Towards Atmospheric Characterisation of Exoplanets

— James Michael Frith —

Centre for Astrophysics Research
Science and Technology Research Institute
— University of Hertfordshire —

Submitted to the University of Hertfordshire in partial fulfilment of the requirements of the degree of Ph.D.

Principal Supervisor: Prof. David Pinfield

— October 2013 —

Declaration

This Ph.D. thesis consists of five chapters and an appendix. Chapter 4 is an unedited journal publication produced from research conducted during the course of the Ph.D which can be found in volume 435, issue 3, pages 2161-2170 of the Monthly Notices of the Royal Astronomical Society. I certify that the content presented in this thesis is my own work. Any results, diagrams and tables used from other published works have been properly cited.

James M. Frith

Acknowledgements

On a professional level, I must first thank my supervisors without whom none of this would be possible. Thanks to Dr Craig Brown for handling all the arrangements that made my work experience at Astrium educational and without any logistical hiccups. Also thank you for all the experience working with spacecraft engineering that will prove to be invaluable and for providing insight into the mine field of European politics. Thank you to Dr John Barnes who simultaneously educated me about echelle spectroscopy and the complicated field of exoplanet atmospheres. And Professor David Pinfield who helped me with everything from being an inspirational scientific mentor to lifts from the airport and without whom there would have been no funding for my PhD. I'd like to thank Dr Kevin Jim and Dr Rita Cognion who pushed me to do a PhD in the first place. And finally I would like to thank Professor Janet Drew and Professor Sean Ryan for helping to support my final few months of writing my thesis.

On a personal level, the person who is responsible more than any other in helping me get to this point is my wife, "You got this" Maria. She has somehow remained sane going through two pregnancies and taking care of two screaming (but lovely) children on her own for the majority of the time while I strained to give birth to my own scientific endeavours. She shot down all of my pursuing proverbial TIE fighters and shouted "you're all clear, kid" just as things seemed most dire. It was only because of her that I was able to stay on target.

With that horrible metaphor out of the way, I would like to thank my parents who, regardless of the fact that I would not exist without them, provided endless emotional and financial support. They have been an inspiration in every way. My brothers are also to thank, both the one that is absent and the other whom I'm very glad is still around. David, Carol, and Ellen Baldam have also helped out immensely with their support and love.

Much Support has also come from amongst my peers as well along the way and it is difficult to name all of those that have kept me sane through this PhD. One that I would like to thank in particular is Andy Gallagher for his many talks about radiative transfer, stellar evolution, and whether blowing up Vulcan was a useful plot tool or just a shameless action scene that ruined the franchise. I would also like to thank Elizabeth Dodd for providing me with noodle soup and good friendship particularly in the final writing phases of my PhD. I would like to thank my fellow UH ROPACS ESRs, Brigitta and Joana, for all of the fun experiences in different countries around the world and shared stresses during all of our ROPACS adventures as well as all of the other ESRs. Hywel, Federico, Beatriz, Simon, Carla, Silvia, Kieran, Carlos, Roberto, Gemma, Chris and others I am probably forgetting have all been amazing people to be associated with and have helped me professionally and personally. Thanks to all of you.

Abstract

This thesis provides a multi-pronged approach towards paving the way for future space and ground based exoplanet characterisation efforts as well as providing new analysis of the atmosphere of the exoplanet HD 179949 b. This is done, firstly, by outlining engineering trade studies conducted for the attitude and orbit control system (AOCS) and sun shield for the Exoplanet Characterisation Observatory (EChO) spacecraft (a proposed European Space Agency exoplanet space mission). These trade studies were conducted in collaboration with EADS Astrium. A cold gas system with the possibility of a hybrid system which would include the use of reaction wheels is recommend for the design of the AOCS. For the sun shield, a V-groove cone shield is concluded to provide the best thermal coverage while also providing stay light protection as well as being more mechanically symmetric than other options. Simulations are then conducted to determine the number of transiting planets future surveys should expect to find around stars within 50 parsecs of the sun. This is done by taking the known stars within 50 parsecs and adding a simulated planet population based on current models and observations to each star. Assumptions are made regarding observability of a planetary transit and a Monte Carlo simulation run to gain statistics on the number and type of planetary systems that can be expected to be found. The results of the simulation show a mean expected number of 27 detectable transiting planets within 50 parsecs. Next, using the Position and Proper Motion Extended-L (PPMXL) catalogue, optical and near-infrared colour cuts were used together with a reduced proper motion cut to find bright M dwarfs for future exoplanet transit studies. PPMXL's low proper motion uncertainties allow this work to probe down to smaller proper motions than previous similar studies. Unique objects found with this method were combined with that of previous work to produce 8479 K $<$ 9 M dwarfs. Low-resolution spectroscopy was obtained of a sample of the objects found using this selection method to gain

statistics on their spectral type and physical properties. Results show a spectral-type range of K7-M4V. This catalogue is the most complete collection of K $<$ 9 M dwarfs currently available and is made available here. High resolution spectroscopy and model spectra of planetary atmospheres is then used along with a spectral deconvolution technique to attempt to detect the Doppler shifted signal of the non-transiting planet HD 179949 b. The signal was not detected but new upper limits were set ruling out the presence of TiO down to a $\log_{10}\ \epsilon_0$ = -4.09 with 99.9 per cent confidence. Simulations conducted by this work imply a loss of sensitivity occurring possibly due to varying telluric interference or instrumental systematics.

Contents

List of Figures

List of Tables

Chapter 1: Introduction

There are very few subjects within the sciences that excite the public quite like the idea of other worlds, possibly similar to our own, existing elsewhere in the universe. Philosophers, scientists, and leaders of different faiths have expressed their opinions over the centuries on whether these celestial bodies exist but only in the last 20 years has there been proof, not only of their existence, but also of their ubiquity. Recent estimates by Bonfils et al. (2013) set the number of planets within the Milky Way in the many billions with these estimates being refined regularly. The next major milestone in exoplanet science, which is on the horizon, is the ability to characterize the chemistry and composition of the atmospheres of these distant bodies with an eye always towards habitability. This chapter will discuss the history of this still maturing branch of science and set the scene for how this work fits in with the current state-of-the art and future of exoplanet science.

1.1 History of Exoplanet Detection

The first credible discovery of a planetary-mass body outside the Solar System was done by Wolszczan & Frail (1992) who used variations in pulsar timing to conclude the presence of at least 2, roughly Earth-mass planets orbiting the neutron star PSR1257 + 12. Three years later, the first radial velocity planetary detection (the radial velocity technique is discussed in Section 1.2.1) was made by Mayor & Queloz (1995) which found a Jupiter sized object around 51 Peg with an orbit much closer to its host star than previously theorized possible. Though other radial velocity surveys had looked at 51 Peg previously (Marcy & Butler, 1995), its short period oscillations had been overlooked. This is partly because it had been theorized that planets of such large size could not form within such close proximity to their parent star due to the incident stellar flux preventing the accretion of large amounts of material (Wuchterl, 1994).

Since these "hot Jupiter" planets had now been found to exist, many similar detections followed in a short time frame due to the re-analysis of previous data sets and

more focused searches (Marcy & Butler (1996), Butler & Marcy (1996), Butler et al. (1997)). These discoveries, advancements in technology and observational techniques ushered in an age of exoplanet discovery that is still ongoing and led to new theories on the possible migration of giant planets from the outer regions whence they formed (Ward (1997), Bryden et al. (1999), Nelson et al. (2000)).

Because they were more easily identifiable with the radial velocity technique, the initial planetary systems discovered consisted of a single hot Jupiter and its host star. However, observations of υ Andromedae by Butler et al. (1997), which announced the detection of a closely orbiting giant planet, and later by Butler et al. (1999) found the first evidence of an exoplanet system containing multiple planets. This, though still very different in its content, was the first planetary system to which the Solar System could easily be compared and hinted that more planets may be hiding below the detection limit of these early radial velocity surveys.

A radial velocity result by Mazeh et al. (2000) of a hot Jupiter around the G0V star HD 209458 showed that the plane of the planet's orbit was very near edge-on implying that the planet may appear to traverse the disc of the star at some point during its orbit. Photometric observations were later simultaneously carried out by Charbonneau et al. (2000) and Henry et al. (2000) that witnessed a periodic dip in brightness of the star that coincided with the inferior conjunction of the planet's radial velocity orbit. This brightness drop was the first observation of a planetary transit (discussed further in Section 1.2.2) where the planet's orbit is randomly orientated such that these types of observations can be carried out. This technique has many advantages over the radial velocity technique as far as characterisation of the planet but is at the mercy of nature to provide the geometry necessary for such a transit and therefore can only be observed for a limited number exoplanet systems.

While the odds of observing a planetary transit are extremely unlikely when looking at only a handful of stars, the Universe is quite good at providing a large data set in which to look for these transits and a large number have been observed. Several large scale ground-based transit searches have been enacted since 1999 but, due to the precise photometric stability and constant monitoring necessary for these types of ob-

servations, the most impressive discoveries using the transit technique have been those from space-based observatories. The COnvection ROtation and planetary Transits (CoRoT) satellite (Baglin et al., 2007) was launched in late 2007 and took data until the end of 2012 and in that time discovered 24 planets. Additionally, the exoplanet-focused Kepler satellite (Koch et al., 2007), launched two years later than CoRoT, has discovered 151 confirmed planets and potentially thousands more yet to be confirmed. Kepler's discoveries have provided valuable statistics on the number of planets that exist within the Milky Way and found some very interesting systems. Kepler 16b was announced by Doyle et al. (2011) as being a Saturn-mass circumbinary planet orbiting and eclipsing its two host stars where all three objects orbit each other to within 0.5^o of the same orbital plane. This implied that all three had been formed from the same collapsing disk of material. Kepler 42 and Kepler 32 (Muirhead et al., 2012; Swift et al., 2013) both host multi-planet transiting systems and are some of the smallest exoplanets discovered. To date the CoRoT and Kepler satellites together have detected 175 confirmed planets, with Kepler still claiming 3548 "objects of interest" or still to be confirmed planetary candidates (Wright et al., 2013). The ground-based transit surveys are not to be overlooked, however, and their contributions and future will be discussed later.

Parallel to the transiting and radial velocity searches, there have been many attempts at directly imaging exoplanet systems using space and ground-based equipment. This detection method is more reliant on technology that has only come into fruition recently so their numbers are few. Detection by this method is one of the few ways to unambiguously observe light directly emitted or reflected from the planet.

Figure 1.1 shows the first successful image of the sub-stellar object 2M1207b and its brown dwarf companion produced by Chauvin et al. (2005). 2M1207b is often referred to as the first imaged exoplanet but at a mass 4 times that of Jupiter, as is the case with many sub-stellar objects, it skirts the line between what could be called a brown dwarf or a giant planet. Regardless of its designation, this image was produced using the European Southern Observatory's Very Large Telescope (ESO,VLT) which was able to resolve the two objects at an angular separation of 0.7 arc seconds (Mohanty

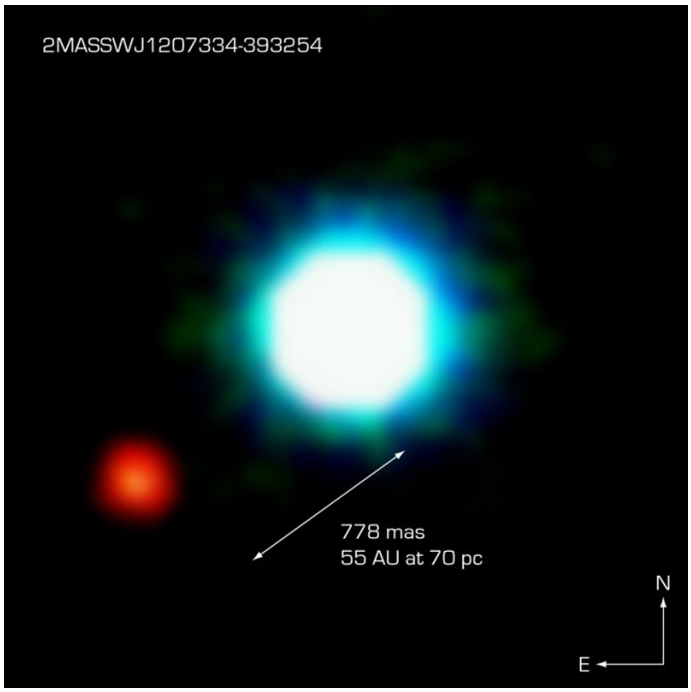

Fig. 1.1: Sub-stellar object 2M1207 b and its M dwarf companion (Chauvin et al., 2004).

et al., 2007), pushing the limits of the technology of the time.

Two discoveries that happened simultaneously were the imaging of a planet around Fomalhaut using the Hubble Space Telescope (HST) (Kalas et al., 2008) and a multi-planet system around HR 8799 (Marois et al., 2009) using the Keck and Gemini telescopes. The validity of the detection of Fomalhaut b has been called into question by the results of Janson et al. (2012) who were unable to reproduce the original result. However, further results by Galicher et al. (2013) and Kalas et al. (2014) claim to authenticate its existence. HR 8799's existence is not in question and remains one of the better studied multi-planet systems and is shown in Figure 1.2.

Initially, only 3 planets were found around HR 8799 but the discovery of a fourth planet was announced a year later by Marois et al. (2010). Similar to the transiting method, direct imaging is highly dependent on the orientation of the exoplanet's orbit and is more sensitive to planets that orbit perpendicularly to the plane of the sky. But a discovery by Lagrange et al. (2009) around the young star β Pictoris's dusty environment appears to be an imaged planet that is orientated such that it is possible the planet may transit its host star (Lecavelier Des Etangs & Vidal-Madjar, 2009). Images taken several years apart showed the planet disappear and reappear on the

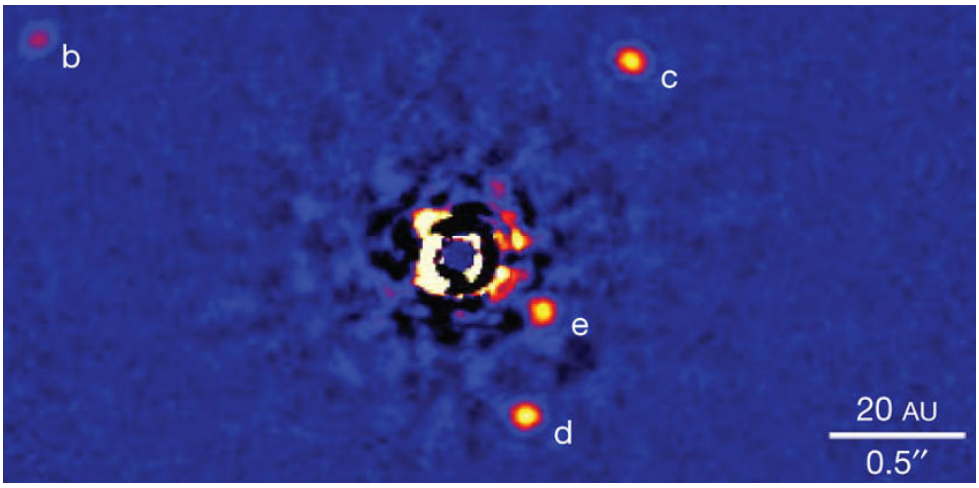

Fig. 1.2: Directly imaged planets HR 8799b,c,d,and e made using the Keck observatory (Marois et al., 2010).

opposite side relative to its primary star implying that either it passed behind or in front of its companion. These images can be seen in Figure 1.3.

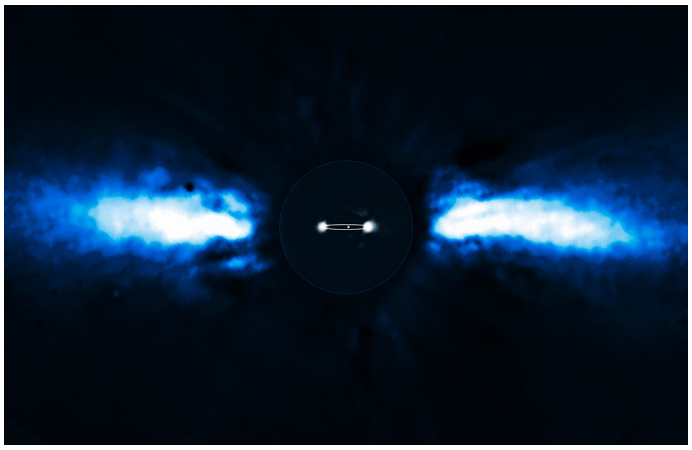

Fig. 1.3: Two images of β Pictoris at different epochs showing its orbital motion around its star (Lagrange et al., 2010). Images taken several years apart showed the planet disappear and reappear on the opposite side relative to its primary star implying that either it passed behind or in front of its companion.

It is worth also mentioning that the microlensing technique has produced several detections of exoplanets, the first being Bond et al. (2004). This method relies on the extremely unlikely event of a planet passing in front of a background star in the precise geometry such that its gravitational influence lenses the background star's light causing a distinct but unrepeatable brightness peak. This technique also detects more widely separated planetary systems that are not possible to detect via other methods but their unrepeatable nature only allows statistics of the population of these objects to be

acquired without an possibility for follow up observations. Because of the seemingly extreme unlikeliness of this to occur, the many detections that have been observed so far by Sumi et al. (2011) have lead them to estimate that there are hundreds of billions of free floating, sub-stellar objects in the Milky Way.

With the ever increasing precision in angular resolution brought about by the use of adaptive optics and detector advancements, measuring the wobble of stars caused by orbiting planets astrometrically may also provide another method to detect exoplanets but none so far have been found using this method.

Even though exoplanet science is a young field, this is, of course, only an overview of some of the important advancements in the methods of discovering exoplanets. The developments towards exoplanet characterisation is a separate matter and will be discussed in Section 1.3.

1.2 Overview of Relevant Detection Techniques

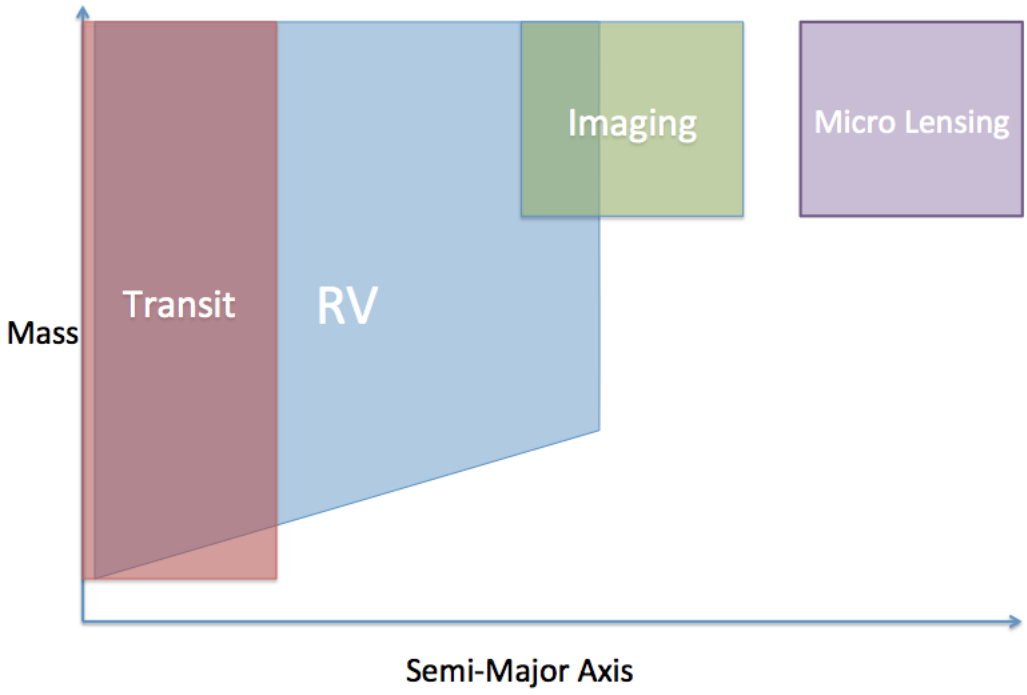

Fig. 1.4: An illustration of the advantages of different detection techniques of exoplanets as a function of mass and semi-major axis of the planet. All techniques require specific geometries for them to be viable but this assumes that those geometries are met for each method.

All of the different exoplanet detection techniques have advantages and disadvantages to finding exoplanets of a particular mass and distance from their host star. Figure 1.4 illustrates the basic parameter space covered by different detection techniques for finding planets of a certain mass and semi-major axis.

While microlensing, and direct detection are very important towards our full understanding of the exoplanet population and characteristics, it would be worth while to further expand on the methods that are more relevant to this work; namely, the radial velocity and the transit techniques.

1.2.1 Radial Velocity

The radial velocity (RV) or Doppler method is the work horse of exoplanet detection and is responsible for the very first detection of 51 Peg and continues today to find dozens of planets. It works off of the simple principle that the wave nature of light causes the wavelength of a constantly emitting source to be slightly shorter when it is moving towards an observer and longer when moving away. Gravitational effects of a planet orbiting a star cause the two bodies to orbit around their combined centre of mass and the star's (and planet's) light is periodically shifted. This period, P, and the amplitude of the shift, K_*, are the observables that allow the planetary system's mass distribution to be determined using the following relationship

$$K_* = \left(\frac{2\pi G}{P_{orb}}\right)^{1/3} \frac{M_p \sin i}{(M_p + M_*)^{2/3}} \frac{1}{(1-e^2)^{1/2}} \tag{1.1}$$

where M_p and M_* are the masses of the planet and star, respectively, i, is the system's inclination with respect to the observer, and e is the eccentricity (Hilditch, 2001). Estimates for the star's mass can usually be made using mass-spectral type relationships or other observables with relatively low uncertainties. Therefore, with the observation of K_* and P and the assumption of a near circular orbit, one can determine M_p sin i. But, without knowing the inclination of the system, this is the limit of information that this method can provide. Therefore, since sin i$\leq$1, for most cases this technique only provides a minimum estimate of the planet's mass.

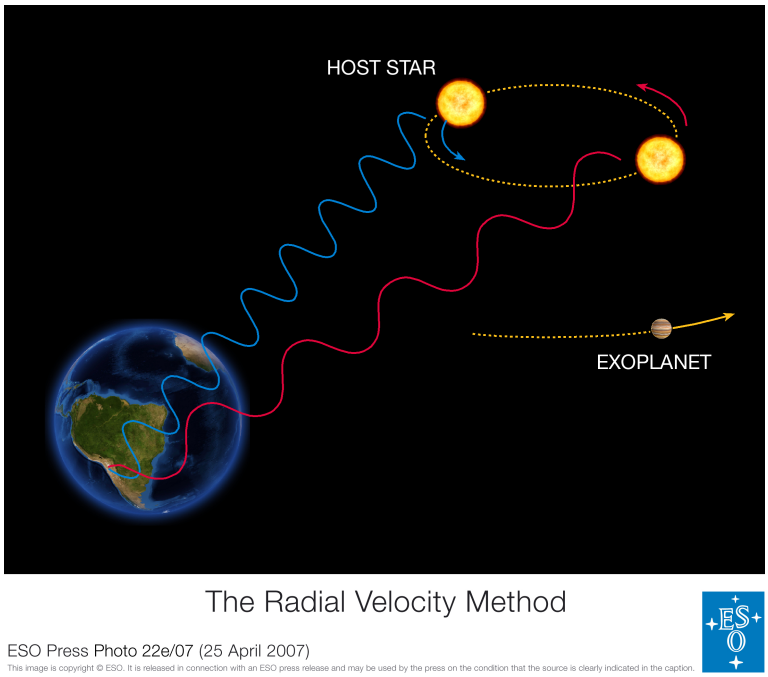

Fig. 1.5: Image describing the radial velocity detection technique. Light from the host star is Doppler shifted as the star and planet orbit each other causing the light to periodically shift from longer to shorter wavelengths. Image taken from www.eso.org.

K_* has been observed for the multitude of planetary systems discovered with this method and varies from hundreds of meters per second for the hot Jupiter systems down to 9 cm s^{-1} to detect an Earth-mass planet around a Sun-type star (Mégevand et al., 2012). This is far below the current detection limit for even the most advanced spectrographs which are sensitive down to $\sim$ 1 m s^{-1}. The sensitivity of these instruments is highly dependent on their ability to remain thermally and physically stable over the course of the observations since even a minuscule fluctuation or vibration will affect the miliangstroms wavelength calibration necessary. The most sensitive and successful spectrograph for finding exoplanets as of now is the High Accuracy Radial velocity Planet Searcher (HARPS) spectrograph (Pepe et al., 2000) on the 3.6m telescope in La Silla, Chile and its twin, HARPS-N (Cosentino et al., 2012), in the northern hemisphere installed on the Telescopio Nazionale Galileo telescope in La Palma, Spain. Their sensitivity is achieved by using simultaneous wavelength calibrations superimposed onto observed spectra as reference and placing all of the instruments in an environmentally enclosed vacuum chamber using thorium arc lamps for the reference spectra. This allows for the majority of thermal drift or fluctuations within the system to be accounted

for since the reference spectra is affected in the same way as the observed.

Sensitivities are not only limited by instrumentation. The stellar properties themselves play a role due to seismic and magnetic activity causing cells of material within the star to rise and fall producing a Doppler jitter indistinguishable from the orbital motion of the star. Signals produced in this way can be partly discounted by simultaneously monitoring the star's activity indicators (such as the Ca II H and K lines) and correlating activity to spurious signals. Activity can also be distinguished from an RV signal caused by a perturbing companion by looking for minute changes in the stellar line profiles that, if caused by a planet, should remain stable. This is done by bisecting the stellar profile line and looking to see if the bisector's position changes over time with respect to the centre of the line (Queloz et al., 2001).

Other methods of breaking the 1 m s^{-1} limit include statistical techniques put forth by Tuomi & Jones (2012) and Anglada-Escudé & Tuomi (2012) who apply Bayesian statistics to archived HARPS data to identify RV signals around lower mass stars. This has produced encouraging results including the discovery of 3 super-Earth mass planets ($\sim$10 M_{Earth}) that were previously missed by earlier RV results (Anglada-Escudé et al., 2013). These statistical methods are cheaper and easier than developing new instruments to achieve lower sensitivities due to the many difficulties involved in overcoming and limitations of the hardware, but good models of the low level systematics in the data are required.

A major driver for pushing the sensitivities lower is the desire to find Earth-like planets but, as mentioned, the precision necessary is an order of magnitude smaller than what is available. One way to skirt the need for better sensitivities is by looking for Earth-type planets that orbit around lower mass stars at a distance that is much closer to the star but where the incident stellar flux is the same as Earth's. Because the mass ratio between a lower mass star and an Earth-mass planet is much greater, K_* can more easily be observed. This is one of many advantages that lower mass stars, particularly M dwarfs, offer to observers looking for planets that may be habitable.

This is not a new idea and M dwarfs have become the focus amongst radial velocity and transit surveys alike (Charbonneau et al., 2008; Bonfils et al., 2013). But these

inherently dim stars emit most of their light in the infrared beyond the optical range in which most RV instruments are sensitive so it is difficult to receive enough photons, using these high resolution spectroscopic techniques, from the M dwarfs to obtain an accurate RV signal. This, and other factors discussed in Section 1.4, has made the few M dwarfs that are bright enough to be observed to become of interest to those searching for and characterizing exoplanets.

1.2.2 Planetary Transits

As mentioned in Section 1.1, a planetary transit is a rare occurrence dependent on the fortuitous alignment of the orbital plane of the planet such that it periodically traverses its host star causing a drop in the observed brightness.

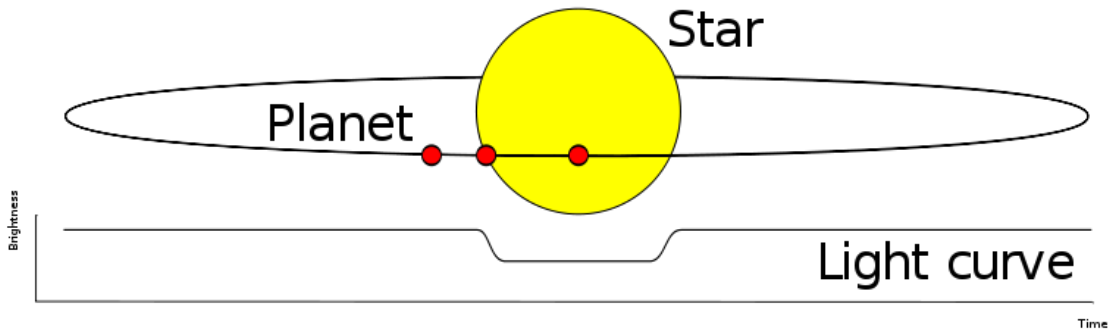

Fig. 1.6: Illustration of a planet transiting in front of its host star and the associated drop in magnitude during the transit. Image produced by Nikola Smolenski.

The change in flux approximates to the ratio of the area of the disk to that of the planet, expressed as

$$\frac{\Delta L}{L} = \left(\frac{R_p}{R_*}\right)^2 \tag{1.2}$$

where L and R_* are the surface brightness and radius of the host star and R_p is the radius of the planet (Winn, 2010). Similarly to the RV method, constraints can be placed on the star's radius using either spectral type information or other observables so Equation 1.2 is an immediate way of discerning an approximation of the radius of the planet.

Equation 1.2 is not completely accurate because it does not take limb darkening

into account which causes the ratio to change as a function of the star's optical depth and the planet's location on the disk with respect to the observer. This is an important effect that must be included for precise measurements (Kipping, 2013). Also, the optical depth of the planet's atmosphere can cause discrepancies in radius measurements between observations made in different passbands. This is obviously highly dependent on the scale height of the planet's atmosphere since a rocky planet with no atmosphere will have less of a discrepancy than a gas giant with an inflated atmosphere (Fortney et al., 2007).

In addition to size estimates of the planet, an advantage one obtains with a planet that has an observable transit is that its inclination is directly measurable. When combined with RV measurements, it is relatively straight forward to obtain mass, radius (and therefore density) and precise orbital elements that describe its periodic motion (Gilliland et al., 2013). This makes transiting planets the most well understood amongst the known population and newly discovered transiting planets highly desired candidates for future study.

As mentioned, the the light from the star can be affected as it passes through the planet's atmosphere interfering with the determination of the planet's radius. This effect can also be measured and spectroscopic measurements taken during transit can give insight into the composition of the planet's atmosphere (Huitson et al., 2013). For most transit geometries, a comparison can be made between the spectroscopy of the light of the star-planet combined to that of the light when the planet passes behind the star where the planet's reflected or emitted light cannot contribute. The usefulness and specifics of these characterisation methods will be discussed more in Section 1.3.

The Kepler satellite, the highly successful exoplanet transit observatory mentioned in Section 1.1, was originally designed to have a 3.5 year long mission. This requirement was directly connected to it's primary science goal which was to gain statistics on the number of Earth-analogues (EA) that exist within the Milky Way. EA's are defined as 1 Earth mass planets around G dwarf stars orbiting at 1 astronomical unit (au). In order for Kepler to safely confirm that it has observed a transiting planet, 3 transit observations are needed to establish any level of certainty. Therefore, in order to

observe 3 transits of an EA, Kepler required at least 3 years (the length of time it takes for an EA to orbit its star 3 times). This time scale is manageable for EA's but the likelihood of observing planets at greater distances from their star decreases as a function of Kepler's 3rd law ($P^2 \propto a^3$, P being period of the orbit and a the semi-major axis). For example, if one wanted to gain statistics on the number of Jupiter-analogues, the Kepler satellite would need to be operational for more than 30 years. This is, of course, impractical (and likely impossible) but it does illustrate that the Kepler statistics are not complete for all orbital regimes.

Though we are understandably biased towards wanting to find exoplanets that are similar to our own, the observability of EA's is very difficult for the transit method and not possible at the moment using the RV technique due to the sensitivity limits discussed in Section 1.2.1. Also mentioned in Section 1.2.1 is the usefulness of bright M dwarfs. This is true of of low mass stars for the transit method as well. The radius of an M dwarf can be comparable to that of Jupiter (Chabrier & Baraffe, 2000) which means that the ΔL measurement of an Earth-sized planet around an M dwarf is much easier to detect. Also, to maintain our bias towards finding planets similar to our own, a planet orbiting an M dwarf at a distance where it receives the same incident flux as an EA places is much closer to its host star (Fortney et al., 2007) and, therefore, is much easier to confirm via multiple transits. Three transits of a planet around an M dwarf at a distance where it receives the same flux as Earth take approximately 3–10 days as opposed to three years for an EA (Ramsey et al., 2008).

Since it is near impossible to obtain precision comparable to Kepler from Earth, ground based surveys have already started to focus on the known low mass stellar population to search for transit light curves. 5 transiting planets around M dwarfs are currently known, 3 of which were discovered via ground based observatories (See Chapter 4). One such discovery was made by the Mearth survey (Charbonneau et al., 2008) which consists of an array of cheap commercial telescopes and cameras that perform a focused search for transits around M dwarfs. They observed one transiting super-Earth around an M 4.5 dwarf (Charbonneau et al., 2009) very soon after beginning operation in 2008 but have not found another in the years since. The survey is ongoing.

An alternative to the queued, single-object-at-a-time Mearth survey, is the super Wide Angle Search for Planets (Street et al., 2003, superWASP) that employs an array of very wide field-of-view cameras that give it a total effective field-of-view of 9.5 square degrees. Their goal is to plough the sky nightly and look for any possible dip in light that may be a transit. They have two installations covering both the northern and southern hemispheres currently in operation. This project has observed 65 exoplanet transits thus far and is one of the most successful (in quantity of exoplanets discovered) ground based transiting surveys. Similar in design and coverage is the Hungarian Automated Telescope Network (Bakos et al., 2002, HATNet) which had first light at around the same time as superWASP and have a total of 29 transiting planets discovered.

1.3 Towards Atmospheric characterisation

Meaningful understanding of the surfaces and interiors of exoplanets is most likely unobtainable for many generations to come. However, using innovative applications of the techniques discussed so far, real understanding of exoplanet atmospheres is possible and, in fact, well underway. With the tools of detection now outlined, this section will focus on the milestones and the state-of-the-art techniques that have produced information of the composition and structure of exoplanet atmospheres.

1.3.1 A side note on the "Habitability" of Exoplanets

As mentioned, much of the driving force of exoplanet discovery has been the interest of the public and professional community to find another planet besides Earth that is deemed "Habitable". This is often confused with a planet that is found to orbit in the "Habitable Zone" (HZ): the radial distance from an exoplanet's host star where enough incident flux is received that liquid water can exist and is not restricted to either a gaseous or solid phase (Kasting et al., 1993); the motivation being that liquid water is a requirement shared by all life on Earth. It is important to note, however, that nothing about the HZ necessitates the habitability of a planet within nor does

being outside the HZ necessitate its un-inhabitability. A planet in the HZ around a G dwarf is in a completely different environment than that of the HZ of an M dwarf where gravitational interaction and the spectral energy distribution of the incident light can change the atmospheric chemistry and geological environment (Barnes et al., 2011b).

A holistic approach towards the definition of "habitable", such as undertaken by Gaidos et al. (2005) and Barnes et al. (2011a), where the effects from tidal heating, the local astronomical environment, plate tectonic carbon recycling, rate of delivery and evaporation of water and other elements to the planet, as well as other factors need to be understood before a planet can truly be deemed habitable. More exotic environments must be considered as well as has been done by Barnes & Heller (2013) and Kipping (2013) who have looked into the possibility of white dwarfs and brown dwarfs as potential hosts to habitable planets as well as exomoons around giant planets.

With all that now being mentioned, one must start somewhere. Determining whether a planet is in the HZ is an easily obtainable metric using the methods outlined in Section 1.2.1 and 1.2.2 and many of the factors needed as an input to a holistic approach are not obtainable with current technology. And since our one empirical data point available to us, the Earth, is in the habitable zone of the Sun, it is as good a place to start as any.

1.3.2 Overview of Relevant characterisation Techniques

Background Information

A few key observatories have been instrumental in providing data to the exoplanet community. The Spitzer space telescope (Werner et al., 2004) has been an essential provider of data products that have contributed greatly to the understanding of this discipline. Launched in 2003, its instruments, sensitive in the infrared, have played an important roll in setting constraints on the atmospheric properties of exoplanets. On board Spitzer are the Infrared Array Camera (IRAC), the Infrared Spectrograph (IRS), and the Multiband Imaging Photometer for Spitzer (MIPS). IRAC takes photometric images across 4 passbands simultaneously at 3.6, 4.5, 5.8 and 8 microns while MIPS

consists of 3 separate photometric detectors in the far infrared from 24, 70, and 160 microns. The IRS allows infrared spectroscopy to be taken with four channels which observe at the wavelengths 5.3 to 14 microns at low resolution, 10 to 19.5 microns at high resolution, 14 to 40 m at low resolution, and 19 to 37 microns at high resolution (Houck et al., 2004).

The Hubble Space Telescope (HST) has also been used to a great degree especially the Space Telescope Imaging Spectrograph (STIS) and the Near Infrared Camera and Multi-Object Spectrometer (NICMOS) Freudling et al. (1997). Between STIS and NICMOS, the HST has provided space-based spectroscopic observations in the optical to near infrared.

Because of the reasons discussed in Section 1.2.2, transiting planets are the obvious choices as targets for characterisation techniques and the majority of attempts to examine exoplanet atmospheres thus far have been done using planets that transit. Photometric observations of a planetary transit, combined with an RV signal, provide constraints on radius, mass, and orbital information which are essential inputs into any estimation of its composition. In addition to providing those constraints, there are several methods that have been developed to take advantage of transiting planets as a way of providing insight into their atmospheric composition and chemistry.

Two transiting planets in particular have been studied significantly more than others so it would be useful to have a brief description of their fundamental characteristics gained from their initial transit and RV observations. The first is HD 189733 b which was discovered by Bouchy et al. (2005) in an RV survey. It is a 1.114 M_{Jup} hot Jupiter orbiting at ∼0.031 au around a K1-K2V primary with a period of 2.2185 days (Wright et al., 2013). The second, mentioned in Section 1.1 as the first transiting planet discovered, is HD 209458 b. It is smaller than HD 189733 b at 0.690 M_{Jup} and orbits around a star similar to the Sun (G0V) at approximately 0.047 au every 3.5247 days Wright et al. (2013). The observations and inferences of these two planet's atmospheres will be discussed below but their basic information is listed here for reference.

Transmission and Eclipse Spectroscopy

During a transit, the planet blocks out a percentage of the star's light as it passes between the star and the observer. During these events, some of the light from the star passes through the atmosphere and can be absorbed or attenuated by the atmosphere. Observing how the intensity of light changes as a function of wavelength using spectroscopy during a transit is therefore one technique to examine the composition of the atmosphere (Coustenis et al., 1997; Seager & Sasselov, 2000). Also, as the planet approaches superior conjunction, the point in a planet's orbit when it is furthest away from the observer, the day side of the planet comes into view and emission spectra can be observed.

Of particular use to atmospheric characterisation is where, in addition to the primary transit during which the planet passes directly in front of the star, a secondary transit can occur where the planet passes behind the star and is hidden from view of the observer. This is useful because it provides the observer with an opportunity to detect both the light from the planet-star combined and, during the secondary transit, an opportunity to only observe the light from the star. This allows comparison between the flux difference as a function of wavelength during the different geometries and to infer the planet's structure and chemical composition. The combination of these two transit events has yielded many encouraging results.

Charbonneau et al. (2002) were the first to successfully use transmission spectroscopy with observations of HD 209458 b. The HST, using STIS, was used to observe HD 209458 b in and out of transit and a deficiency in the abundance of sodium in the atmosphere, contrary to predictions by Seager & Sasselov (2000), was detected.

HD 209458 b was observed later by Vidal-Madjar et al. (2003) with the STIS during 3 transits. They found a large drop in flux in the stellar Lyman-α line during transit that was larger than should be for the measured radius estimations for the planet. Subsequent observations by Ben-Jaffel (2007) and Ben-Jaffel & Sona Hosseini (2010) produced similar results implying that HD 209458 b has a highly extended atmosphere. Lecavelier Des Etangs et al. (2010) and Lecavelier des Etangs et al. (2012) found a

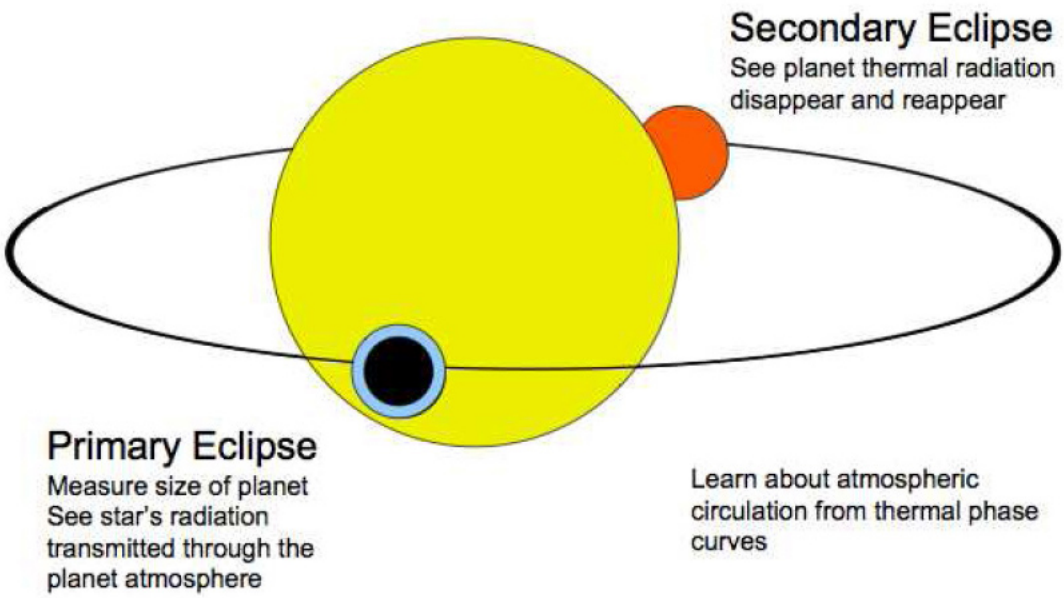

Fig. 1.7: This shows the geometry of the primary and secondary eclipse. During a primary eclipse, when the star passes in front of the star, the observer sees the cool (night) side of planet while light from the star passes through its atmosphere. Just before the secondary eclipse, the observer sees the hot (day) side of the planet and can see its reflected or emitted light. When the planet passes behind the star, only stellar light is observed so one can differentiate between the signal with and without the planet. Image taken from the University of Arizona website (http://ircamera.as.arizona.edu/MIRI/).

similar discrepancy with their HST observations of HD 189733 b and concluded that hot Jupiters such as these can have highly extended atmospheres that trail their orbit and can possibly approach or go beyond their Roche Limit (Eggleton, 1983) where the planet may be in a state of evaporation.

Specific molecules have been inferred using similar methods. Tinetti et al. (2007) used IRAC on Spitzer to observe several transits of HD 189733 b and saw the percentage of light attenuated due to the planetary transit vary as a function of wavelength. This essentially provided data points along the planet's spectral energy distribution (SED) and model planetary atmospheres could be compared to observations. They found their observations consistent with an atmosphere that contained water vapour. Spitzer was also used by Grillmair et al. (2008) and found significant water absorption present in the emission spectra of HD 189773 b. Swain et al. (2008) also observed HD 189773 using NICMOS and saw evidence for a water-methane atmosphere. Similarly, Barman (2007) and Swain et al. (2009) found water, methane, and carbon dioxide in HD 209458 b again using NICMOS measurements.

Pont et al. (2008) used HST to observe 3 transits of HD 189773 b and found evidence for stellar spots on the surface of the star as well as evidence for sub-micrometer particles in the upper atmosphere. Later, Sing et al. (2011) observed HD 189773 b with the HST STIS in the near-uv and obtained 2 transit events. Their resulting transmission spectrum was consistent with Rayleigh scattering potentially caused by high altitude haze which may result in the planet being highly reflective (or large albedo) at higher wavelengths. More recently, observations by Ben-Jaffel & Ballester (2013) during transits of HD189733 b found evidence of neutral oxygen using HST archive data.

An example of ground based transmission spectroscopy was carried out by Wood et al. (2011) who used optical spectroscopy with the VLT's GIRAFFE spectrograph (Flores et al., 2004) to observe Wasp-17 b: a transiting hot Jupiter around an F6-type star (Anderson et al., 2010). They found a depletion of sodium in the atmosphere when compared to solar-abundance models and hypothesize that ionized sodium may have rained to the surface and is now obscured by a cloud layer. Other ground based observations were done by Sing et al. (2012) using the Gran Telescopio Canarias (GTC) during 2 transits of the exoplanet X0-2b (Burke et al., 2007). This was done using the Optical System for Imaging and low Resolution Integrated Spectroscopy (OSIRIS) (Cepa et al., 2000).

Direct Detection

The emerging field of characterizing exoplanets atmospheres via direct detection is obviously highly dependent on first finding planets that can be directly observed. The few mentioned in Section 1.1 (HR 8799 b,c,d,e, and β Pictoris b) have been joined by the recently discovered GJ 504 b, a directly imaged $\sim$4 M_{Jup} planet around a Sun-like star. Without including the debatable Fomalhaut b (Janson et al., 2012), there are three systems currently available to attempt characterisation (Wright et al., 2013). HR 8799's 4 distinct planets has made it the target of multiple observations to detect light directly from the planet and has been the study of multiple observing campaigns (Janson et al. (2010),Bowler et al. (2010), Barman et al. (2011)). Most

recently, the detection of carbon and oxygen in the preliminary results of Konopacky et al. (2013) and Oppenheimer et al. (2013) tentatively announced the detection of methane, ammonia or possibly acetylene, and possibly carbon dioxide. The advantages of directly observing light from a planet opens up possible tomographic techniques proposed by Kostov & Apai (2013) who propose inverting the light curves of directly detected planets using future observatories as the come available.

This is a field in development with very interesting possibilities but is dependent on advanced chronographic techniques that are still being developed. Recent prototypes of a vortex chronograph (Wahl et al. (2013),Mawet et al. (2013)) which uses a phase mask to cancel out light from the primary star, have reproduced detections of the HR 8799 planetary system and may lead to the ability for smaller observatories to obtain spectroscopy of systems like HR 8799 in the future

High Resolution Spectroscopic Characterisation

Spectroscopic characterisation relies on distinguishing the light absorbed, reflected, or directly emitted from the planet by its Doppler shift produced by its orbital motion around the primary. This can be done during a transit or can be applied to non-transiting planets to some extent where the planet's Doppler shift will vary as a function of phase. This is a technique that has been heavily applied to binary star systems and is used regularly to find new binary stars that are unresolved (Szabados et al., 2013; Debosscher et al., 2013).

One of the first to establish albedo constraints on the Close Orbiting Giant Planet (CEGP) orbiting τ Boo using reflected light studies was done by Charbonneau et al. (1999). In the same year, Collier Cameron et al. (1999) reported directly detecting the reflected light of the same system; however, their findings were found to be inconsistent with later observations. Further reflected light studies were done by Collier Cameron et al. (2002) using high resolution spectroscopy and a similar Doppler tomographic signal-analysis technique again placing physical constraints on υ And's innermost planet. There has been recent success by Snellen et al. (2010) who detected carbon monoxide in HD 209458 b and Rodler et al. (2013) performed similar observa-

tions on HD 189733 b where they were also able to discern a Doppler shifted signal indicating carbon monoxide. This method relies on the planet being bright enough to detect since the host star signal will dominate otherwise. This is therefore restricted to only certain planet-star combinations (hot Jupiters being the obvious application). However, one advantage it has, as mentioned, is that it does not necessarily require a transiting planet to gain information about the planet in this way (as this work will show in Chapter 5), enabling a greater sample of objects to be studied.

1.4 A Need for targets: Advantages of M dwarfs as Host Stars

Making use of transmission spectroscopy and the secondary transit are arguably the best current methods to obtain information about an exoplanet's atmosphere but is obviously only applicable to planets that transit. Although there are hundreds of such targets already detected, very few have been found that have star-planet combinations that both have a sizeable transit depth and are bright enough to obtain spectroscopic information. The two planet's outlined above, HD 189733 b and HD 209458, are targets that fulfil this criteria well. Figure 1.8 shows the current known transiting population and the 2MASS Ks band magnitude of the primary versus the percentage drop in flux during the transit. A box has been drawn for illustration to show why HD 189733 b and HD 209458 b have been good targets for spectroscopic characterisation. The box does not necessarily represent any specific observational limitations; it is only a way of emphasizing the usefulness of those two planets.

The other important element that needs to be considered is the period of the planet which dictates how many transits can be observed in a reasonable time frame. The short periods of HD 189733 b and HD 209458 b have allowed many transits to be observed. A counter example is HD 80606 b (Naef et al., 2001) which, though having a favourable transit depth to host star brightness ratio, has a period of $\sim$111 days (Wright et al., 2013) making multiple transit observations difficult to obtain. Coupling those

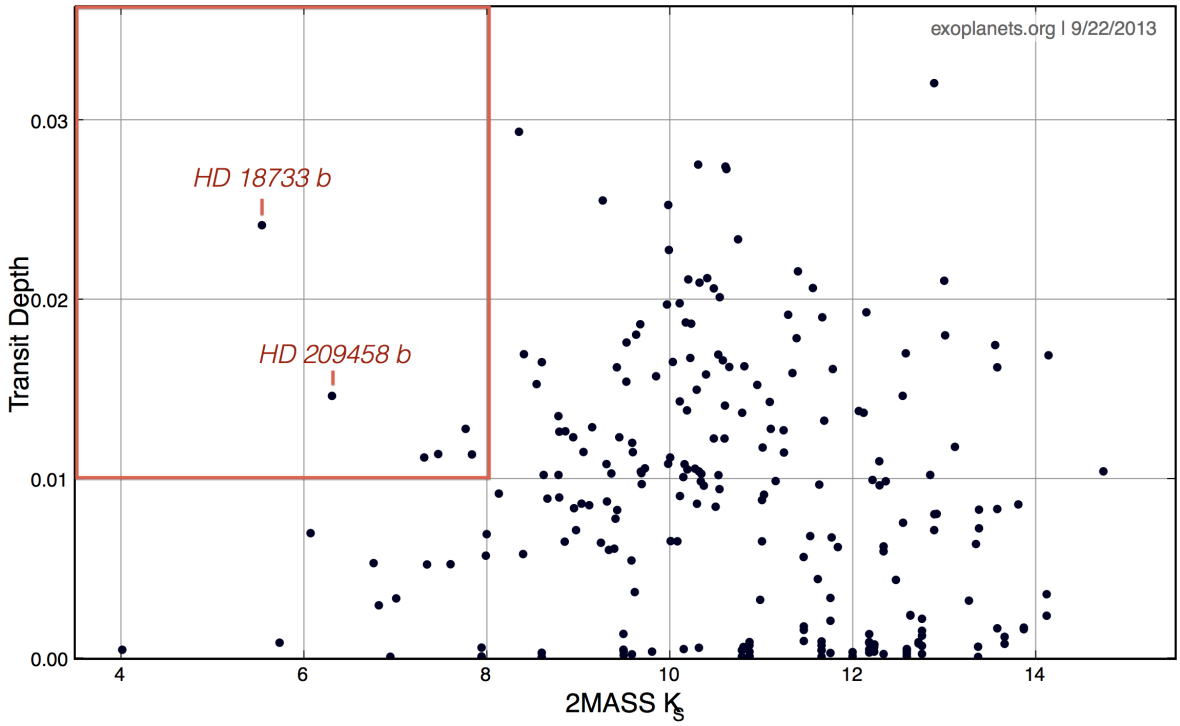

Fig. 1.8: This shows the known transiting planets and the depth of the transit induced by the planet verses the 2MASS Ks magnitude of the primary. The red box is drawn for reference to illustrate the relatively low number of planets that have been found around bright primarys that still produce an easily detectable drop in flux. A bright enough primary to obtain quality spectroscopic information and a measurable drop in flux across multiple wavelengths is useful for transmission spectroscopy measurements. Information and plot produced using www.exoplanets.org (Wright et al., 2013).

requirements with the desire to search for Earth sized planets in the HZ makes finding Earth analogues very difficult. A way of fulfilling the optimal transiting requirements and still being able to detect an Earth mass planet in the HZ is, as mentioned, by extending the target list to cool, low mass stars.

Bright M dwarfs have become heavily sought after as targets for future transit surveys due to their ability to fulfil all of the above requirements. Their cooler nature means that the HZ is much closer to the star, resulting in much shorter periods in the HZ. They are relatively small in comparison to Solar-type stars so the same sized planet transiting an M dwarf has a greater overall depth. They have been somewhat overlooked in RV surveys since their peak flux lies outside the optical which is where most RV studies are sensitive. As a result, the interest in the local M dwarf population has grown in recent years but the current M dwarf population is not well known. This is one motivation for this work and is the subject of Chapter 4.

1.5 The Future

Several ground and space projects are on the horizon that could have a significant impact on exoplanet science and part of the motivation for this work is to help pave the way for these future instruments and observatories. These future projects can be broken up into two categories: Ones that focus on detecting new exoplanets and ones with the goal to characterize known exoplanets. These categories are further broken up into space and ground based observatories. This is a brief overview of some of those projects and how this work will contribute.

1.5.1 Detection

Space Based

The Transiting Exoplanet Survey Satellite (TESS) has been selected by NASA to be launched in 2017 and is an all sky survey program to look for transits around nearby bright stars (Ricker et al., 2010). TESS will search in the optical bands and focus on bright (V$\leq$12) G and K dwarfs less than 50 parsecs away.

Similar to TESS but still competing to be selected is the PLAnetary Transits and Oscillations of stars (PLATO) satellite (Catala et al., 2011): a possible M-class European Space Agency (ESA) mission. PLATO would have a very large field of view and also focus on finding transits around bright stars with a V $\leq$11. In addition to searching for transits, PLATO's mission will also be to characterize the stars themselves through trying to detect the astroseismic p-mode oscillations which give insight into the age and composition of the stars (Bonanno et al., 2002).

Ground Based

As discussed in Section 1.1, the MEarth survey continues to operate and look for transits around M dwarfs. New optimization techniques are being implemented (Berta et al., 2012) to mitigate false-positive transit detections and hope to increase the known number of transiting planets around M dwarfs.

A similar project to MEarth, A PAthway toward the characterisation of Habitable

Earths (APACHE) Sozzetti et al. (2013) which is also focusing on detecting planet's orbiting around M Dwarfs. The project consists of an array of cheap, small telescopes based in the Italian Alps and uses the same single-target approach as MEarth with the intention to be able to compliment their results.

It is arguable that RV surveys skirt both categories of detection and characterisation but, regardless of which category they are presented in here, they continue to be essential. Confirmation of transits by detection of a planet-induced RV signal will still be needed for mass estimates for all transiting planets detected by future surveys and HARPS North and South will continue their own independent RV searches. Additionally, two separate surveys using new state-of-the art optical and IR spectrograph are being implemented by Ge et al. (2013). The optical is using the EXtremely high Precision ExtrasolaR planet Tracker (EXPERT) III and the IR is using the Florida IR Silicon immersion grating spectromeTer (FIRST). Both plan on targeting cool stars (not hotter than K0) with FIRST focusing on the cooler population. They are claiming 0.3 m $s^{-}1$ precision for EXPERT and 3 m $s^{-}1$ for FIRST. This is the first high resolution RV survey dedicated to searching for planets around nearby, bright late K and M dwarfs. Similarly, the Calar Alto high-Resolution search for M dwarfs with Exoearths with Near-infrared and optical *É*chelle Spectrographs (CARMENES,Quirrenbach et al. (2012)) and the Habitable Zone Planet Finder (HPF;Mahadevan et al. (2012)) are other programs that will target bright M dwarfs to search for Earth sized planets in the HZ.

Another project that will be able to push the limits of current detection abilities is the Echelle SPectrograph for Rocky Exoplanet - and Stable Spectroscopic Observations (ESPRESSO;Mégevand et al. (2012)) which is a high resolution spectrograph to be coupled with the VLT. The VLT's large aperture will allow high resolution spectroscopic observations of dimmer objects to have usable signal-to-noise ratios (S/N) and therefore be able to obtain RV measurements of these dimmer objects.

1.5.2 Characterisation

Space Based

The CHaracterizing ExOPlanets Satellite (CHEOPS) has already been selected by ESA as an S class mission to be launched in 2017 (Broeg et al., 2013). It will be a pointable small telescope (30cm) using photometry in the optical with the mission to constrain radii measurements for known transiting exoplanets. Because of the precision available to space based instruments, it is hoped to be able to constrain radii down to Neptune and super-Earth size transiting planets. Like most of the characterisation missions below, this mission relies on ground based surveys to expand upon the current list of transiting planets around bright (for this mission a $V < 12.5$) host stars.

The James Webb Space Telescope (Gardner & JWST Science Working Group, 2005) is a tool that is expected to revolutionize astronomy and its applications towards exoplanet science will be no exception. Its 6.5 meter aperture, infrared instruments covering 0.6 to 27 microns, and not having to contend with the Earth's atmosphere make it well poised to be an extremely useful tool for exoplanet transmission spectroscopy. However, one of its strengths is a possible disadvantage to the exoplanet community. Namely, JWST is such a useful tool for all astronomical disciplines that its time will be heavily sought after and potentially difficult to obtain for the sometimes time-consuming observations required for transmission spectroscopy.

The Exoplanet CHacertisation Observatory (EChO) is competing for the same slot as PLATO as an ESA M-class mission (Tinetti et al., 2012) and is a proposed observatory designed to do transmission spectroscopy of known exoplanets. In addition to its time being completely dedicated to the characterisation of exoplanet atmospheres, its design allows it to simultaneously obtain spectroscopy of its targets from .4 - 16 microns. It also would benefit from a target list of transiting planets around bright M dwarfs for which it predicts it can determine atmospheric characteristics for orbiting super-Earths in the HZ (Tessenyi et al., 2012). Barstow et al. (2013) has predicted that EChO, as currently designed, should be able to detect H_2O, CO_2 and CH_4 from a single transit measurement for a hot Jupiter orbiting a Sun-like star as well as a hot

Neptune orbiting an M dwarf. More about the design and the direct contributions of this work towards EChO can be found in Chapter 2.

Ground Based

In addition to the RV surveys mentioned above, which skirt between the detection and characterisation categories, a new generation of large, ground based telescopes will be built in the next 10 years that will provide instruments 100 times more sensitive than current telescopes (Gladysz et al., 2011). Three of them are the European Extremely Large Telescope (EELT) currently designed to be 39.3 meters in diameter (Liske et al., 2012) to be built in Cerro Armazones, Chile, the Thirty Meter Telescope (TMT) which is to be built on Mauna Kea (Sanders, 2013), Hawaii, and the 24.4 m Giant Magellan Telescope that will be built in Las Campanas, Chile (Prieto et al., 2010). All three of these projects have very ambitious adaptive optics programs (Diolaiti et al. (2010), Conan et al. (2012), Herriot et al. (2012)) to account for fluctuations in the atmosphere and are hoping to achieve the diffraction limit of the telescope. They will therefore have unprecedented angular resolution which could lead to many more exoplanets being detected and characterized by direct imaging. With the increased aperture, sensitivities towards Doppler imaging is increased as well as RV studies being sensitive to dimmer objects. Transmission spectroscopy will be possible for some of the dimmer transiting planets as well.

1.6 The Contributions Of This Thesis

This work focuses on three different topics: one industrial and two scientific. The industrial contribution involves working on the preliminary designs of the EChO spacecraft on site at EADS–Astrium and is outlined in Chapter 2. The scientific contributions consist of providing more targets for future space and ground-based characterisation efforts and exploring the limit of current ground-based methods to directly study the atmospheres of exoplanets using high resolution spectroscopy. In Chapters 3 and 4, this is done by expanding the known bright, M dwarf population and by providing realistic

statistics on the number of transiting planets we can expect to find within 50 parsecs from the Sun. These M dwarfs provide ongoing and future transit surveys with targets that can be prioritized and searched for a new transiting planet population. These new planets will then be further targeted by a future spaced-based characterisation mission.

To explore ground-based characterisation methods, in Chapter 5, high resolution spectroscopy of the non-transiting hot Jupiter HD 179949 b is used to search for molecules in its atmosphere and set constraints on the contrast ratio between the star and planet.

References

Anderson, D. R., Hellier, C., Gillon, M., Triaud, A. H. M. J., Smalley, B., Hebb, L., Collier Cameron, A., Maxted, P. F. L., Queloz, D., West, R. G., Bentley, S. J., Enoch, B., Horne, K., Lister, T. A., Mayor, M., Parley, N. R., Pepe, F., Pollacco, D., Ségransan, D., Udry, S., & Wilson, D. M. 2010, ApJ, 709, 159 [ADS]

Anglada-Escudé, G. & Tuomi, M. 2012, A&A, 548, A58 [ADS]

Anglada-Escudé, G., Tuomi, M., Gerlach, E., Barnes, R., Heller, R., Jenkins, J. S., Wende, S., Vogt, S. S., Butler, R. P., Reiners, A., & Jones, H. R. A. 2013, A&A, 556, A126 [ADS]

Baglin, A., Auvergne, M., Barge, P., Michel, E., Catala, C., Deleuil, M., & Weiss, W. 2007, in American Institute of Physics Conference Series, Vol. 895, Fifty Years of Romanian Astrophysics, 201–209 [ADS]

Bakos, G. Á., Lázár, J., Papp, I., Sári, P., & Green, E. M. 2002, PASP, 114, 974 [ADS]

Barman, T. 2007, ApJ, 661, L191 [ADS]

Barman, T. S., Macintosh, B., Konopacky, Q. M., & Marois, C. 2011, ApJ, 733, 65 [ADS]

Barnes, R. & Heller, R. 2013, Astrobiology, 13, 279 [ADS]

Barnes, R., Heller, R., Jackson, B., Leconte, J., Greenberg, R., Mullins, K., & Raymond, S. N. 2011a, in Bulletin of the American Astronomical Society, Vol. 43, American Astronomical Society Meeting Abstracts 217, 221.05 [ADS]

Barnes, R., Meadows, V. S., Domagal-Goldman, S. D., Heller, R., Jackson, B., López-Morales, M., Tanner, A., Gómez-Pérez, N., & Ruedas, T. 2011b, in Astronomical Society of the Pacific Conference Series, Vol. 448, 16th Cambridge Workshop on Cool Stars, Stellar Systems, and the Sun, 391 [ADS]

Barstow, J. K., Aigrain, S., Irwin, P. G. J., Bowles, N., Fletcher, L. N., & Lee, J.-M. 2013, MNRAS, 430, 1188 [ADS]

Ben-Jaffel, L. 2007, ApJ, 671, L61 [ADS]

Ben-Jaffel, L. & Ballester, G. E. 2013, A&A, 553, A52 [ADS]

Ben-Jaffel, L. & Sona Hosseini, S. 2010, ApJ, 709, 1284 [ADS]

Berta, Z. K., Irwin, J., Charbonneau, D., Burke, C. J., & Falco, E. E. 2012, AJ, 144, 145 [ADS]

Bonanno, A., Schlattl, H., & Paternò, L. 2002, A&A, 390, 1115 [ADS]

Bond, I. A., Udalski, A., Jaroszyński, M., Rattenbury, N. J., Paczyński, B., Soszyński, I., Wyrzykowski, L., Szymański, M. K., Kubiak, M., Szewczyk, O., Żebruń, K., Pietrzyński, G., Abe, F., Bennett, D. P., Eguchi, S., Furuta, Y., Hearnshaw, J. B., Kamiya, K., Kilmartin, P. M., Kurata, Y., Masuda, K., Matsubara, Y., Muraki, Y., Noda, S., Okajima, K., Sako, T., Sekiguchi, T., Sullivan, D. J., Sumi, T., Tristram, P. J., Yanagisawa, T., Yock, P. C. M., & OGLE Collaboration. 2004, ApJ, 606, L155 [ADS]

Bonfils, X., Delfosse, X., Udry, S., Forveille, T., Mayor, M., Perrier, C., Bouchy, F., Gillon, M., Lovis, C., Pepe, F., Queloz, D., Santos, N. C., Ségransan, D., & Bertaux, J.-L. 2013, A&A, 549, A109 [ADS]

Bouchy, F., Udry, S., Mayor, M., Moutou, C., Pont, F., Iribarne, N., da Silva, R., Ilovaisky, S., Queloz, D., Santos, N. C., Ségransan, D., & Zucker, S. 2005, A&A, 444, L15 [ADS]

Bowler, B. P., Liu, M. C., Dupuy, T. J., & Cushing, M. C. 2010, ApJ, 723, 850 [ADS]

Broeg, C., Fortier, A., Ehrenreich, D., Alibert, Y., Baumjohann, W., Benz, W., Deleuil, M., Gillon, M., Ivanov, A., Liseau, R., Meyer, M., Oloffson, G., Pagano, I., Piotto, G., Pollacco, D., Queloz, D., Ragazzoni, R., Renotte, E., Steller, M., & Thomas, N. 2013, in European Physical Journal Web of Conferences, Vol. 47, European Physical Journal Web of Conferences, 3005 [ADS]

Bryden, G., Chen, X., Lin, D. N. C., Nelson, R. P., & Papaloizou, J. C. B. 1999, ApJ, 514, 344 [ADS]

Burke, C. J., McCullough, P. R., Valenti, J. A., Johns-Krull, C. M., Janes, K. A., Heasley, J. N., Summers, F. J., Stys, J. E., Bissinger, R., Fleenor, M. L., Foote, C. N., García-Melendo, E., Gary, B. L., Howell, P. J., Mallia, F., Masi, G., Taylor, B., & Vanmunster, T. 2007, ApJ, 671, 2115 [ADS]

Butler, R. P. & Marcy, G. W. 1996, ApJ, 464, L153 [ADS]

Butler, R. P., Marcy, G. W., Fischer, D. A., Brown, T. M., Contos, A. R., Korzennik, S. G., Nisenson, P., & Noyes, R. W. 1999, ApJ, 526, 916 [ADS]

Butler, R. P., Marcy, G. W., Williams, E., Hauser, H., & Shirts, P. 1997, ApJ, 474, L115 [ADS]

Catala, C., Appourchaux, T., & Plato Mission Consortium. 2011, Journal of Physics Conference Series, 271, 012084 [ADS]

Cepa, J., Aguiar, M., Escalera, V. G., Gonzalez-Serrano, I., Joven-Alvarez, E., Peraza, L., Rasilla, J. L., Rodriguez-Ramos, L. F., Gonzalez, J. J., Cobos Duenas, F. J., Sanchez, B., Tejada, C., Bland-Hawthorn, J., Militello, C., & Rosa, F. 2000, in Society of Photo-Optical Instrumentation Engineers (SPIE) Conference Series, Vol. 4008, Society of Photo-Optical Instrumentation Engineers (SPIE) Conference Series, 623–631 [ADS]

Chabrier, G. & Baraffe, I. 2000, ARA&A, 38, 337 [ADS]

Charbonneau, D., Berta, Z. K., Irwin, J., Burke, C. J., Nutzman, P., Buchhave, L. A., Lovis, C., Bonfils, X., Latham, D. W., Udry, S., Murray-Clay, R. A., Holman, M. J., Falco, E. E., Winn, J. N., Queloz, D., Pepe, F., Mayor, M., Delfosse, X., & Forveille, T. 2009, Nature, 462, 891 [ADS]

Charbonneau, D., Brown, T. M., Latham, D. W., & Mayor, M. 2000, ApJ, 529, L45 [ADS]

Charbonneau, D., Brown, T. M., Noyes, R. W., & Gilliland, R. L. 2002, ApJ, 568, 377 [ADS]

Charbonneau, D., Irwin, J., Nutzman, P., & Falco, E. E. 2008, in Bulletin of the American Astronomical Society, Vol. 40, American Astronomical Society Meeting Abstracts 212, 242 [ADS]

Charbonneau, D., Noyes, R. W., Korzennik, S. G., Nisenson, P., Jha, S., Vogt, S. S., & Kibrick, R. I. 1999, ApJ, 522, L145 [ADS]

Chauvin, G., Lagrange, A.-M., Dumas, C., Zuckerman, B., Mouillet, D., Song, I., Beuzit, J.-L., & Lowrance, P. 2004, A&A, 425, L29 [ADS]

—. 2005, A&A, 438, L25 [ADS]

Collier Cameron, A., Horne, K., Penny, A., & James, D. 1999, Nature, 402, 751 [ADS]

Collier Cameron, A., Horne, K., Penny, A., & Leigh, C. 2002, MNRAS, 330, 187 [ADS]

Conan, R., Bennet, F., Bouchez, A. H., van Dam, M. A., Espeland, B., Gardhouse, W., d'Orgeville, C., Parcell, S., Piatrou, P., Price, I., Rigaut, F., Trancho, G., & Uhlendorf, K. 2012, in Society of Photo-Optical Instrumentation Engineers (SPIE) Conference Series, Vol. 8447, Society of Photo-Optical Instrumentation Engineers (SPIE) Conference Series [ADS]

Cosentino, R., Lovis, C., Pepe, F., Collier Cameron, A., Latham, D. W., Molinari, E., Udry, S., Bezawada, N., Black, M., Born, A., Buchschacher, N., Charbonneau, D., Figueira, P., Fleury, M., Galli, A., Gallie, A., Gao, X., Ghedina, A., Gonzalez, C., Gonzalez, M., Guerra, J., Henry, D., Horne, K., Hughes, I., Kelly, D., Lodi, M., Lunney, D., Maire, C., Mayor, M., Micela, G., Ordway, M. P., Peacock, J., Phillips, D., Piotto, G., Pollacco, D., Queloz, D., Rice, K., Riverol, C., Riverol, L., San Juan, J., Sasselov, D., Segransan, D., Sozzetti, A., Sosnowska, D., Stobie, B., Szentgyorgyi, A., Vick, A., & Weber, L. 2012, in Society of Photo-Optical Instrumentation Engineers (SPIE) Conference Series, Vol. 8446, Society of Photo-Optical Instrumentation Engineers (SPIE) Conference Series [ADS]

Coustenis, A., Schneider, J., Bockelée-Morvan, D., Rauer, H., Wittemberg, R., Chassefière, E., Greene, T., Penny, A., & Guillot, T. 1997, in Astronomical Society of the Pacific Conference Series, Vol. 119, Planets Beyond the Solar System and the Next Generation of Space Missions, 101 [ADS]

Debosscher, J., Aerts, C., Tkachenko, A., Pavlovski, K., Maceroni, C., Kurtz, D., Beck, P. G., Bloemen, S., Degroote, P., Lombaert, R., & Southworth, J. 2013, A&A, 556, A56 [ADS]

Diolaiti, E., Conan, J.-M., Foppiani, I., Marchetti, E., Baruffolo, A., Bellazzini, M., Bregoli, G., Butler, C. R., Ciliegi, P., Cosentino, G., Delabre, B., Lombini, M., Petit, C., Robert, C., Rossettini, P., Schreiber, L., Tomelleri, R., Biliotti, V., D'Odorico, S., Fusco, T., Hubin, N., & Meimon, S. 2010, in Society of Photo-Optical Instrumentation Engineers (SPIE) Conference Series, Vol. 7736, Society of Photo-Optical Instrumentation Engineers (SPIE) Conference Series [ADS]

Doyle, L. R., Carter, J. A., Fabrycky, D. C., Slawson, R. W., Howell, S. B., Winn, J. N., Orosz, J. A., Prsa, A., Welsh, W. F., Quinn, S. N., Latham, D., Torres, G., Buchhave, L. A., Marcy, G. W., Fortney, J. J., Shporer, A., Ford, E. B., Lissauer, J. J., Ragozzine, D., Rucker, M., Batalha, N., Jenkins, J. M., Borucki, W. J., Koch, D., Middour, C. K., Hall, J. R., McCauliff, S., Fanelli, M. N., Quintana, E. V., Holman, M. J., Caldwell, D. A., Still, M., Stefanik, R. P., Brown, W. R., Esquerdo, G. A., Tang, S., Furesz, G., Geary, J. C., Berlind, P., Calkins, M. L., Short, D. R., Steffen, J. H., Sasselov, D., Dunham, E. W., Cochran, W. D., Boss, A., Haas, M. R., Buzasi, D., & Fischer, D. 2011, Science, 333, 1602 [ADS]

Eggleton, P. P. 1983, ApJ, 268, 368 [ADS]

Flores, H., Puech, M., Hammer, F., Garrido, O., & Hernandez, O. 2004, A&A, 420, L31 [ADS]

Fortney, J. J., Marley, M. S., & Barnes, J. W. 2007, ApJ, 659, 1661 [ADS]

Freudling, W., Storrs, A., Pirzkal, N., & Pasquali, A. 1997, in Bulletin of the American Astronomical Society, Vol. 29, American Astronomical Society Meeting Abstracts, 1225 [ADS]

Gaidos, E., Deschenes, B., Dundon, L., Fagan, K., Menviel-Hessler, L., Moskovitz, N., & Workman, M. 2005, Astrobiology, 5, 100 [ADS]

Galicher, R., Marois, C., Zuckerman, B., & Macintosh, B. 2013, ApJ, 769, 42 [ADS]

Gardner, J. P. & JWST Science Working Group. 2005, in Bulletin of the American Astronomical Society, Vol. 37, American Astronomical Society Meeting Abstracts, 115.01 [ADS]

Ge, J., Powell, S., Zhao, B., Wang, J., Fletcher, A., Chang, L., Groot, J., Wan, X., Jakeman, H., Myers, D., Grafer, E., Liu, J., Varosi, F., Schofield, S., Moore, A., van Olphen, M., Katz, J., Muterspaugh, M. W., Barnes, R., & Blake, C. 2013, in American Astronomical Society Meeting Abstracts, Vol. 221, American Astronomical Society Meeting Abstracts, 109.05 [ADS]

Gilliland, R. L., Marcy, G. W., Rowe, J. F., Rogers, L., Torres, G., Fressin, F., Lopez, E. D., Buchhave, L. A., Christensen-Dalsgaard, J., Désert, J.-M., Henze, C. E., Isaacson, H., Jenkins, J. M., Lissauer, J. J., Chaplin, W. J., Basu, S., Metcalfe, T. S., Elsworth, Y., Handberg, R., Hekker, S., Huber, D., Karoff, C., Kjeldsen, H., Lund, M. N., Lundkvist, M., Miglio, A., Charbonneau, D., Ford, E. B., Fortney, J. J., Haas, M. R., Howard, A. W., Howell, S. B., Ragozzine, D., & Thompson, S. E. 2013, ApJ, 766, 40 [ADS]

Gladysz, S., Castella, B. F., Rebolo, R., Kissler-Patig, M., & Jolissaint, L. 2011, in European Physical Journal Web of Conferences, Vol. 16, European Physical Journal Web of Conferences, 7003 [ADS]

Grillmair, C. J., Burrows, A., Charbonneau, D., Armus, L., Stauffer, J., Meadows, V., van Cleve, J., von Braun, K., & Levine, D. 2008, Nature, 456, 767 [ADS]

Henry, G. W., Marcy, G. W., Butler, R. P., & Vogt, S. S. 2000, ApJ, 529, L41 [ADS]

Herriot, G., Andersen, D., Atwood, J., Byrnes, P., Boucher, M.-A., Boyer, C., Caputa, K., Correia, C., Dunn, J., Ellerbroek, B., Fitzsimmons, J., Gilles, L., Hickson, P., Hill, A., Kerley, D., Pazder, J., Reshetov, V., Roberts, S., Smith, M., Véran, J.-P., Wang, L., & Wevers, I. 2012, in Society of Photo-Optical Instrumentation Engineers (SPIE) Conference Series, Vol. 8447, Society of Photo-Optical Instrumentation Engineers (SPIE) Conference Series [ADS]

Hilditch, R. W. 2001, An Introduction to Close Binary Stars [ADS]

Houck, J. R., Roellig, T. L., van Cleve, J., Forrest, W. J., Herter, T., Lawrence, C. R., Matthews, K., Reitsema, H. J., Soifer, B. T., Watson, D. M., Weedman, D., Huisjen, M., Troeltzsch, J., Barry, D. J., Bernard-Salas, J., Blacken, C. E., Brandl, B. R., Charmandaris, V., Devost, D., Gull, G. E., Hall, P., Henderson, C. P., Higdon, S. J. U., Pirger, B. E., Schoenwald, J., Sloan, G. C., Uchida, K. I., Appleton, P. N., Armus, L., Burgdorf, M. J., Fajardo-Acosta, S. B., Grillmair, C. J., Ingalls, J. G., Morris, P. W., & Teplitz, H. I. 2004, ApJS, 154, 18 [ADS]

Huitson, C. M., Sing, D. K., Pont, F., Fortney, J. J., Burrows, A. S., Wilson, P. A., Ballester, G. E., Nikolov, N., Gibson, N. P., Deming, D., Aigrain, S., Evans, T. M., Henry, G. W., Lecavelier des Etangs, A., Showman, A. P., Vidal-Madjar, A., & Zahnle, K. 2013, MNRAS, 434, 3252 [ADS]

Janson, M., Bergfors, C., Goto, M., Brandner, W., & Lafrenière, D. 2010, ApJ, 710, L35 [ADS]

Janson, M., Carson, J. C., Lafreniere, D., Spiegel, D. S., Bent, J. R., & Wong, P. 2012, ApJ, 747, 116 [ADS]

Kalas, P., Graham, J. R., Chiang, E., Fitzgerald, M. P., Clampin, M., Kite, E. S., Stapelfeldt, K., Marois, C., & Krist, J. 2008, Science, 322, 1345 [ADS]

Kalas, P., Graham, J. R., Fitzgerald, M. P., & Clampin, M. 2014, in IAU Symposium, Vol. 299, IAU Symposium, 204–207 [ADS]

Kasting, J. F., Whitmire, D. P., & Reynolds, R. T. 1993, Icarus, 101, 108 [ADS]

Kipping, D. M. 2013, MNRAS[ADS]

Koch, D., Borucki, W., Basri, G., Brown, T., Caldwell, D., Christensen-Dalsgaard, J., Cochran, W., Devore, E., Dunham, E., Gautier, T. N., Geary, J., Gilliland, R., Gould, A., Jenkins, J., Kondo, Y., Latham, D., Lissauer, J., & Monet, D. 2007, in IAU Symposium, Vol. 240, IAU Symposium, 236–243 [ADS]

Konopacky, Q. M., Barman, T. S., Macintosh, B., & Marois, C. 2013, in American Astronomical Society Meeting Abstracts, Vol. 221, American Astronomical Society Meeting Abstracts, 126.03 [ADS]

Kostov, V. & Apai, D. 2013, ApJ, 762, 47 [ADS]

Lagrange, A.-M., Bonnefoy, M., Chauvin, G., Apai, D., Ehrenreich, D., Boccaletti, A., Gratadour, D., Rouan, D., Mouillet, D., Lacour, S., & Kasper, M. 2010, Science, 329, 57 [ADS]

Lagrange, A.-M., Gratadour, D., Chauvin, G., Fusco, T., Ehrenreich, D., Mouillet, D., Rousset, G., Rouan, D., Allard, F., Gendron, É., Charton, J., Mugnier, L., Rabou, P., Montri, J., & Lacombe, F. 2009, A&A, 493, L21 [ADS]

Lecavelier des Etangs, A., Bourrier, V., Wheatley, P. J., Dupuy, H., Ehrenreich, D., Vidal-Madjar, A., Hébrard, G., Ballester, G. E., Désert, J.-M., Ferlet, R., & Sing, D. K. 2012, A&A, 543, L4 [ADS]

Lecavelier Des Etangs, A., Ehrenreich, D., Vidal-Madjar, A., Ballester, G. E., Désert, J.-M., Ferlet, R., Hébrard, G., Sing, D. K., Tchakoumegni, K.-O., & Udry, S. 2010, A&A, 514, A72 [ADS]

Lecavelier Des Etangs, A. & Vidal-Madjar, A. 2009, A&A, 497, 557 [ADS]

Liske, J., Padovani, P., & Kissler-Patig, M. 2012, in Society of Photo-Optical Instrumentation Engineers (SPIE) Conference Series, Vol. 8444, Society of Photo-Optical Instrumentation Engineers (SPIE) Conference Series [ADS]

Mahadevan, S., Ramsey, L., Bender, C., Terrien, R., Wright, J. T., Halverson, S., Hearty, F., Nelson, M., Burton, A., Redman, S., Osterman, S., Diddams, S., Kasting, J., Endl, M., & Deshpande, R. 2012, in Society of Photo-Optical Instrumentation Engineers (SPIE) Conference Series, Vol. 8446, Society of Photo-Optical Instrumentation Engineers (SPIE) Conference Series [ADS]

Marcy, G. W. & Butler, R. P. 1995, in Bulletin of the American Astronomical Society, Vol. 27, American Astronomical Society Meeting Abstracts, 1379 [ADS]

Marcy, G. W. & Butler, R. P. 1996, ApJ, 464, L147 [ADS]

Marois, C., Macintosh, B., Barman, T., Zuckerman, B., Song, I., Patience, J., Lafreniere, D., & Doyon, R. 2009, in American Astronomical Society Meeting Abstracts, Vol. 214, American Astronomical Society Meeting Abstracts 214, 230.03 [ADS]

Marois, C., Zuckerman, B., Konopacky, Q. M., Macintosh, B., & Barman, T. 2010, Nature, 468, 1080 [ADS]

Mawet, D., Absil, O., Girard, J. H., Milli, J., O'Neal, J., Delacroix, C., Baudoz, P., Boccaletti, A., Bourget, P., Christiaens, V., Forsberg, P., Gonté, F., Habraken, S., Hanot, C., Karlsson, M., Kasper, M., Lagrange, A., Lizon, J., Muzic, K., Peña, E., Olivier, R., Slusarenko, N., Tacconi-Garman, L. E., & Surdej, J. 2013, The Messenger, 152, 8 [ADS]

Mayor, M. & Queloz, D. 1995, Nature, 378, 355 [ADS]

Mazeh, T., Naef, D., Torres, G., Latham, D. W., Mayor, M., Beuzit, J.-L., Brown, T. M., Buchhave, L., Burnet, M., Carney, B. W., Charbonneau, D., Drukier, G. A., Laird, J. B., Pepe, F., Perrier, C., Queloz, D., Santos, N. C., Sivan, J.-P., Udry, S., & Zucker, S. 2000, ApJ, 532, L55 [ADS]

Mégevand, D., Zerbi, F. M., Cabral, A., Di Marcantonio, P., Amate, M., Pepe, F., Cristiani, S., Rebolo, R., Santos, N. C., Dekker, H., Abreu, M., Affolter, M., Avila, G., Baldini, V., Bristow, P., Broeg, C., Carvas, P., Cirami, R., Coelho, J., Comari, M., Conconi, P., Coretti, I., Cupani, G., D'Odorico, V., De Caprio, V., Delabre, B., Figueira, P., Fleury, M., Fragoso, A., Genolet, L., Gomes, R., Gonzalez Hernandez, J., Hughes, I., Iwert, O., Kerber, F., Landoni, M., Lima, J., Lizon, J.-L., Lovis, C., Maire, C., Mannetta, M., Martins, C., Moitinho, A., Molaro, P., Monteiro, M., Rasilla, J. L., Riva, M., Santana Tschudi, S., Santin, P., Sosnowska, D., Sousa, S., Spanò, P., Tenegi, F., Toso, G., Vanzella, E., Viel, M., & Zapatero Osorio, M. R. 2012, in Society of Photo-Optical Instrumentation Engineers (SPIE) Conference Series, Vol. 8446, Society of Photo-Optical Instrumentation Engineers (SPIE) Conference Series [ADS]

Mohanty, S., Jayawardhana, R., Huélamo, N., & Mamajek, E. 2007, ApJ, 657, 1064 [ADS]

Muirhead, P. S., Johnson, J. A., Apps, K., Carter, J. A., Morton, T. D., Fabrycky, D. C., Pineda, J. S., Bottom, M., Rojas-Ayala, B., Schlawin, E., Hamren, K., Covey, K. R., Crepp, J. R., Stassun, K. G., Pepper, J., Hebb, L., Kirby, E. N., Howard, A. W., Isaacson, H. T., Marcy, G. W., Levitan, D., Diaz-Santos, T., Armus, L., & Lloyd, J. P. 2012, ApJ, 747, 144 [ADS]

Naef, D., Latham, D. W., Mayor, M., Mazeh, T., Beuzit, J. L., Drukier, G. A., Perrier-Bellet, C., Queloz, D., Sivan, J. P., Torres, G., Udry, S., & Zucker, S. 2001, A&A, 375, L27 [ADS]

Nelson, R. P., Papaloizou, J. C. B., Masset, F., & Kley, W. 2000, MNRAS, 318, 18 [ADS]

Oppenheimer, B. R., Baranec, C., Beichman, C., Brenner, D., Burruss, R., Cady, E., Crepp, J. R., Dekany, R., Fergus, R., Hale, D., Hillenbrand, L., Hinkley, S., Hogg, D. W., King, D., Ligon, E. R., Lockhart, T., Nilsson, R., Parry, I. R., Pueyo, L., Rice, E., Roberts, J. E., Roberts, Jr., L. C., Shao, M., Sivaramakrishnan, A., Soummer, R., Truong, T., Vasisht, G., Veicht, A., Vescelus, F., Wallace, J. K., Zhai, C., & Zimmerman, N. 2013, ApJ, 768, 24 [ADS]

Pepe, F., Mayor, M., Delabre, B., Kohler, D., Lacroix, D., Queloz, D., Udry, S., Benz, W., Bertaux, J.-L., & Sivan, J.-P. 2000, in Society of Photo-Optical Instrumentation Engineers (SPIE) Conference Series, Vol. 4008, Society of Photo-Optical Instrumentation Engineers (SPIE) Conference Series, 582–592 [ADS]

Pont, F., Knutson, H., Gilliland, R. L., Moutou, C., & Charbonneau, D. 2008, MNRAS, 385, 109 [ADS]

Prieto, G., Thomas-Osip, J. E., Phillips, M. M., McCarthy, P., & Johns, M. 2010, in Society of Photo-Optical Instrumentation Engineers (SPIE) Conference Series, Vol. 7733, Society of Photo-Optical Instrumentation Engineers (SPIE) Conference Series [ADS]

Queloz, D., Henry, G. W., Sivan, J. P., Baliunas, S. L., Beuzit, J. L., Donahue, R. A., Mayor, M., Naef, D., Perrier, C., & Udry, S. 2001, A&A, 379, 279 [ADS]

Quirrenbach, A., Amado, P. J., Seifert, W., Sánchez Carrasco, M. A., Mandel, H., Caballero, J. A., Mundt, R., Ribas, I., Reiners, A., Abril, M., Aceituno, J., Alonso-Floriano, J., Ammler-von Eiff, M., Anglada-Escude, G., Antona Jiménez, R., Anwand-Heerwart, H., Barrado y Navascués, D., Becerril, S., Bejar, V., Benitez, D., Cardenas, C., Claret, A., Colome, J., Cortés-Contreras, M., Czesla, S., del Burgo, C., Doellinger, M., Dorda, R., Dreizler, S., Feiz, C., Fernandez, M., Galadi, D., Garrido, R., González Hernández, J., Guardia, J., Guenther, E., de Guindos, E., Gutiérrez-Soto, J., Hagen, H. J., Hatzes, A., Hauschildt, P., Helmling, J., Henning, T., Herrero, E., Huber, A., Huber, K., Jeffers, S., Joergens, V., de Juan, E., Kehr, M., Klutsch, A., Kürster, M., Lalitha, S., Laun, W., Lemke, U., Lenzen, R., Lizon, J.-L., López del Fresno, M., López-Morales, M., López-Santiago, J., Mall, U., Martin, E., Martín-Ruiz, S., Mirabet, E., Montes, D., Morales, J. C., Morales Muñoz, R., Moya, A., Naranjo, V., Oreiro, R., Pérez Medialdea, D., Pluto, M., Rabaza, O., Ramon, A., Rebolo, R., Reffert, S., Rhode, P., Rix, H.-W., Rodler, F., Rodríguez, E., Rodríguez López, C., Rodríguez Pérez, E., Rodriguez Trinidad, A., Rohloff, R.-R., Sánchez-Blanco, E., Sanz-Forcada, J., Schäfer, S., Schiller, J., Schmidt, C., Schmitt, J., Solano, E., Stahl, O., Storz, C., Stürmer, J., Suarez, J. C., Thiele, U., Ulbrich, R., Vidal-Dasilva, M., Wagner, K., Winkler, J., Xu, W., Zapatero Osorio, M. R., & Zechmeister, M. 2012, in Society of Photo-Optical Instrumentation Engineers (SPIE) Conference Series, Vol. 8446, Society of Photo-Optical Instrumentation Engineers (SPIE) Conference Series [ADS]

Ramsey, L., Wolszczan, A., Bongiorno, S., Redman, S., Engel, L., Barnes, J., & Jones, H. R. A. 2008, in Astronomical Society of the Pacific Conference Series, Vol. 398, Extreme Solar Systems, 505 [ADS]

Ricker, G. R., Latham, D. W., Vanderspek, R. K., Ennico, K. A., Bakos, G., Brown, T. M., Burgasser, A. J., Charbonneau, D., Clampin, M., Deming, L. D., Doty, J. P., Dunham, E. W., Elliot, J. L., Holman, M. J., Ida, S., Jenkins, J. M., Jernigan, J. G., Kawai, N., Laughlin, G. P., Lissauer, J. J., Martel, F., Sasselov, D. D., Schingler, R. H., Seager, S., Torres, G., Udry, S., Villasenor, J. N., Winn, J. N., & Worden, S. P. 2010, in Bulletin of the American Astronomical Society, Vol. 42, American Astronomical Society Meeting Abstracts 215, 450.06 [ADS]

Rodler, F., Kürster, M., & Barnes, J. R. 2013, MNRAS, 432, 1980 [ADS]

Sanders, G. H. 2013, Journal of Astrophysics and Astronomy [ADS]

Seager, S. & Sasselov, D. D. 2000, ApJ, 537, 916 [ADS]

Sing, D. K., Huitson, C. M., Lopez-Morales, M., Pont, F., Désert, J.-M., Ehrenreich, D., Wilson, P. A., Ballester, G. E., Fortney, J. J., Lecavelier des Etangs, A., & Vidal-Madjar, A. 2012, MNRAS, 426, 1663 [ADS]

Sing, D. K., Pont, F., Aigrain, S., Charbonneau, D., Désert, J.-M., Gibson, N., Gilliland, R., Hayek, W., Henry, G., Knutson, H., Lecavelier Des Etangs, A., Mazeh, T., & Shporer, A. 2011, MNRAS, 416, 1443 [ADS]

Snellen, I. A. G., de Kok, R. J., de Mooij, E. J. W., & Albrecht, S. 2010, Nature, 465, 1049 [ADS]

Sozzetti, A., Bernagozzi, A., Bertolini, E., Calcidese, P., Carbognani, A., Cenadelli, D., Christille, J.-M., Damasso, M., Giacobbe, P., Lanteri, L., Lattanzi, M. G., & Smart, R. 2013, in European Physical Journal Web of Conferences, Vol. 47, European Physical Journal Web of Conferences, 3006 [ADS]

Street, R. A., Pollaco, D. L., Fitzsimmons, A., Keenan, F. P., Horne, K., Kane, S., Collier Cameron, A., Lister, T. A., Haswell, C., Norton, A. J., Jones, B. W., Skillen, I., Hodgkin, S., Wheatley, P., West, R., & Brett, D. 2003, in Astronomical Society of the Pacific Conference Series, Vol. 294, Scientific Frontiers in Research on Extrasolar Planets, 405–408 [ADS]

Sumi, T., Kamiya, K., Bennett, D. P., Bond, I. A., Abe, F., Botzler, C. S., Fukui, A., Furusawa, K., Hearnshaw, J. B., Itow, Y., Kilmartin, P. M., Korpela, A., Lin, W., Ling, C. H., Masuda, K., Matsubara, Y., Miyake, N., Motomura, M., Muraki, Y., Nagaya, M., Nakamura, S., Ohnishi, K., Okumura, T., Perrott, Y. C., Rattenbury, N., Saito, T., Sako, T., Sullivan, D. J., Sweatman, W. L., Tristram, P. J., Udalski, A., Szymański, M. K., Kubiak, M., Pietrzyński, G., Poleski, R., Soszyński, I., Wyrzykowski, Ł., Ulaczyk, K., & Microlensing Observations in Astrophysics (MOA) Collaboration. 2011, Nature, 473, 349 [ADS]

Swain, M. R., Tinetti, G., Vasisht, G., Deroo, P., Griffith, C., Bouwman, J., Chen, P., Yung, Y., Burrows, A., Brown, L. R., Matthews, J., Rowe, J. F., Kuschnig, R., & Angerhausen, D. 2009, ApJ, 704, 1616 [ADS]

Swain, M. R., Vasisht, G., & Tinetti, G. 2008, Nature, 452, 329 [ADS]

Swift, J. J., Johnson, J. A., Morton, T. D., Crepp, J. R., Montet, B. T., Fabrycky, D. C., & Muirhead, P. S. 2013, ApJ, 764, 105 [ADS]

Szabados, L., Anderson, R. I., Derekas, A., Kiss, L. L., Szalai, T., Székely, P., & Christiansen, J. L. 2013, MNRAS, 434, 870 [ADS]

Tessenyi, M., Ollivier, M., Tinetti, G., Beaulieu, J. P., Coudé du Foresto, V., Encrenaz, T., Micela, G., Swinyard, B., Ribas, I., Aylward, A., Tennyson, J., Swain, M. R., Sozzetti, A., Vasisht, G., & Deroo, P. 2012, ApJ, 746, 45 [ADS]

Tinetti, G., Beaulieu, J. P., Henning, T., Meyer, M., Micela, G., Ribas, I., Stam, D., Swain, M., Krause, O., Ollivier, M., Pace, E., Swinyard, B., Aylward, A., van Boekel, R., Coradini, A., Encrenaz, T., Snellen, I., Zapatero-Osorio, M. R., Bouwman, J., Cho, J. Y.-K., Coudé de Foresto, V., Guillot, T., Lopez-Morales, M., Mueller-Wodarg, I., Palle, E., Selsis, F., Sozzetti, A., Ade, P. A. R., Achilleos, N., Adriani, A., Agnor, C. B., Afonso, C., Allende Prieto, C., Bakos, G., Barber, R. J., Barlow, M., Batista, V., Bernath, P., Bézard, B., Bordé, P., Brown, L. R., Cassan, A., Cavarroc, C., Ciaravella, A., Cockell, C., Coustenis, A., Danielski, C., Decin, L., De Kok, R., Demangeon, O., Deroo, P., Doel, P., Drossart, P., Fletcher, L. N., Focardi, M., Forget, F., Fossey, S., Fouqué, P., Frith, J., Galand, M., Gaulme, P., Hernández, J. I. G., Grasset, O., Grassi, D., Grenfell, J. L., Griffin, M. J., Griffith, C. A., Grözinger, U., Guedel, M., Guio, P., Hainaut, O., Hargreaves, R., Hauschildt, P. H., Heng, K., Heyrovsky, D., Hueso, R., Irwin, P., Kaltenegger, L., Kervella, P.,

Kipping, D., Koskinen, T. T., Kovács, G., La Barbera, A., Lammer, H., Lellouch, E., Leto, G., Lopez Morales, M., Lopez Valverde, M. A., Lopez-Puertas, M., Lovis, C., Maggio, A., Maillard, J. P., Maldonado Prado, J., Marquette, J. B., Martin-Torres, F. J., Maxted, P., Miller, S., Molinari, S., Montes, D., Moro-Martin, A., Moses, J. I., Mousis, O., Nguyen Tuong, N., Nelson, R., Orton, G. S., Pantin, E., Pascale, E., Pezzuto, S., Pinfield, D., Poretti, E., Prinja, R., Prisinzano, L., Rees, J. M., Reiners, A., Samuel, B., Sánchez-Lavega, A., Forcada, J. S., Sasselov, D., Savini, G., Sicardy, B., Smith, A., Stixrude, L., Strazzulla, G., Tennyson, J., Tessenyi, M., Vasisht, G., Vinatier, S., Viti, S., Waldmann, I., White, G. J., Widemann, T., Wordsworth, R., Yelle, R., Yung, Y., & Yurchenko, S. N. 2012, Experimental Astronomy, 34, 311 [ADS]

Tinetti, G., Vidal-Madjar, A., Liang, M.-C., Beaulieu, J.-P., Yung, Y., Carey, S., Barber, R. J., Tennyson, J., Ribas, I., Allard, N., Ballester, G. E., Sing, D. K., & Selsis, F. 2007, Nature, 448, 169 [ADS]

Tuomi, M. & Jones, H. R. A. 2012, A&A, 544, A116 [ADS]

Vidal-Madjar, A., Lecavelier des Etangs, A., Désert, J.-M., Ballester, G. E., Ferlet, R., Hébrard, G., & Mayor, M. 2003, Nature, 422, 143 [ADS]

Wahl, M., Metchev, S. A., Patel, R., Serabyn, G., & PALM-3000 Adaptive Optics Team. 2013, in American Astronomical Society Meeting Abstracts, Vol. 221, American Astronomical Society Meeting Abstracts, 144.22 [ADS]

Ward, W. R. 1997, ApJ, 482, L211 [ADS]

Werner, M. W., Roellig, T. L., Low, F. J., Rieke, G. H., Rieke, M., Hoffmann, W. F., Young, E., Houck, J. R., Brandl, B., Fazio, G. G., Hora, J. L., Gehrz, R. D., Helou, G., Soifer, B. T., Stauffer, J., Keene, J., Eisenhardt, P., Gallagher, D., Gautier, T. N., Irace, W., Lawrence, C. R., Simmons, L., Van Cleve, J. E., Jura, M., Wright, E. L., & Cruikshank, D. P. 2004, ApJS, 154, 1 [ADS]

Winn, J. N. 2010, ArXiv e-prints [ADS]

Wolszczan, A. & Frail, D. A. 1992, Nature, 355, 145 [ADS]

Wood, P. L., Maxted, P. F. L., Smalley, B., & Iro, N. 2011, MNRAS, 412, 2376 [ADS]

Wright, J. T., Kakhouri, O., Marcy, G. W., Han, E., Feng, Y., Johnson, J. A., Howard, A. W., Fischer, D. A., Valenti, J. A., Anderson, J., & Piskunov, N. 2013, VizieR Online Data Catalog, 612, 30412 [ADS]

Wuchterl, G. 1994, Earth Moon and Planets, 67, 51 [ADS]

Chapter 2: Preliminary Design Studies for the Exoplanet Characterisation Observatory

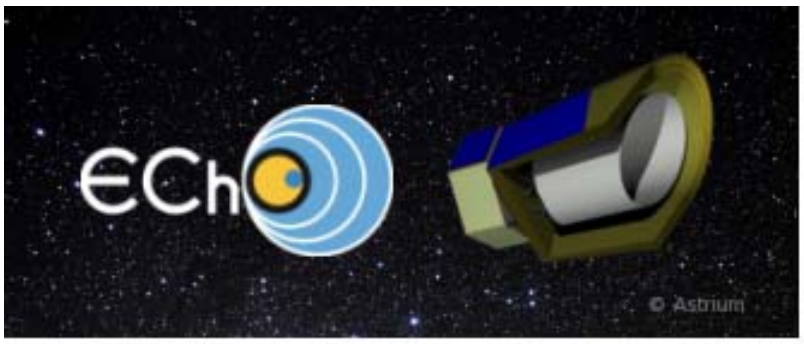

Fig. 2.1: Conceptual Image of The Exoplanet Characterisation Observatory. Image Provided by Astrium.

As a condition of receiving the funding for this project, part of this work was to be conducted with collaboration between an industrial partner and the scientific community to help facilitate communication and cooperation between the two. The following appendix will outline this work's contributions towards The Exoplanet Characterisation Observatory (EChO) as conducted via such a partnership with EADS Astrium.

2.1 ESA's Cosmic Vision

Development of spacecraft is a long and meticulous process that requires much planning and forethought in order to be successful. This is partly due to the difficulties of constructing an extremely complicated, unique, state-of-the-art machine but emphasized by its need to operate in extreme environments with no possibility of servicing. Also, given the amount of money that is involved in designing and building a scientific spacecraft and the multitude of possibilities for it to fail, space agencies must make long term plans that span decades. The strategy has been successfully implemented in the past with the Horizon 2000 program which started in 1984 with the designing of

Cassini and ending with the successful launch of Plank and Herschel in 2009.

ESA's current long term plan to develop new spacecraft for the scientific community is entitled Cosmic Vision and covers the 2015-2025 time frame. The core questions hoping to be addressed during this plan are:

1. What are the conditions for planet formation and the emergence of life?
2. How does the Solar System work?
3. What are the fundamental physical laws of the Universe?
4. How did the Universe originate and what is it made of?

ESA's implementation of this plan consists of asking the scientific community for proposals for space missions that conduct space-based experiments toward answering the questions above. These proposals can be in the form of missions classified as small (S), medium (M), or large (L) which are primarily classifiers of the technological development required to implement the mission. This often translates into a greater cost and complexity as you go from the S to the L class. Currently, 4 missions have been selected with one final one to be decided. One is CHEOPS, the S-class mission mentioned in Chapter 1, which will help to characterize known exoplanet radii. There are 2 M-class missions that have been selected which are the Euclid and Solar Orbiter missions, and one large mission entitled Jupiter Icy Moons Explorer (JUICE). None of these M or L-class missions have direct applications to exoplanet studies but it has been suggested that Euclid would be very useful for a microlensing survey for exoplanet detection (Beaulieu et al., 2010). Regardless of their applications towards exoplanet research, they will answer very important questions about the Solar System and the Universe. There is a third M-class mission left to be selected which will be launched in ∼2022 time frame. The final M3 candidates are now in the last stages of being selected. Two of the candidates have direct application to exoplanet science: PLAnetary Transits and Oscillations of stars (PLATO) and Exoplanet Characterisation Observatory (EChO) (both discussed briefly in Chapter 1). PLATO is a mission designed for detection while the EChO is focused on characterisation.

2.2 An Exoplanet Roadmap

In 2008, ESA appointed a group of scientists to produce a document that would advise them in the best way to address the pertinent questions of exoplanet science as they relate to the Cosmic Vision program (Fridlund, 2009). This group was designated the ExoPlanet Roadmap Advisory Team (EPRAT) and collaborated over the next two years to produce a document summarizing their input to ESA. The document was released in 2010 and 3 specific space missions were suggested as high priority:

1. A mission to characterise exoplanet atmospheres down to 5 M_{Earth}.
2. A mission to photometrically detect the all sky transiting terrestrial planet population.
3. An astrometric mission which would identify low mass non-transiting planets.

While they designated all of these missions as "high priority", they specifically did not state which of these missions was of greater priority than the other and left ESA to make the decision between the various proposals it received. It is no surprise, therefore, that 2 of the 3 high priority missions are currently M3 selection candidates.

2.3 The Exoplanet Characterisation Observatory

EChO is a concept currently being proposed for ESAs Cosmic Visions to be considered for launch around 2022. The main objective of EChO is to use spectroscopic data to determine the chemical composition and physical properties, such as temperature, of transiting exoplanet atmospheres, with a view towards observing Super-Earths down to the habitable zone of late type stars.

EChO will utilize several techniques to attempt to gain information about exoplanet atmospheres as outlined in Section 1.3.2. In particular, EChO will take advantage of the transmission and eclipse spectroscopy of transiting planets as well as potentially exploiting flux phase variations of non-transiting planets. The uniqueness of EChO lies in its ability to constantly monitor such planets (given its location in space) and

also to observe across all available passbands simultaneously allowing information to be gathered across the spectrum for every transit.

During the last few months of 2010, studies were conducted, while consulting with Astrium engineers, to assess the feasibility and technological trade offs of EChOs key systems as an input into the ESA proposal which was submitted early December 2010. The following is a summary of that process.

2.4 Considerations During Spacecraft Design

The design of a successful space mission is an optimization problem spanning a huge parameter space with little margin for error. Given most of this work involves attempting to solve this optimization problem for a select set of subsystems, it is useful to outline a few of the parameters that need to be considered when individual designs were considered. The following are some of the factors that were considered.

1. **Cost**: This is probably the most obvious limitation to consider that is set very early in the process and usually determined long before the selection of a design is made.

2. **Time**: Though some equate time with money, such is not always the case. There are a limited number of manufactures that can provide space worthy components and if there is a back log of other missions requiring their services then the mission could be significantly delayed. For example, the production of a large primary mirror of a particular optical quality is a meticulous process that cannot be done in a short amount of time no matter how much money is available. If a mission is required to be lunched within a certain time frame, the time to acquire or manufacture all of the different components must be considered.

3. **Mass**: Getting anything into space takes a lot of energy and every space mission must follow a very strict mass budget. These are broken up into “dry” and “wet” masses where the “wet” mass includes any propellent that the spacecraft would require for its lifetime in addition to all of its hardware components.

4. **Lifetime**: A mission designed to operate for 10 years will require many more redundant systems and more propellent than a mission for 2 years. This will increase mass, cost, and design time to mitigate chances of failure.

5. **Size**: Even if a spacecraft is well within its mass budget, their are physical limitations to the size of mission imposed by the size of the launch vehicle's fairing.

6. **Technological Readiness**: Technologies that have a long history of reliable operation are considered to have a high Technological Readiness and therefore lower the overall risk of the mission. If the spacecraft design includes technologies that are still being developed with no history of successful operation, the risk of the mission increases.

All of these factors were considered for this work when performing the trade studies of different subsystems.

2.5 EChO's Basic Design

The EChO telescope will be a small, 1.2 Cassegrain or Ritchey Chretien design with a possibility of an off-axis system to avoid potential diffraction problems from the secondary. While the telescope is proposed to be of a straightforward design, the focal plane will require a very wide wavelength range to access the information needed to determine the exoplanet atmospheres composition. As a consequence, EChO is proposed to provide low resolution spectroscopy for a spectral range between 0.4-16 microns. This will give EChO access to many molecular signatures expected to be found in exoplanet atmospheres as can be seen in Figure 2.4. This also creates some specific design requirements that must be fulfilled to ensure the telescope can access the specified wavelengths.

One design concern that arose during this work was the availability of detectors at the wavelengths for which EChO is proposed to operate. While the benefits of having such a broad spectral range are apparent, one key challenge of this mission will be

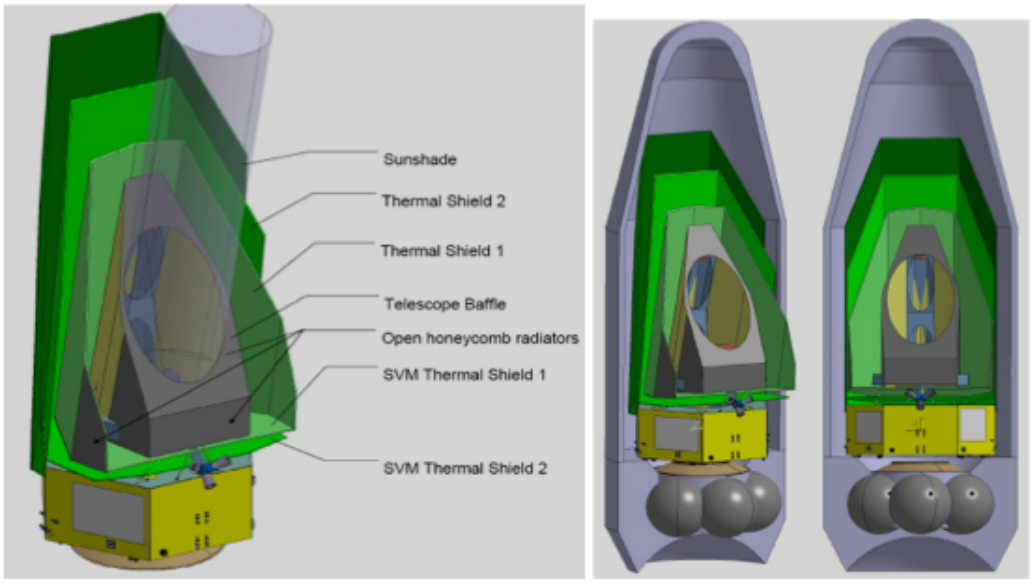

Fig. 2.2: One proposed design for the EChO spacecraft. Image taken from Tinetti et al. (2012)

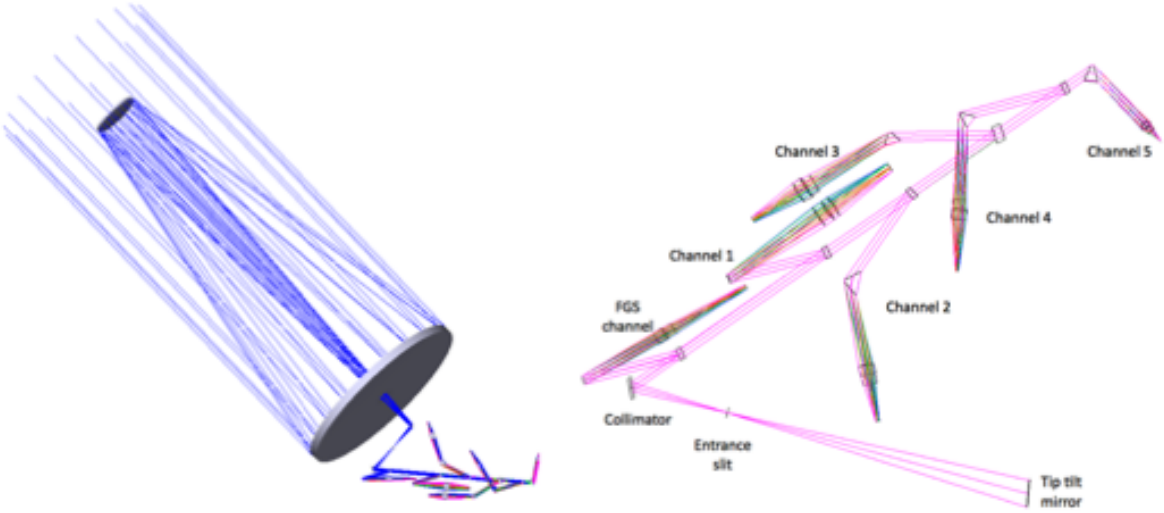

Fig. 2.3: One design for the multi-channel spectrograph placed at the focal plane. The proposed spectral coverage will be 0.6–16 microns. Image taken from Tinetti et al. (2012)

in acquiring adequate detectors that can fulfil these requirements. Although detectors currently exist that are capable of working at these wavelengths, they are only available through vendors from the United States. Given this is an ESA mission, the preference would be to develop this technology in Europe rather than outsourcing to a country outside of Europe. There are European options that possibly could be developed in the time frame for the launch of EChO but this does constitute a lower Technology

	0.4-1 μm	1-5 μm	5-11 μm	11-16 μm
R, baseline	500	300	300	20
R, desired	500	300	300	300
Species				
*H_2O	0.51, 0.57, 0.65, 0.72, 0.82, 0.94	1.13, 1.38, 1.9, **2.69**	6.2	continuum
*CO_2	-	1.21, 1.57, 1.6, 2.03, **4.25**	-	**15.0**
C_2H_2	-	1.52, **3.0**	7.53	**13.7**
HCN	-	**3.0**	-	**14.0**
C_2H_6	-	3.4	-	**12.1**
O_3	0.45-0.75 (the Chappuis band)	4.7	9.1, **9.6**	14.3
HDO	-	2.7,3.67	7.13	-
*CO	-	1.57, 2.35, **4.7**	-	-
O_2	0.58, 0.69, 0.76, 1.27	-	-	-
NH_3	0.55, 0.65, 0.93	1.5, 2, 2.25, 2.9, **3.0**	6.1, **10.5**	-
PH_3	-	4.3	8.9, 10.1	-
*CH_4	0.48, 0.57. 0.6, 0.7, 0.79, 0.86,	1.65, 2.2, 2.31, 2.37, **3.3**	6.5, **7.7**	-
CH_3D	?	3.34, **4.5**	6.8, 7.7, **8.6**	-
C_2H_4	-	**3.22**, 3.34	6.9, **10.5**	-
H_2S	-	2.5, 3.8 ...	7	-
SO_2	-	4	**7.3**, 8.8	-
N_2O	-	2.8, 3.9, **4.5**	7.7, 8.5	-
NO_2	-	3.4	**6.2**, 7.7	13.5
H_2	-	2.12	-	-
H_3^+	-	2.0, 3-4.5	-	-
He	-	1.083	-	-
*Na	0.589	1.2	-	-
*K	0.76	-	-	-
TiO	0.4-1	1-3.5	-	-
VO	0.4-1	1-2.5	-	-
FeH	0.6-1	1-2	-	-
TiH	0.4-1	1-1.6	-	-
Rayleigh	0.4-1	-	-	-
Cloud/haze	yes	possible	silicates, etc.	-
H α	**0.66**			
H β	0.486			
Ca	0.8498, 0.8542, 0.8662		-	-

Fig. 2.4: Molecular and atomic spectral lines that would be available to EChO. The asterisk denotes that that feature has already been detected in an exoplanet atmosphere. Image taken from Tinetti et al. (2012)

Readiness Level (TRL) and therefore a higher risk factor for EChOs development. However, as a mitigation, ESA may decide to relax the requirements of the mission such that the spectrum of interest is reduced.

2.6 Trade Studies

2.6.1 Attitude and Orbit Control System

Scientific Impact

The spacecraft's attitude and orbit control system (AOCS) is integral to the daily operation and survival of a spacecraft and its scientific mission. The AOCS determines the spacecraft's ability to point at a particular location on the celestial sphere as well as its ability to maintain its pointing over a period of time. This, in turn, affects the sensitivity of the mission due to the limitation it sets on the spacecraft's ability to keep a target within a particular region of the detector.

The AOCS can be a highly complex system requiring consumables and/or moving parts which can decrease the lifetime of the spacecraft as well as add significant mass depending on the design. Because of these concerns, a trade study was conducted to attempt to optimize the benefits and limit the risk of a particular AOCS design as it would apply to the EChO mission concept.

Trade Study

Two options were considered for the spacecraft's AOCS: Reaction wheels (spinning wheels that change the attitude of the spacecraft by varying their rotation rate) and a cold gas system (compressed nitrogen expelled from thrusters). The Euclid and PLATO missions, which have similar designs, have also undergone a trade study between these options. The conclusion of the Euclid trade study was that the telescope should baseline a cold gas thruster solution, whereas PLATO uses wheels as its baseline AOCS method. The trades conducted for both of these missions show that the choice of AOCS system is marginal. A third option can also exist which would comprise of a hybrid system

consisting of both reaction wheels and cold gas. Reaction wheels could be used to provide a rapid re-pointing capability while a gas system would be used for fine-tuning attitude during observation to avoid image degradation. The drawback of such a hybrid system is that increases complexity and cost.

The conclusion of this trade study was, since micro vibrations are an important factor for EChO's stability and sensitivity, a cold gas solution is preferred. Clearly this trade needs to be performed in greater detail during future assessment studies.

2.6.2 Sun Shield

Scientific Impact

A sun shield is used when part or all of a spacecraft needs to be kept in shadow to passively cool detectors or optics to increase sensitivity at the redder wavelengths. Since they are designed to have one side of the shield always facing the sun, they are also natural locations for solar panels to help provide the spacecraft with power.

Their design usually involves several layers of reflective material that are angled such that most of the incident flux is reflected back and forth between the layers and eventually re-radiated into space. The specific orientation of the shield can vary and is dependent on the size of the faring within the launch vehicle and the slewing requirements of the particular mission. Because they often need to cover the entire body of the spacecraft, they can be very large and can require a complicated deployment process. The many moving parts can therefore increases the risk of mission failure if one of the deployments is incomplete. The spacecraft's required solar exclusion angle can also drive the design of the sun shield given certain observations could expose the protected areas if particular designs are chosen. An asymmetric design can also complicate the balance of the spacecraft launch vehicle. These considerations were all taken into account for the requirements of the EChO spacecraft and discussed in the following below.

Trade Study

The EChO mirror will need to be passively cooled to 50 K. A heat reflective sun shield is therefore required in order to achieve this. To passively reach such low temperatures, EChO is proposed to use a V-groove sun shield similar to the one employed by JWST. There is also a requirement for EChO which states that up to 2π of the sky should be visible at any point in time, with a ± 30 degrees by 360 degrees annulus being the requirement. In order to try and maximize the sky view of the telescope a number of sun shield configurations were considered. The three configurations looked at were a parasol configuration, a side sun shield, or a V-groove cone.

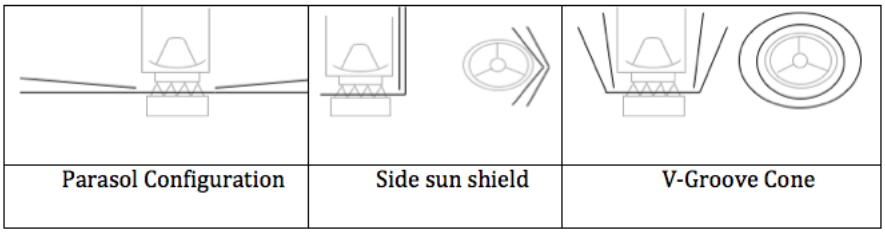

Fig. 2.5: Three possible designs for a thermal reflective sun shield to passively cool the optics of the spacecraft. Image provided by EADS Astrium.

The conclusion of this preliminary trade from a thermal perspective is that the choice between the side sun shield and the V-groove cone is marginal. The side sun shield will provide a slightly better view of the sky but requires greater complexity in spacecraft operations and it requires a roll manoeuvre to slew beyond 90 degrees. There is also more heritage in the side sun shield solution, with missions such as Herschel and Euclid using such systems. From a mechanical perspective, the V-groove cone option is better because the design is symmetric and allows a more natural launch load path. It also has the potential to be more lightweight as the sunshield doubles as a stray light baffle, removing the need for this heavy additional structure.

Further analysis of the systems and mass/power budgets for EChO can be found in the Astrium Technical note ECHO-ASU-TN.001.

2.7 EChO's Final Design and Status

The results of this trade study was folded into the Phase-A design studies conducted by Astrium and the information was carried on through the process in a more rigorous way by other Astrium and ESA. The final design for EChO that was proposed to ESA consisted of an AOCS using a hybrid cold gas/reaction wheel system and a V-groove cone sun shield design, consistent with the conclusions of this preliminary study.

After ESA conducted industrial studies to determine the feasibility, cost, and scientific merit for all of the M3 candidates, ESA selected PLATO as the mission to fill the M3 slot. However, the work done towards the design and potential science of EChO may be applied to a future ESA mission which can use the EChO design as a framework for a similar or possibly more ambitious mission.

References

Beaulieu, J. P., Bennett, D. P., Batista, V., Cassan, A., Kubas, D., Fouqué, P., Kerrins, E., Mao, S., Miralda-Escudé, J., Wambsganss, J., Gaudi, B. S., Gould, A., & Dong, S. 2010, in Astronomical Society of the Pacific Conference Series, Vol. 430, Pathways Towards Habitable Planets, 266

Fridlund, M. 2009, in American Institute of Physics Conference Series, Vol. 1158, American Institute of Physics Conference Series, 351–358

Tinetti, G., Beaulieu, J. P., Henning, T., Meyer, M., Micela, G., Ribas, I., Stam, D., Swain, M., Krause, O., Ollivier, M., Pace, E., Swinyard, B., Aylward, A., van Boekel, R., Coradini, A., Encrenaz, T., Snellen, I., Zapatero-Osorio, M. R., Bouwman, J., Cho, J. Y.-K., Coudé de Foresto, V., Guillot, T., Lopez-Morales, M., Mueller-Wodarg, I., Palle, E., Selsis, F., Sozzetti, A., Ade, P. A. R., Achilleos, N., Adriani, A., Agnor, C. B., Afonso, C., Allende Prieto, C., Bakos, G., Barber, R. J., Barlow, M., Batista, V., Bernath, P., Bézard, B., Bordé, P., Brown, L. R., Cassan, A., Cavarroc, C., Ciaravella, A., Cockell, C., Coustenis, A., Danielski, C., Decin, L., De Kok, R., Demangeon, O., Deroo, P., Doel, P., Drossart, P., Fletcher, L. N., Focardi, M., Forget, F., Fossey, S., Fouqué, P., Frith, J., Galand, M., Gaulme, P., Hernández, J. I. G., Grasset, O., Grassi, D., Grenfell, J. L., Griffin, M. J., Griffith, C. A., Grözinger, U., Guedel, M., Guio, P., Hainaut, O., Hargreaves, R., Hauschildt, P. H., Heng, K., Heyrovsky, D., Hueso, R., Irwin, P., Kaltenegger, L., Kervella, P., Kipping, D., Koskinen, T. T., Kovács, G., La Barbera, A., Lammer, H., Lellouch, E., Leto, G., Lopez Morales, M., Lopez Valverde, M. A., Lopez-Puertas, M., Lovis, C., Maggio, A., Maillard, J. P., Maldonado Prado, J., Marquette, J. B., Martin-Torres, F. J., Maxted, P., Miller, S., Molinari, S., Montes, D., Moro-Martin, A., Moses, J. I., Mousis, O., Nguyen Tuong, N., Nelson, R., Orton, G. S., Pantin, E., Pascale, E., Pezzuto, S., Pinfield, D., Poretti, E., Prinja, R., Prisinzano, L., Rees, J. M., Reiners, A., Samuel, B., Sánchez-Lavega, A., Forcada, J. S., Sasselov, D., Savini, G., Sicardy, B., Smith, A., Stixrude, L., Strazzulla, G., Tennyson, J., Tessenyi, M., Vasisht, G., Vinatier, S., Viti, S., Waldmann, I., White, G. J., Widemann, T., Wordsworth, R., Yelle, R., Yung, Y., & Yurchenko, S. N. 2012, Experimental Astronomy, 34, 311

Chapter 3: Simulated Exoplanet Targets for Ground and Space Based Surveys

3.1 Introduction

If a space based exoplanet characterisation mission were to be launched today, there are many transiting planets that would make viable targets. It has been estimated that hot Jupiters around FGK stars with a V magnitude of 10 or brighter would be able to be characterized by a space based mission like EChO (Tessenyi et al., 2012) assuming a certain number of observed primary and secondary transits. Currently, there are at least 13 hot Jupiters that fulfil this requirement (Wright et al., 2013). However, characterizing planets that fall within the HZ is always of particular interest to the community and there are few transiting planets currently known to which a mission like EChO would be sensitive. An expansion of the target list, particularly of transiting super Earths around bright low mass stars, would allow EChO to provide statistics on cool, potentially rocky planets as well as the hot giant planets.

Many new ground based transit surveys are either operating or are scheduled to begin prior to a mission like EChO could be launched to search for these new targets. A survey that has been in operation the longest, mentioned in Chapter 1, is MEarth Charbonneau et al. (2008). Its primary goal is to monitor about 2000 late M dwarfs (R $< 0.33\ R_{Earth}$) taken from the Lepine-Shara Proper Motion Catalog of northern stars Lépine & Shara (2005) to search for super Earths, as small as twice the radius of the Earth, in the HZ. Another planned ground based survey that will potentially produce good targets, also mentioned in Chapter 1, is a program entitled (APACHE) (Sozzetti et al., 2013) dedicated to the longterm photometric monitoring of thousands of nearby M dwarfs in the Northern hemisphere. Due to start in early 2014, it will provide a longitudinally distributed network of telescopes dedicated to the search for transits

of small planets. Another program, not focused on low mass stars, is the Multi-site All-Sky CAmeRA (MASCARA) (Snellen et al., 2013) which is another longitudinally separated network of observatories and designed for constant monitoring of the sky's brightest stars (V = 4–8). Also focusing on lower mass transiting planets is the Next Generation Transit Survey (NGTS) which is due to begin in 2014 (Wheatley et al., 2013).

With all of these new surveys soon to begin operation, an estimate of the number and characteristics of the detectable transiting planet population is of use. Statistics of simulated planets around known local stars will provide these surveys and future missions with statistics as a guide for how many transits can be detected over the next 10 years.

3.2 Target Simulations

These simulations use empirical data taken from current exoplanet and local stellar populations and are used to produce a simulated local planetary population around known stars out to 50 parsecs.

3.2.1 Local Stellar Sample

A sample of approximately 9000 Stars from the Gliese (Gliese & Jahreiss, 1995) and Hipparcos catalogue (Perryman et al., 1997) were selected based on their parallactic distance measurements being less than or equal to 50 parsecs. It is noted that this may not be a complete sample of all stars within 50 parsecs and this is discussed further in Section 3.4. The stars covered the whole sky and were chosen to fall within the main sequence. Colour cuts made to restrict the population to nothing bluer than a spectral type of F. These colour cuts were

$$0.25 < B - V < 2.25 \tag{3.1}$$

These B–V values correspond to temperatures of approximately 3000–7500 Kelvin

(Reed, 1998). A Hertzsprung-Russell diagram of the selected stellar sample can be seen in Figure 3.2.

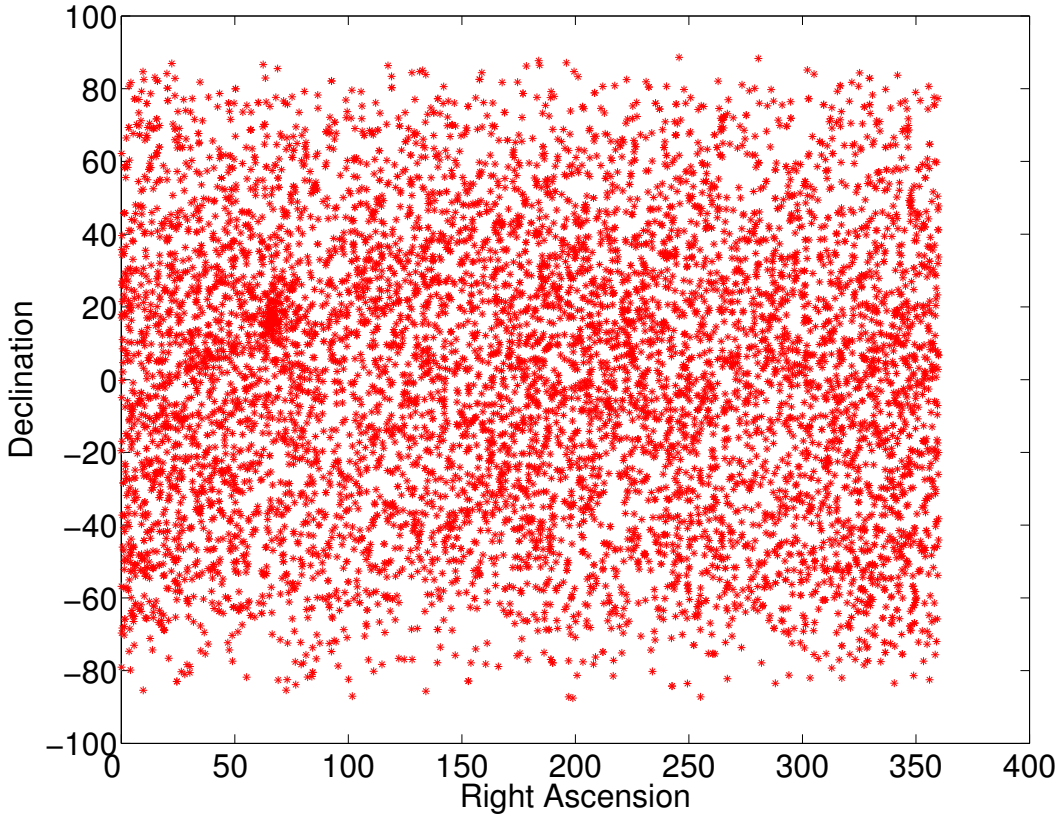

Fig. 3.1: The right ascension and declination of the selected stars. They cover the entire sky including the galactic plane.

Additionally, stars with a parallax error greater than 10 per cent were excluded to limit uncertainties when determining the stellar parameters.

3.2.2 Simulating Stellar Parameters

While distances were available via parallax measurements from Hipparcos, stellar properties such as mass and radius are needed when determining whether a planetary transit will be detectable using modern techniques. While these values weren't directly available, it is possible to estimate them using a combination of empirically derived relationships and known physical relationships.

First, an effective stellar temperature estimation can be made using the available

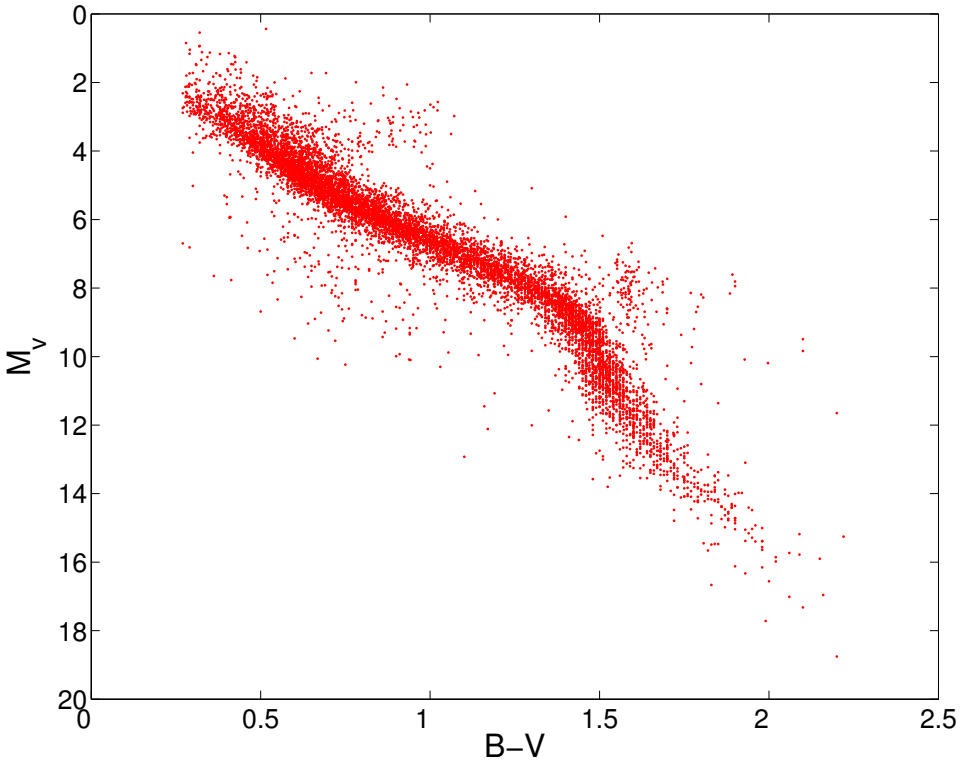

Fig. 3.2: The absolute magnitude and B–V values of the selected Hipparcos and Gliese stars within 50 parsecs. The selected stars were chosen based on their colour and absolute magnitudes being consistent with F, G, K, and M dwarfs.

B–V values based on Reed (1998). The temperature can be estimated using the relation

$$T_* = 10^{(B-V)-\frac{14.551}{-3.684}} \tag{3.2}$$

where T_* is the surface temperature of the star. A temperature estimate then allows many follow on estimations of the stellar population's properties. Also from Reed (1998), an empirically derived fit to data from (Lang, 1992) is given to determine the bolometric correction for each star. The bolometric correction is the conversion from a single bandpass magnitude to an integrated bandpass magnitude which is representative of the objects luminosity. This is stated as

$$\begin{aligned} BC = &-8.499(log_{10}T-4)^4 + 13.421(log_{10}T-4)^3 \\ &-8.131(log_{10}T-4)^2 - 3.901(log_{10}T-4) - 0.438 \end{aligned} \tag{3.3}$$

where BC is the bolometric correction and T is the effective temperature derived in Equation 3.2. This is then used to determine the stars bolometric magnitude and luminosity in the normal way

$$M_{bol} = M_v + BC \tag{3.4}$$

where M_{bol} and M_V are the stars bolometric and absolute magnitude, respectively. The luminosity is then computed in terms of solar luminosities with the following relationship

$$L_* = 2.51(4.83 - M_{bol}) \tag{3.5}$$

The temperature and the luminosity is then used to estimate the stellar radii using

$$R_* = \sqrt{\frac{L_*}{T_*^4}} \tag{3.6}$$

where R_* is in units of Solar radii and T_* is the temperature of the star in units of Solar temperature. This relationship assumes the star is a blackbody. This rather simple relationship tends to break down for lower mass stars and produces radii much too small compared to the estimated lower limit of a main sequence star. Chabrier & Baraffe (2000) have estimated that due to pressure generated by degenerate electron gas, the minimum radius of objects above $M_\odot = 0.07$ is an $R_* \approx 0.08\ R_\odot$. As a result, this value was used as the lower limit for the stellar radii estimations.

The mass-luminosity relationship of main sequence stars has been well constrained by Torres et al. (1997) who looked at eclipsing binary stars with known distances. This can be approximated with one relationship but deviates slightly at the low mass/luminosity end. The approximations used are

$$\begin{aligned} M_* &= L_*^{(1/4.0)}\ (L_* > 0.05 L_\odot) \\ M_* &= L_*^{(1/2.3)}\ (L_* < 0.05 L_\odot) \end{aligned} \tag{3.7}$$

As can be seen in Figure 3.3, this relationship causes a slight discontinuity at 0.5 $M_{\odot}$. However, precise host star mass estimates are not required to determine the probability of whether an exoplanet transit is detectable (as is discussed in Section 3.3) .

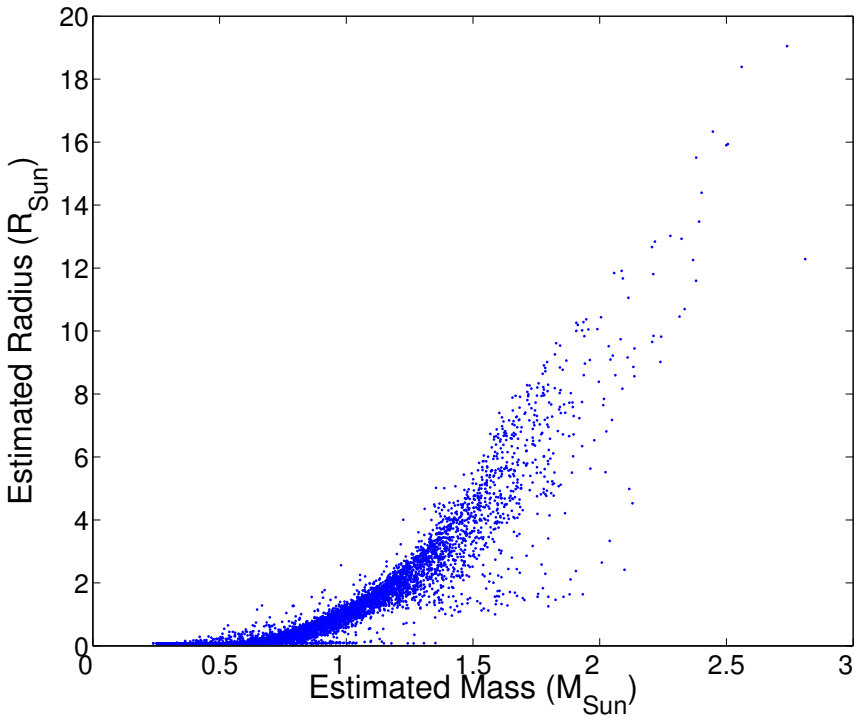

Fig. 3.3: Estimated radii and masses of the host star population. The discontinuity at 0.5 $M_{\odot}$ is caused by the assumptions made in Equation 3.7 but will not affect the transit detection results.

3.2.3 Properties of Simulated Planet Population

Now that the local stellar population has been defined, appropriate simulated exoplanets must be established that are representative of the observed population. This is done by using information from the known transiting population to define a planet fraction and a period distribution then assuming that stellar and planetary mass scale together as suggested by Johnson et al. (2007) and Bonfils et al. (2013).

Assumptions

For simplicity, 3 assumptions have been made that speed up this process while still providing good statistics on the number of transits that can be expected amongst this

stellar population. These assumptions are:

1. Every star has a planet.

This is a practical assumption that can easily be adjusted in the future using the appropriate planet fraction.

2. Only one planet per star.

While many transiting multiple planetary systems have been discovered with Kepler (Kepler 11, Keppler 33, Kepler 32, Kepler 20, and others (Wright et al., 2011)), there are none as of yet that have been discovered via ground based observatories. The majority of the multiple planet systems discovered by Kepler (all but Kepler 9 b and c) have a transit depth that is currently below the average detection limit of ground based observations (0.5 per cent;see Figure 3.4). In addition to this assumption simplifying the simulations, it is also consistent with current transit surveys where only one transiting planet is observable per star from the ground.

3. All planets have circular orbits.

The vast majority of transiting exoplanets have an eccentricity less than 0.2, as seen in Figure 3.5, with the majority of those having an eccentricity lower than 0.02. Though it is a simplification, assuming a circular orbit is again representative of the observed population of transiting planets.

Further precision for these simulations can be achieved in the future by removing these assumptions and are known limitations of this work. That being said, we must now define an exoplanet population to match with the stars discussed above.

Simulations

The primary source of exoplanet statistics comes from The Exoplanet Catalogue, created and maintained by Wright et al. (2011). While this source is well maintained and thorough, many objects exist within the catalogue that may be excluded from this work.

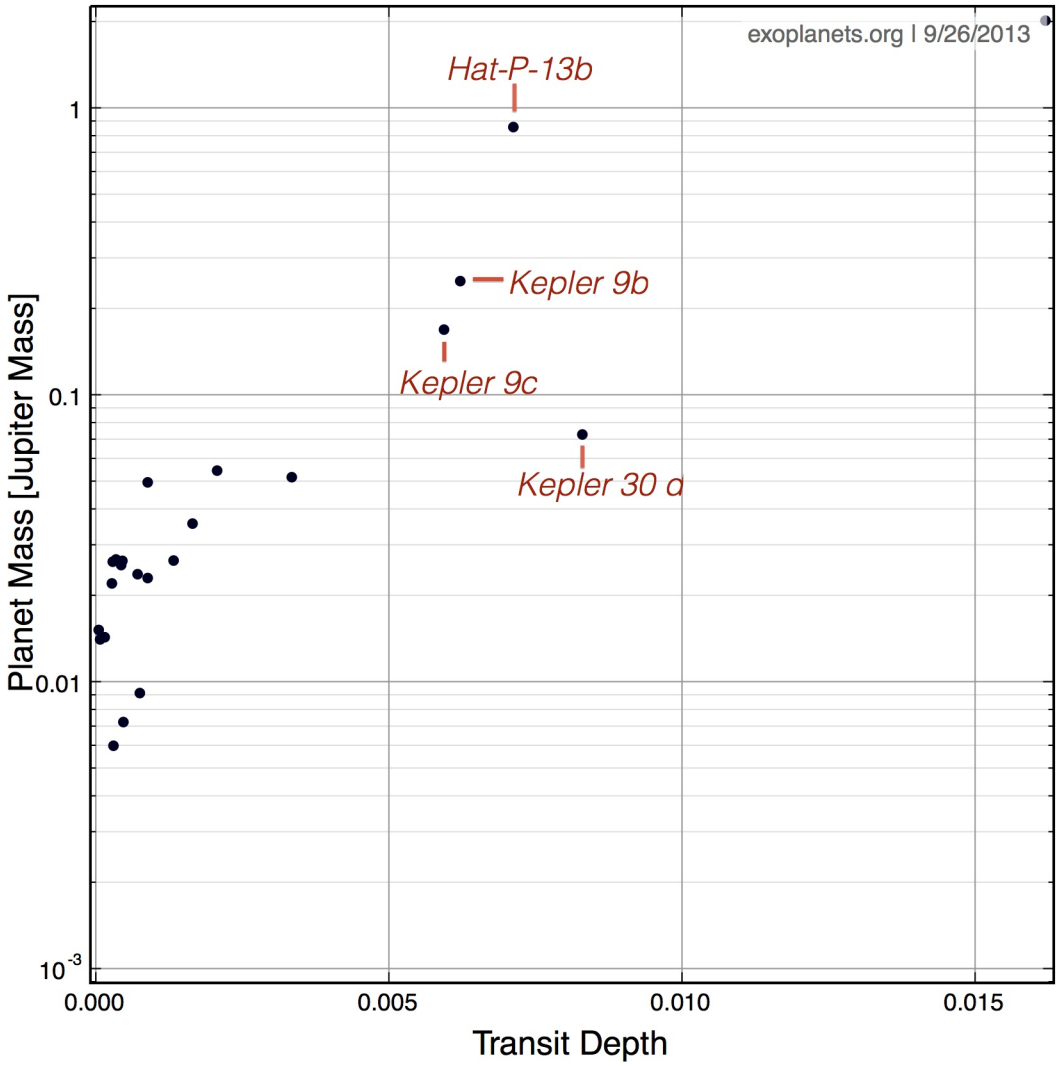

Fig. 3.4: All of the known transiting planets that are part of a multi-planet system. With the exception of Kepler 9, no two transiting planets are found to have a depth that is above the current baseline limitation of ground based observatories of 0.5 per cent. Hat-P-13b's companion does not appear to transit (Bakos et al., 2009) and Kepler 30's reside below the limit. Information and plot produced using www.exoplanets.org (Wright et al., 2013).

The definition of what precisely constitutes a "planet" has been a point of contention amongst different members of the community (Boss et al., 2003). Many believe that the only true distinction between a brown dwarf and a planet is the method in which they were formed (core accretion Vs. disk instability, Matsuo et al. (2007)) while others argue that the distinction should be the upper mass limit where deuterium burning in the object's core will begin (Spiegel et al., 2011). It is beyond the scope of this work to form a concrete distinction between the two but, for the purposes of determining whether a planet's radius is large enough to detect during a transit, the defining characteristic lies with the mass.

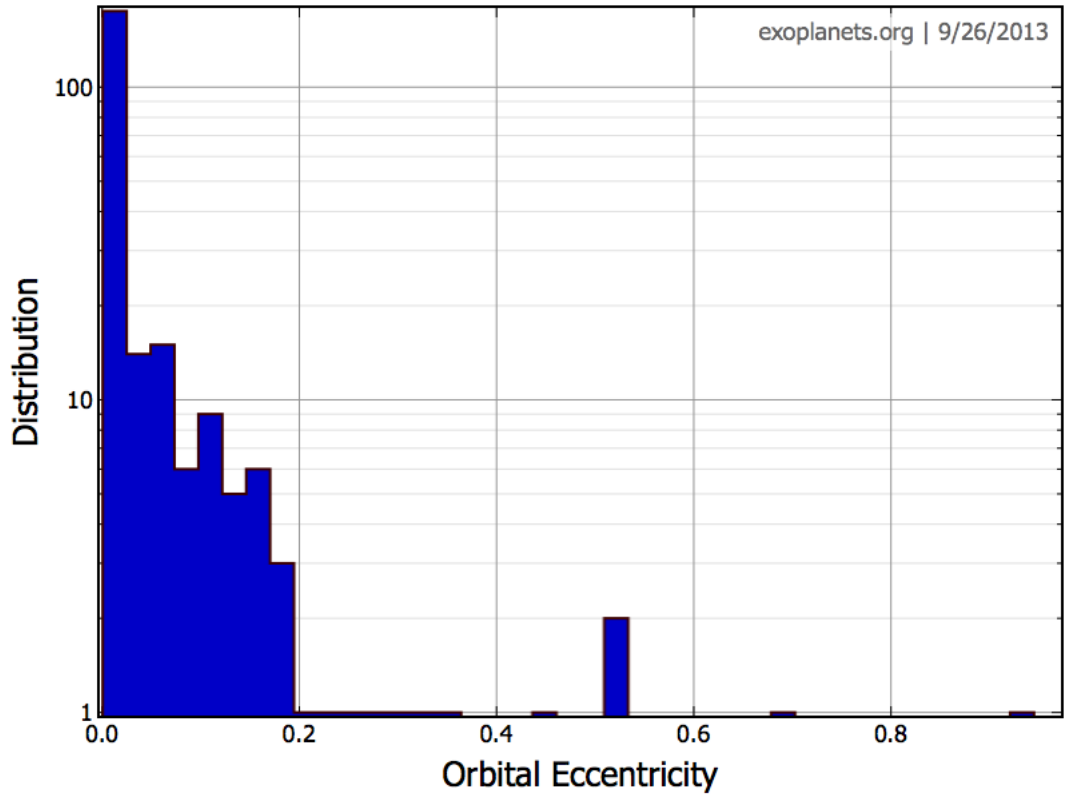

Fig. 3.5: The distribution of the eccentricity of known transiting planets. Information and plot produced using www.exoplanets.org (Wright et al., 2013).

The International Astronomy Union (IAU) discussed the upper mass limit of what can be classified as a planet and decided that the distinction should be whether deuterium burning can occur (Boss et al., 2007). While the general accepted mass for this to begin is at 13 M_{Jup}, Spiegel et al. (2011) find that this is dependent highly on the metallicity of the object. For very low metallicity objects, they conclude that this limit could be up to 16.3 M_{Jup}. At the risk of including what some would call brown dwarfs within these simulations, a conservative upper limit of 18 M_{Jup} is chosen to include as diverse of a planet population as possible. Again, while some may argue that these don't necessarily represent the exoplanet population, it is perfectly feasible that objects such as these can be expected to be found orbiting nearby stars.

A power law fit to known exoplanet masses was used to determine the probability distribution functions necessary to simulate a population consistent with observations. The fit was used from the information within the exoplanet catalogue and simulated masses from the distribution specified by the probability density fit were then gener-

ated. The resulting distribution can be seen in Figure 3.6.

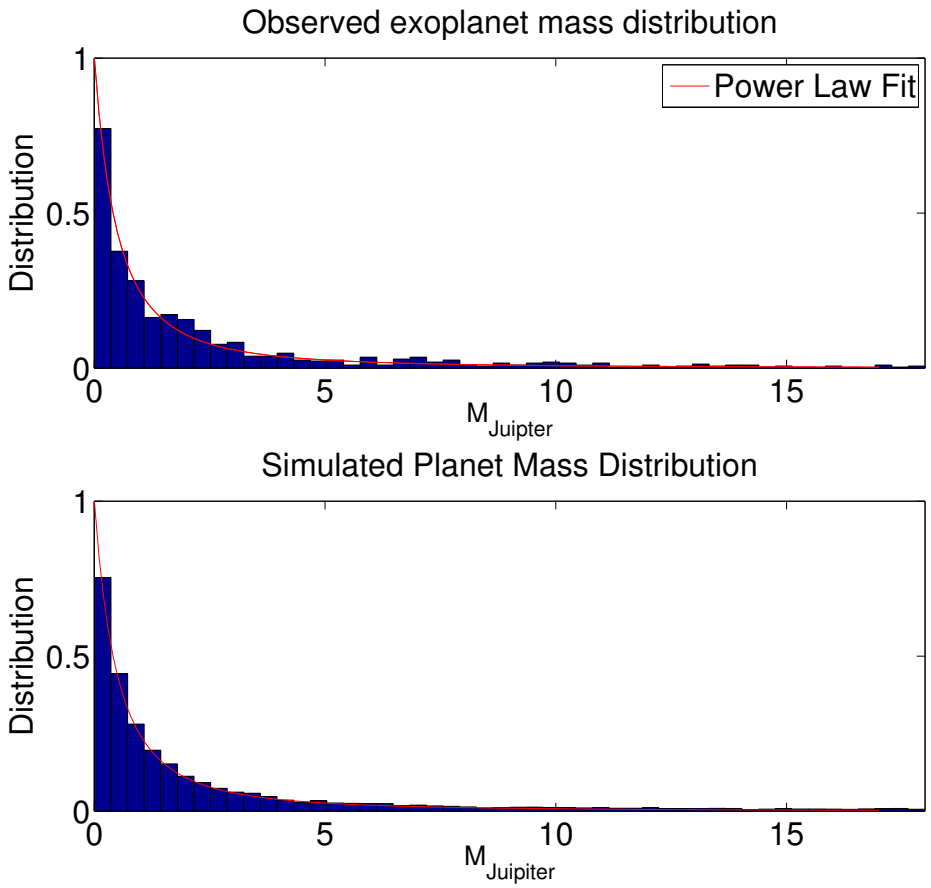

Fig. 3.6: Above: Existing planet population's mass and the corresponding power-law fit. Below: Resulting probability distribution of simulated planetary mass.

A further characteristic that is needed for these simulations is a range of semi-major axes or, in this case, radial distances from its host star. The Exoplanet Catalogue includes objects with semi-major axes out to as far as 3200 au but more than 90 percent of the known objects fall below 10 au. There is a detection bias here from the nature of radial velocity detections (and transits over a short observation time scale) being more sensitive to planets that are closer to their stars. Choosing an upper limit is somewhat arbitrary since it again comes into the realm of the definition of a planet. Using the Solar system as a guide, the last planet-sized object (Neptune) can be found at approximately 30 au, so an upper limit of 40 au was chosen. While planets orbiting further away are entirely possible, this upper limit does not significantly change the probability distribution of the simulated objects and, as is later discussed, transiting

planets beyond 3 au are most likely unobservable within the next 10 years.

The determination of a lower limit to the orbital distance is slightly less clear. The smallest semi-major axis known for a transiting planet to date was discovered by Muirhead et al. (2012) using the Kepler satellite. It is designated Kepler 42c, has an a=0.0059 au, and is likely a rocky, low mass planet. Wasp 43b (Hellier et al., 2011) is a hot Jupiter orbiting at an a=0.0142 au around a K7 dwarf which makes it the shortest period ground based discovery. While Wasp 43b is currently the shortest period planet that has been discovered via ground based transiting detection, there is no reason why other objects may exist at similar orbital distances as Kepler 42c. Therefore, its semi-major axis (a=0.0059 au)is designated as the lower limit for these simulations. Similar to the mass distribution, a power-law fit was done using information from the existing population and the results can be seen in Figure 3.7.

While this describes a distribution of possible orbital radii for the simulated exoplanets, when assigning a particular planet to a host star, certain limitations must be taken into account. In reality, the most influential factor on a planet's orbit is likely the gravitational effects from other bodies in the system (Barnes & Greenberg, 2005). However, since each system is only described by one planet and one star in a circular orbit, there are few limitations to where a planet can be placed with respect to its star. One obvious check to perform is that the orbit of the exoplanet does not fall within the radius of its host star. Another check to perform is that the planet is sufficiently distant from the Roche limit (Williams, 2003) of the host star. This done by applying the formula

$$d_{RL} = 2.44 R_p \left(\frac{M_*}{M_P} \right)^{1/3} \tag{3.8}$$

where d_{RL} is the distance from the surface of the star the planet must be before it is broken apart by tidal forces. There is some evidence that low density, hot gas giants around Sun-like stars may evaporate down to their core at orbital distances less than 0.015 au due mass loss caused by stellar wind ram pressure and coronal mass ejections from the star (Lammer et al., 2009). In fact, this has claimed to have been observed

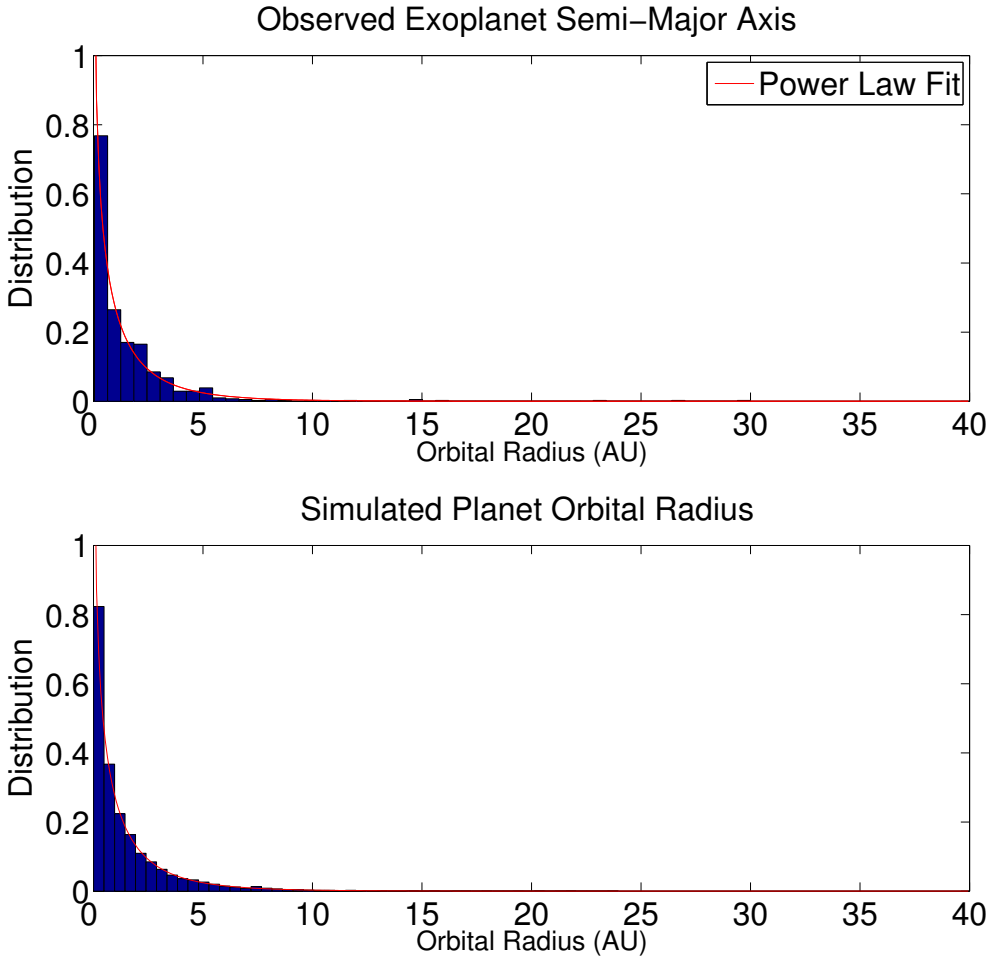

Fig. 3.7: Above: Existing planet population's semi-major axis distribution and the corresponding power-law fit. Below: Resulting probability distribution of simulated planetary orbital radii.

with Wasp-12b which orbits a G0 star at a distance of 0.02 au (Li et al., 2010). In this case, its semi-major axis is only 3.1 stellar radii away from its star. This being the most extreme case of such a system observed thus far, for these simulations, if a planet is assigned with an orbital distance that finds itself within the star or below the Roche limit, its orbital distance is adjusted to be at 4 stellar radii away from its host star.

The highly important, but easy to simulate, inclination of the orbital plane of the system with respect to the Earth was assigned a random number from 0 to 90 degrees.

3.2.4 Pairing Planet to Host Star

If the planet and star formed from the same collapsing cloud of material, it is safe to assume that the more massive stars are more likely to play host to more massive planets and less massive stars are less likely. This has been found to be the case by observations done by Johnson et al. (2007), Johnson et al. (2010) and Bonfils et al. (2013) who gained statistics on the frequency and mass of planets as a function of host star mass. To represent this relationship, the simulated planets and host stars are sorted by mass and paired together so that the least massive planet is matched to the least massive star consecutively upwards to the highest massive pair. The comparison between the star and planet's mass can be seen in Figure 3.8 where the observed planets have also been plotted. The simulated data roughly follow the median distribution found in the observed data where the simulated population runs through the densest part of the observed population in the higher mass regime. This is therefore a reasonable representation of the expected planet-host star distribution for these simulations. Figure 3.8 also shows the lack of planets around low mass stars that have been observed which is primarily due to RV studies focusing on F,G,and K stars.

3.2.5 Simulated Planet Radius

Defining the size of the planet is intrinsically important when discussing transit probabilities and detections. The mass range of the simulated planets so far represent several very different planetary species that, as a first approximation, we have examples of here in the Solar system; namely, low mass planets made up of rock and iron, planets at several Earth-masses consisting of ice and rock, and massive planets dominated by Hydrogen (H) and Helium (He). Fortney, Marley, and Barnes (Fortney et al., 2007, FMB) have developed a method based on planets with these 3 distinct compositions to estimate radii across the large mass range within our simulated sample. Though the models are somewhat old, they provide an accurate enough estimate for purposes of approximating the depth of a simulated transit.

These models are based on the application of equations of state (EOS) for spher-

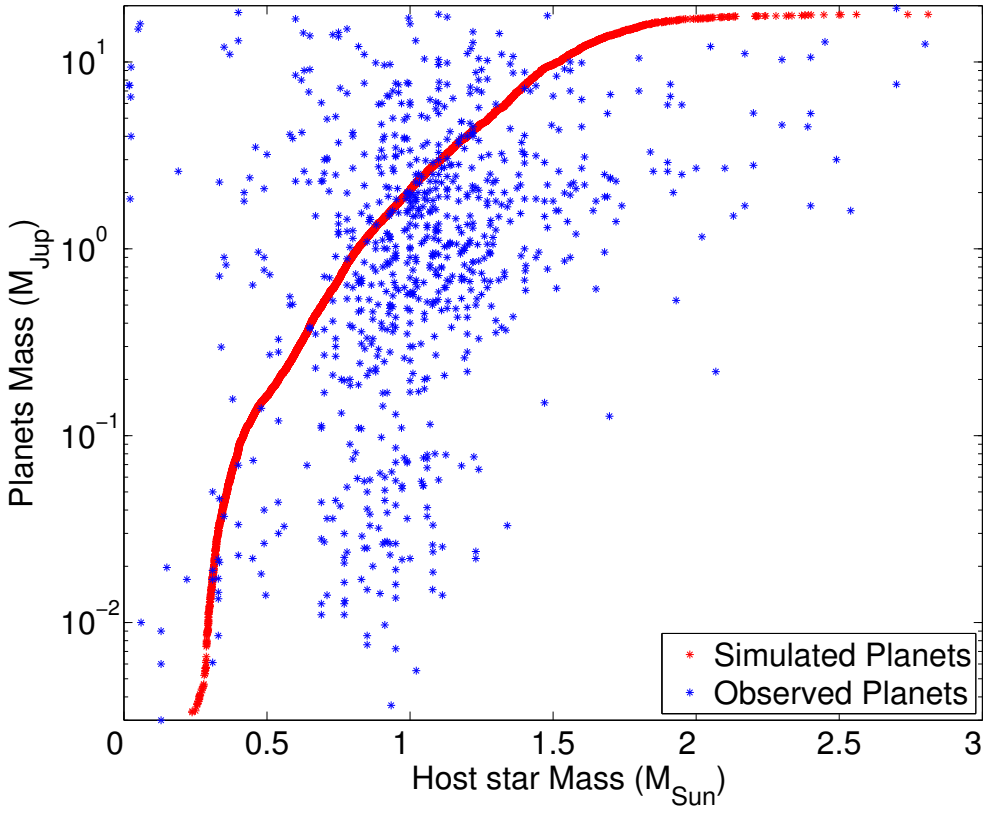

Fig. 3.8: Planet star mass versus host star mass. The observed data are plotted in blue and the simulated in red. The simulated data roughly follows the average distribution found in the observed data and runs through the densest region of the observed population. This implies this sorting is a sufficient method of paring host star to simulated planet. The lack of data points in the lower mass end is caused by RV searches focusing on Solar-type stars.

ically symmetric planets in hydrostatic equilibrium across the different mass ranges. These equations are

$$\frac{\partial r}{\partial m} = \frac{1}{4\pi r^2 \rho} \tag{3.9}$$

$$\frac{\partial P}{\partial m} = \frac{-Gm}{4\pi r^4} \tag{3.10}$$

where m is the mass of a given shell and r is its radius, ρ the local mass density, G the gravitational constant, and P the pressure. While these equations are not in the scope of this work to discuss in detail, it is important to note that, though these two equations are sufficient to define a radius with ice-rock-iron compositions, for planets with a mass dominated by H/He, a third EOS is needed to to account for time varying

influences. That third equation is

$$\frac{\partial L}{\partial m} = -T\frac{\partial S}{\partial t} \tag{3.11}$$

where T is temperature of the planet, L the planet's luminosity, S is the specific entropy, and t is time. Including T and t to define the radius of these giant planets has the implication that the age and spectral type of the host star as well its semi-major axis plays a roll in determining its radius.

For the smaller ice-rock-iron planets, the mass-radius relationship is relatively easy to implement using formula provide by FMB. These equations are

$$\begin{aligned} R = (0.0912\,\mathrm{imf} + 0.1603)(\log M)^2 + (0.3330\,\mathrm{imf}) \\ +0.7387)\log M + (0.4639\,\mathrm{imf} + 1.1193); \end{aligned} \tag{3.12}$$

$$\begin{aligned} R = (0.0592\,\mathrm{rmf} + 0.0592)(\log M)^2 + (0.2337\,\mathrm{rmf}) \\ +0.4938)\log M + (0.3102\,\mathrm{rmf} + 0.7932); \end{aligned} \tag{3.13}$$

where M is the mass of the planet, rmf is the rock-mass fraction (1.0 for pure rock, 0.0 for pure iron), and imf is the ice-mass fraction (1.0 for pure ice and 0.0 for pure rock). Since a planetary mass has already been generated above, all that is needed is to designate what range of masses and ice-rock-iron ratios we want to simulate. Figure 3.9 (taken from FMB) shows the applications of Equation 3.12 and 3.13 using different ice and rock mass fractions.

As can be seen, pure iron produces small, dense planets where pure ice planets have more inflated atmospheres. An Earth-like planet is designated to have an rmf = 0.67 and can be seen plotted in Figure 3.9 just below the 'pure rock' contour.

The gas giant radii are not so well constrained due to the many variables that go into affecting their radii. FMB are not able to describe a directly applicable formula but do provide several look up tables that provide their simulated radii across a range

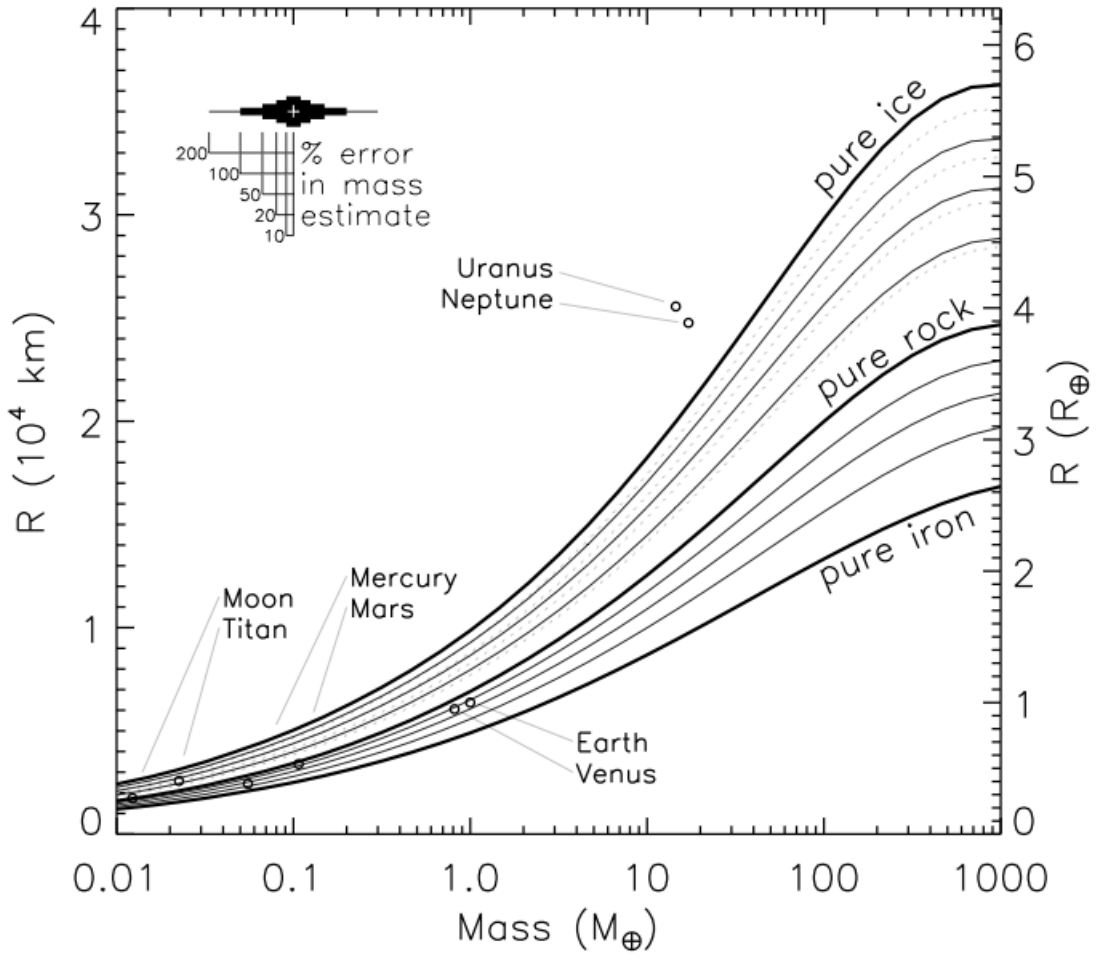

Fig. 3.9: Taken from FMB, this shows the radii of planets after the applications of Equations 3.12 and 3.13 across a range of Earth masses and ice-rock-iron mass fractions. Solar system objects are used as reference points.

of core masses (as opposed to pure H/He), semi-major axes, and masses. The results they present can be seen in Figure 3.10.

While this is a rather convoluted graph, certain trends can be seen that are useful to note for these simulations. More distant gas giants have slightly smaller radii while closer-in planets are inflated. This is due to their convective atmospheres having a much higher incident flux and, subsequently, their atmospheres having more energy pushing the edge of the atmosphere outward. Also useful to note is, from about 1 Jupiter mass, the radii can be constrained to have a minimum radius 0.8 R_J and all but the smallest and closest planets grow larger than 1.4 R_J.

Using these models as a guide, in an attempt to optimize representing the simulated planet radii accurately and limiting complexity, the planets have been separated into

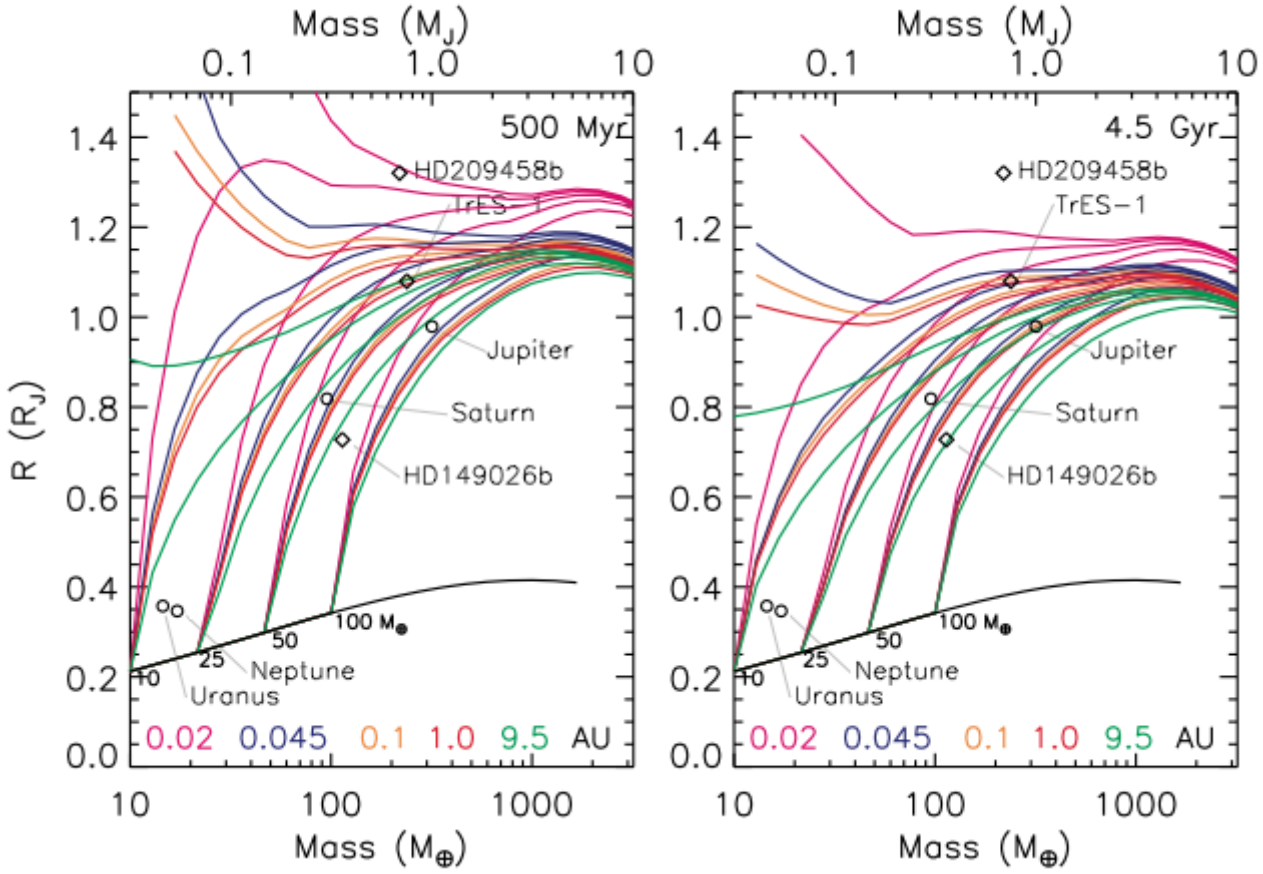

Fig. 3.10: Also Taken from FMB, this shows the radii of H/He dominated planets. Left shows planetary radii for a host star at 500 million years old and right shows radii for a star at 4.5 billion years. The coloured lines represent the track as mass increases for planets at different semi-major axes from 0.02 au to 9.5. The black line whence the lines start represent different core masses with 50 per cent ice and 50 per cent rock. Various Solar system objects and exoplanets are shown for reference.

3 separate mass ranges. For planets with M_{Earth} ≥10, an Earth-like composition is assumed and Equation 3.13 is used to compute the radii. For planets $10 < M_{Earth} \leq 300$, an imf = 0.75 is used (following the line half way between pure ice and pure rock in Figure 3.9) in Equation 3.12.

For planets with M_{Earth} >300, the radius is a function of mass and orbital distance. Similar to FMB, planets in this mass range are separated into orbital distance bins of 0.02, 0.045, 0.1, 1.0, and 9.5 au. Each bin has an initial radius set at 1.2, 1.1, 1.0, 0.9 and 0.8 R_{Jup}, respectively, then a normalized fraction is added based on the object's mass. This produces a population that is consistent with observed data while still primarily following FMBs models. To illustrate this, Figure 3.11 shows the radii and masses for all known exoplanets to date along with the simulated planets.

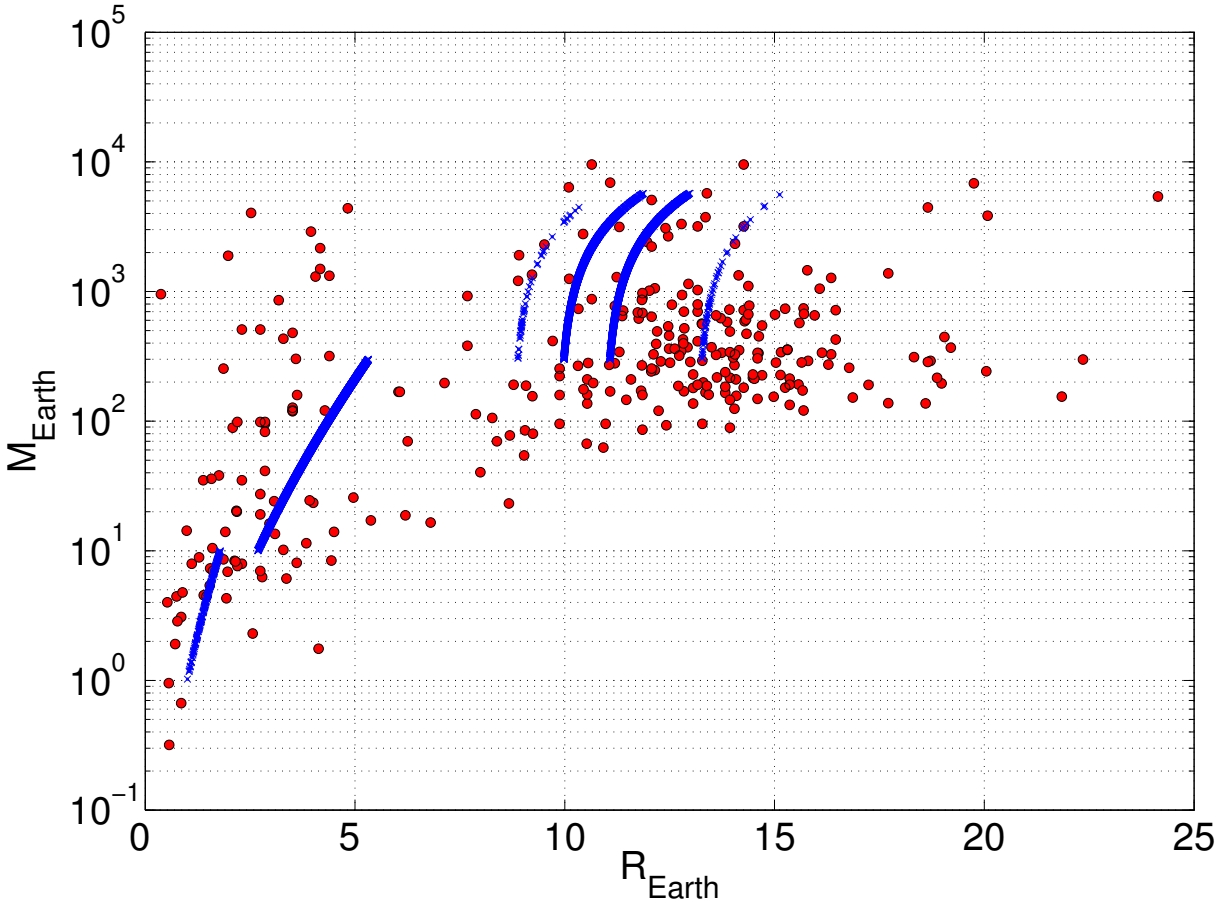

Fig. 3.11: Radius and mass of simulated and observed planets where observed are in red and simulated are blue. The two methods for calculating the radii as discussed in Section 3.2.5 follow the observed distribution and pass through the densest regions.

The simulated planets follow closely along with what has been observed. There is a gap in radii between 6 and 8 R_{Earth} in the simulated data but there is a noticeable drop in the density of observed objects in this radius range as well. The simulated giant planets cover most of the parameter space within the mass limits with many existing exoplanets having similar characteristics.

3.3 Transit Determination and Photometric Detection

With the radii of stars and planets, orbital distances, and orbital inclinations now simulated, it is possible to calculate whether the geometry of the system allows the

planet to transit as well as the resulting drop in flux.

3.3.1 Transit Determination

The first check is whether the planet will traverse the surface of the star from the point of view of an observer. This is made fairly straight forward with the assumption of a circular orbit. Derivations for the following equations can be found in Mandel & Agol (2002), Winn (2010), and Haswell (2010).

The most important factor to determine if a planet is transiting is the impact parameter, b, which is defined as

$$b = \frac{a \cos i}{R_*} \tag{3.14}$$

where a is the distance from the center of the star to the center of the planet (the radius of the orbit), i is the orbital inclination, and R_* is the radius of the star (see Figure 3.13).

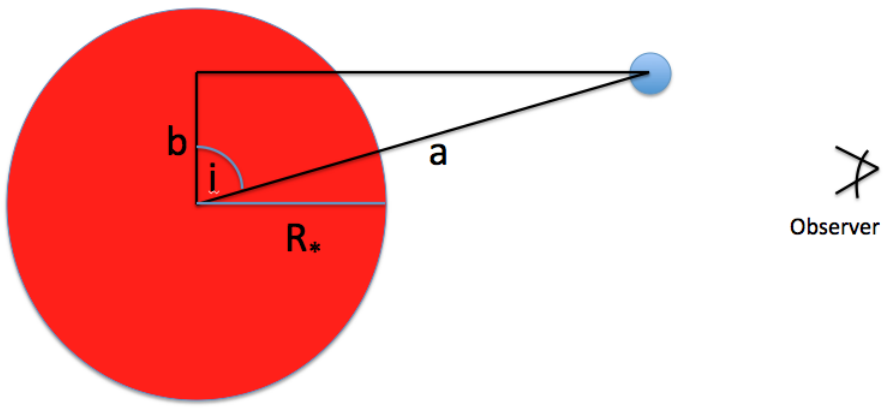

Fig. 3.12: The impact parameter, b, is a function of the planet's orbital distance, a, and the inclination of the plane of its orbit, i, with respect to an observer.

A planet is designated to be fully transiting if

$$\text{Full} : b \leq R_* - R_P \tag{3.15}$$

where R_P, is the radius of the planet. This is true for transits where the the full disc of the planet crosses the disk of the star.

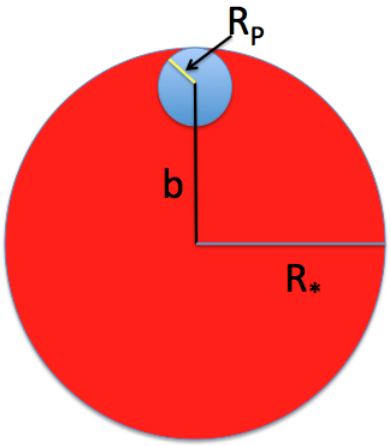

Fig. 3.13: A planet is determined to be fully transiting if the impact parameter, b, is less than or equal to the radius of the star, R_* minus the radius of the planet, R_p.

The drop in flux is easily described by

$$\frac{\Delta F}{F} = \left(\frac{R_P}{R_*}\right)^2 \tag{3.16}$$

However, it is also possible for a planet to go through a partial transit where there is still a drop in flux deep enough to be detected.

These partial transits can be identified by

$$\text{Partial} : R_* - R_P \leq b \leq R_* + R_P \tag{3.17}$$

The partial transit depths are calculated by finding the area of the stellar disk occulted by the partially transiting planet. This is found by calculating the area shared

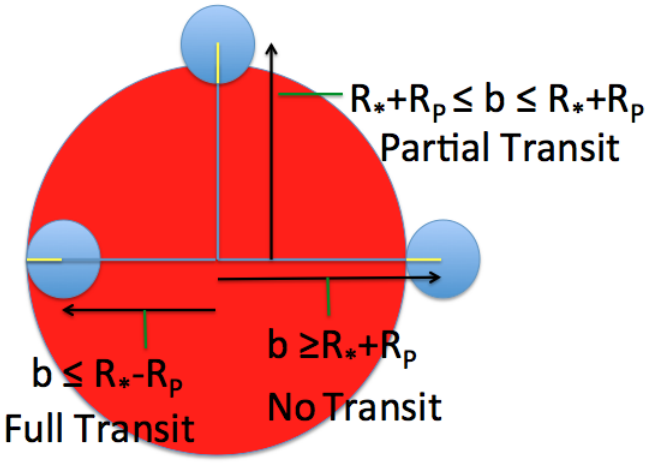

Fig. 3.14: Various possible transits and non-transits of a planet. Partial planets are also possible to detect where the planet's disk grazes the star's. This is described by R_* - R_P ≤ b ≤ R_* + R_P.

by the disk of the star and planet and is described as

$$\frac{\Delta F_{partial}}{F} = \frac{1}{\pi}\left(\theta_1 + \frac{b}{R_*^2}\theta_2 - \frac{R_p}{R_*} sin\,\theta_1\right) \tag{3.18}$$

where

$$\theta_1 = \sin^{-1}\left(\frac{b}{R_*}\right) \tag{3.19}$$

and

$$\theta_2 = \sin^{-1}\left(\frac{b}{R_p/R_*}\right) \tag{3.20}$$

The derivation for the transit depth of a partial transit can be found in Winn (2010).

3.3.2 Detection

Equations 3.16 and 3.18 provide the percentage drop in flux that results from the transit. The Kepler satellite has been able to observe planetary transits down to a precision of better than 0.1 per cent (Borucki et al., 2009) but the photometric precision

of ground-based observations are limited by fluctuations in the atmosphere. Currently, the two transiting planets that have been discovered from ground-based observations with the smallest transiting depth are(Wright et al., 2013): Wasp-72b which has a transit depth of 0.37 per cent (Gillon et al., 2013) and Hat-P-11b with a transit depth of 0.33 per cent (Bakos et al., 2010). However, all others are greater than 0.5 per cent. Therefore, a conservative estimate of the mean precision that is to be expected from ground-based observatories over the next 10 years is 0.5 per cent.

$$\frac{\Delta F}{F} > 0.005 \tag{3.21}$$

It is important to note that the motivation of this work is to gain statistics on how many photometric transits will be detected in the next 10 years. For a detection, it is generally accepted that 3 transits are needed before it can be confirmed. The upper limit for the orbital radius of detectable transiting planets is thus one where 3 transits can be observed in the next 10 years. This can easily be estimated using Kepler's third law, $P^2 M_* = a^3$, where M_* is the mass of the host star in Solar masses, P is the period in years, and a is, in this case, the orbital radius. Using information from Figure 3.3, the most massive host star is $\sim 3\ M_\odot$ and dictates the greatest orbital radius where 3 transits can be observed. After applying Kepler's third law, a maximum orbital distance of 3 au was determined and all planets that were detectable but had an orbital distance above 3 au were not included in the results. However, because of Equations 3.14 and 3.15, as a increases, the likelihood of a transit drops very quickly. For reference, the longest period of a transiting planet discovered from ground based observatories is Hat-P-15b with a period of 10.86 days (Kovács et al., 2010).

3.4 Simulation Results

Because inclinations were assigned randomly, a Monte Carlo simulation was run using the above methods as an input to find the probability of the number of detectable planets that will be detectable in the next 10 years. Out of the 9053 planets and selected

host stars, after iterating the simulation 6000 times, a mean value of 27 (σ=5.53) transiting planets are found to be detectable. This distribution is seen in Figure 3.15. This represents the expected number of transits that are observable within this sample.

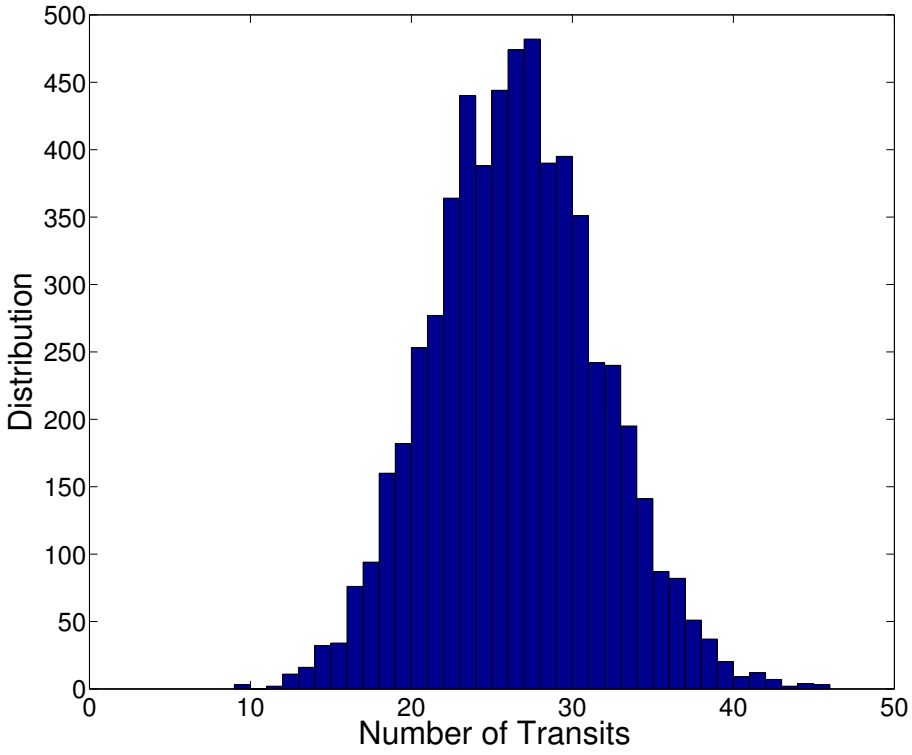

Fig. 3.15: Results of a Monte Carlo simulation showing the number of detectable transits expected over the next 10 years with these simulations. The distribution has a mean value of 27 with σ=5.53.

For each iteration, the mean values of the detected host star and planet properties were also found. The average host star T_{eff} and distance from Earth can be seen in Figures 3.16 and 3.17. The typical detectable transiting planet host star's T_{eff} is about 5300 K and its distance is 32 parsecs. The properties of the planets that were found to be transiting can be seen in Figures 3.18, 3.19, and 3.20. The mean orbital distance is 0.13 au and the mean mass is 3.15 M_{Jup}. The typical radius of the transiting planets is 9.13 R_{Earth}.

While these statistics are applicable to a large sample of the known stellar population within 50 parsecs, it is not entirely complete. Figure 3.21 shows the stellar sample's distance distribution with an obvious drop in numbers past 25 parsecs. This is due to 25 parsecs being the distance limit for the Gliese stars. Figure 3.21 also has

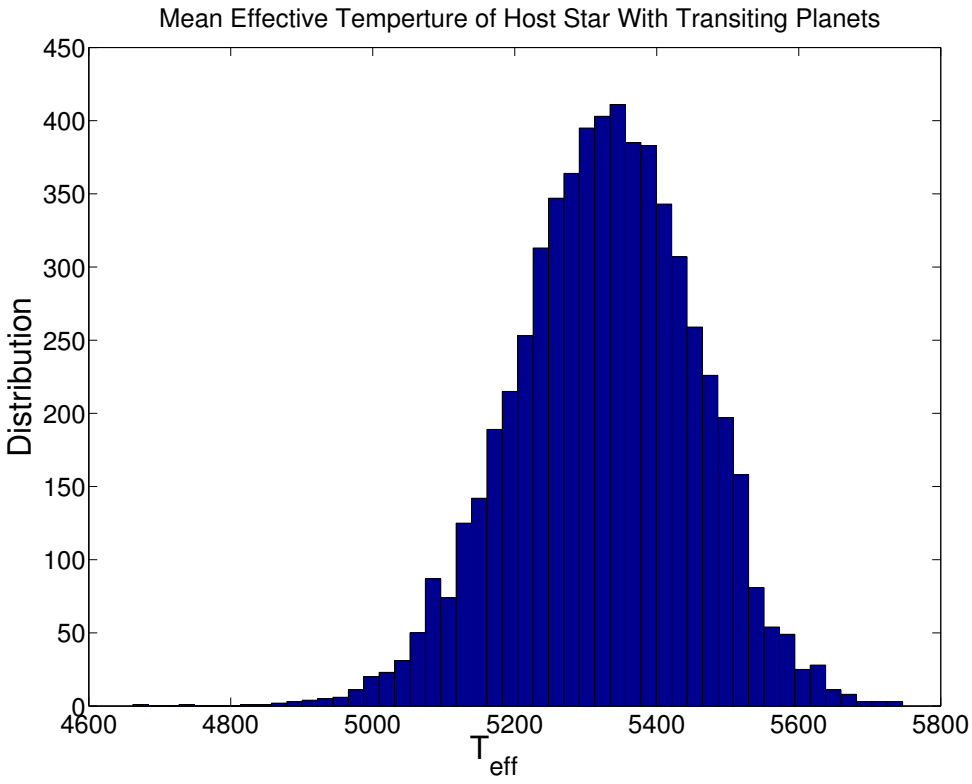

Fig. 3.16: For each iteration of the simulation, the mean T_{eff} of all host stars with a detected transiting planet was calculated and this figure shows the results of 6000 iterations of the simulation code. The mean of the distribution is 5327 K.

a red line showing the distribution that would exist if the density of stars remained constant as distance was increased. This is an approximation but a clear discontinuity begins after 15 parsecs implying that this sample is not complete. Therefore, though these statistics are representative of the known stellar population out to 50 parsecs, a more complete sample of stars is needed for them to be applied to the true local transiting planet population.

The local, dim stellar populations are not well characterized and are the subject of Chapter 4. The absence of this elusive group of objects may well contribute significantly to the apparent incompleteness of the known local population. Looking again at Figure 3.21 and assuming that the population less than 15 parsecs is more representative of the greater population, instead of ∼9000 stars within 50 parsecs, there would be closer to 40,000. Given that increase in the number of stars and assuming the same statistics could be applied as outlined above, that would imply a possible 4 fold increase in the number of nearby transiting planets, taking the mean closer to 140 transiting planets

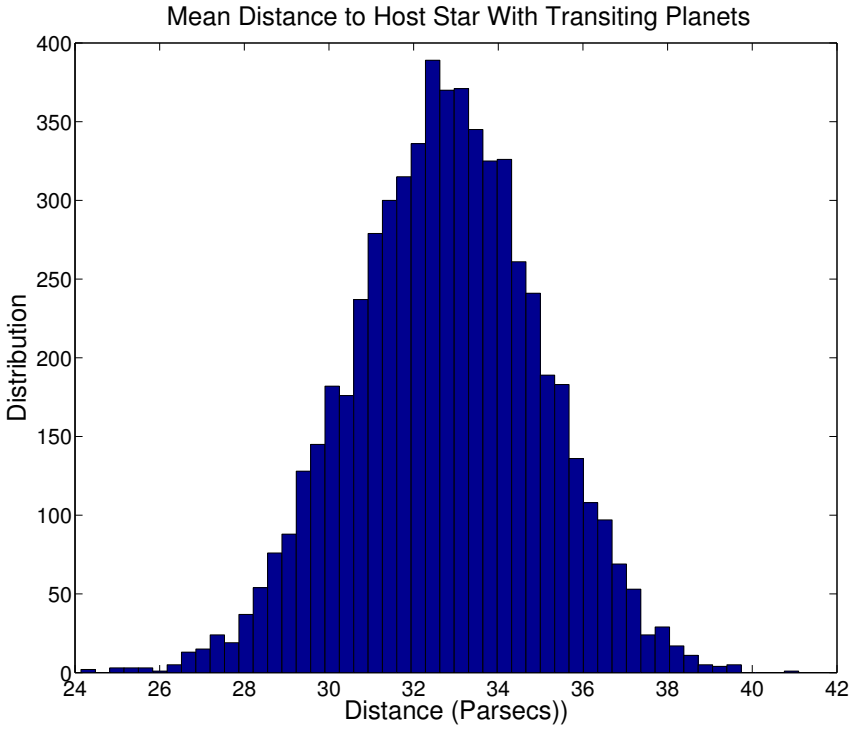

Fig. 3.17: As Figure 3.16 but showing the mean host star's distance in parsecs. The mean of the distribution is 32.75 parsecs away from Earth.

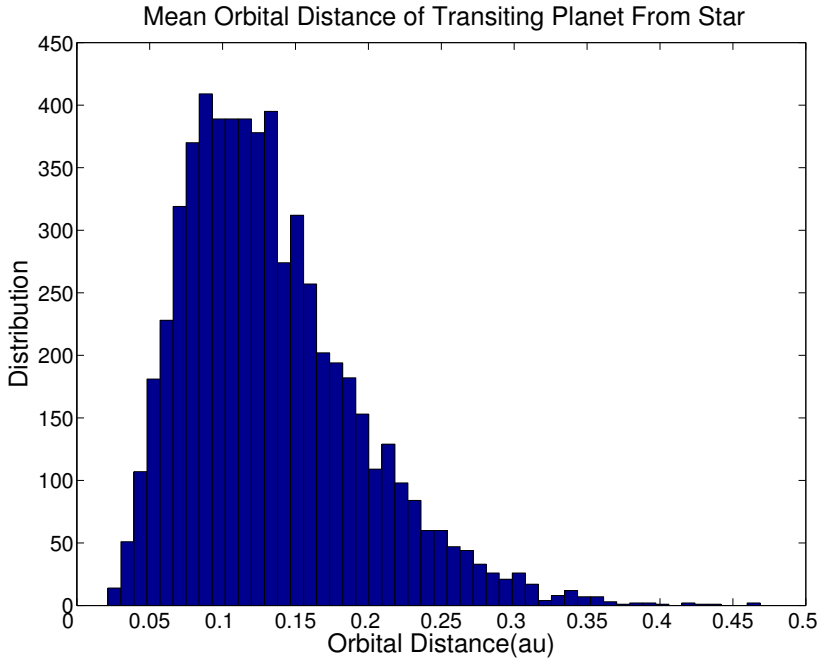

Fig. 3.18: As Figure 3.16 but showing the mean orbital distance of a planet that had a detectable transit. The mean of the distribution is 0.13 au.

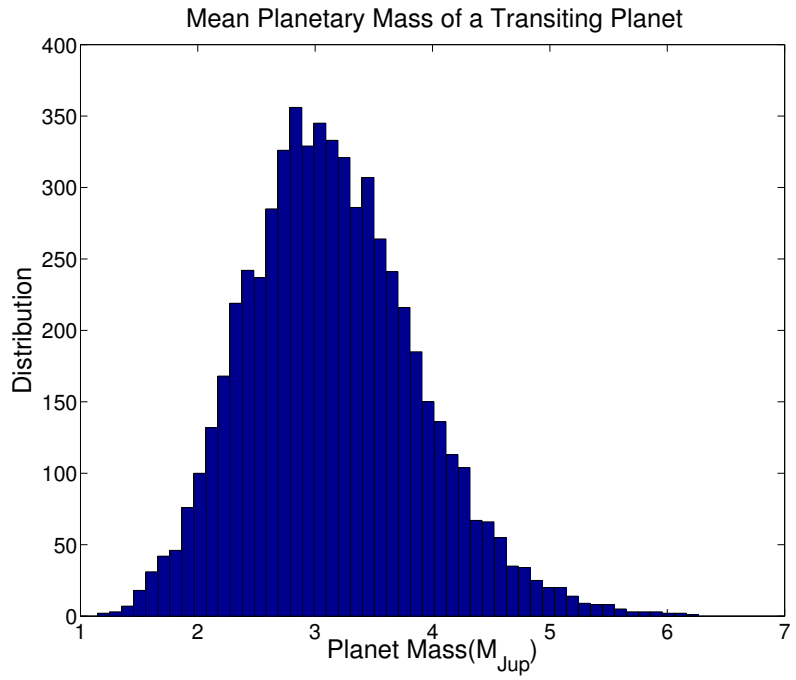

Fig. 3.19: As Figure 3.16 but showing the mean mass of a planet that had a detectable transit. The mean of the distribution is 3.15 M_{Jup}.

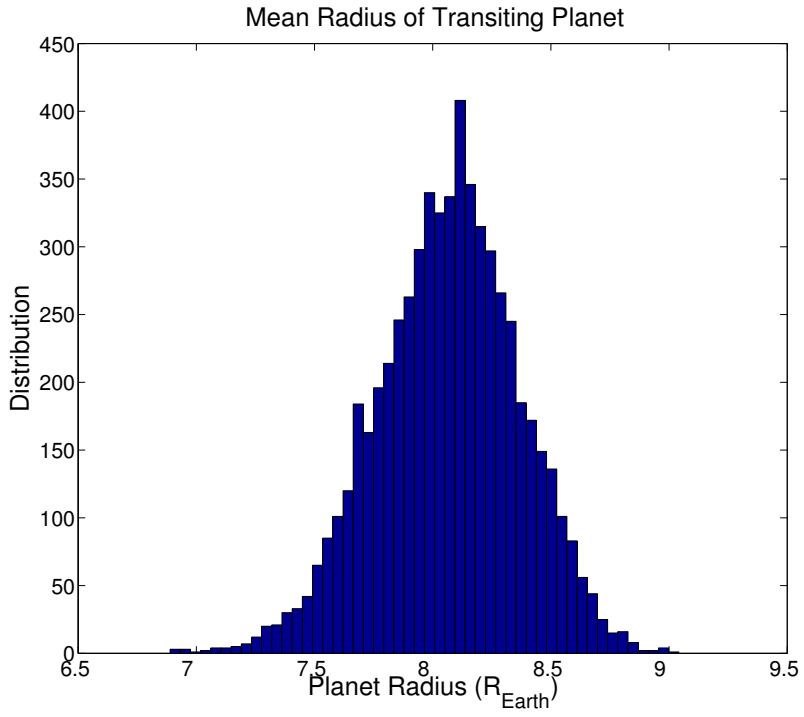

Fig. 3.20: As Figure 3.16 but showing the mean radius of a planet that had a detectable transit. The mean of the distribution is 9.13 R_{Earth}.

instead of 30.

These assumptions rely heavily on the current understanding of the exoplanet pop-

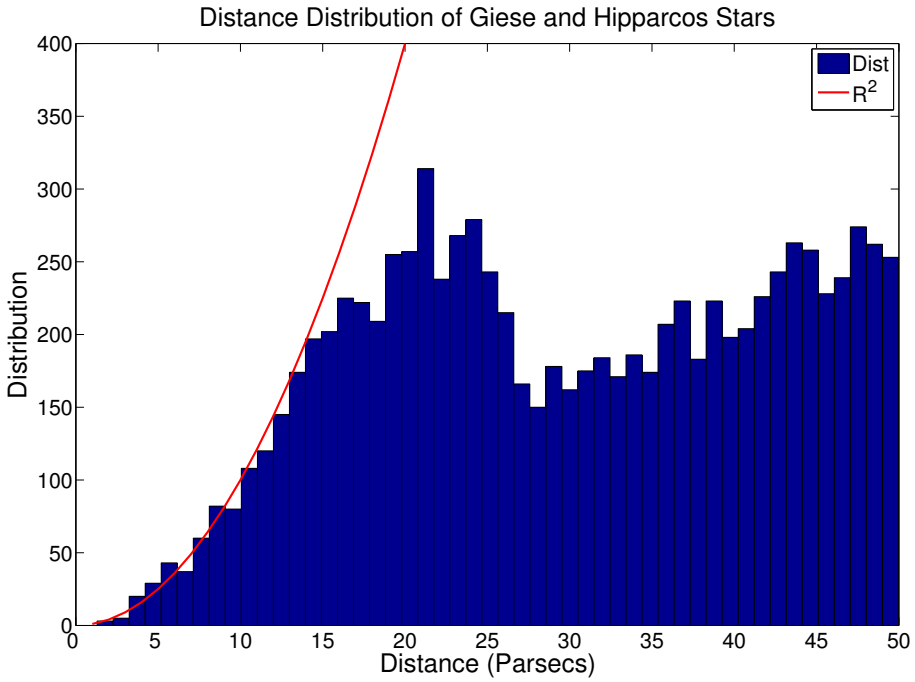

Fig. 3.21: The distance distribution of the stars used for these simulations. A clear drop in numbers is apparent after 25 parsecs which is caused by the Gliese stars only being sensitive down to that distance. The red line shows how the numbers would increase if number density of stars stayed constant as distance increased.

ulation with the mass distribution and orbital distance playing a huge role in whether a transiting planet is detectable. Adapting the simulated planet population's characteristics as new data become available will allow these results to better reflect the number of transiting planets we can expect around nearby stars.

3.5 Conclusions

These simulations have provided an estimate for the number of transits that can be expected to be found around the known local stellar population out to 50 parsecs as well as provided the stellar and planetary properties to expect from those transits. According to 6000 iterations of these simulations, roughly 27 transits can be expected to be found around this stellar population with the typical transiting planet being found around a star about 30 parsecs around a star with a T_{eff} of 5300 K. The typical planet will be about 3 M_{Jup} with a radius of $\sim$9 R_{Earth} at an orbit of 0.13 au.

One caveat to these conclusions is that the local M dwarf population is not well

characterized and is likely to make up 90 per cent of the local stellar population (Peryman & ESA, 1997). Expanding on the local bright M dwarf population is the focus of the following chapter.

References

Bakos, G. Á., Howard, A. W., Noyes, R. W., Hartman, J., Torres, G., Kovács, G., Fischer, D. A., Latham, D. W., Johnson, J. A., Marcy, G. W., Sasselov, D. D., Stefanik, R. P., Sipőcz, B., Kovács, G., Esquerdo, G. A., Pál, A., Lázár, J., Papp, I., & Sári, P. 2009, ApJ, 707, 446

Bakos, G. Á., Torres, G., Pál, A., Hartman, J., Kovács, G., Noyes, R. W., Latham, D. W., Sasselov, D. D., Sipőcz, B., Esquerdo, G. A., Fischer, D. A., Johnson, J. A., Marcy, G. W., Butler, R. P., Isaacson, H., Howard, A., Vogt, S., Kovács, G., Fernandez, J., Moór, A., Stefanik, R. P., Lázár, J., Papp, I., & Sári, P. 2010, ApJ, 710, 1724

Barnes, R. & Greenberg, R. 2005, in Bulletin of the American Astronomical Society, Vol. 37, AAS/Division for Planetary Sciences Meeting Abstracts #37, 672

Bonfils, X., Delfosse, X., Udry, S., Forveille, T., Mayor, M., Perrier, C., Bouchy, F., Gillon, M., Lovis, C., Pepe, F., Queloz, D., Santos, N. C., Ségransan, D., & Bertaux, J.-L. 2013, A&A, 549, A109

Borucki, W. J., Koch, D., Jenkins, J., Sasselov, D., Gilliland, R., Batalha, N., Latham, D. W., Caldwell, D., Basri, G., Brown, T., Christensen-Dalsgaard, J., Cochran, W. D., DeVore, E., Dunham, E., Dupree, A. K., Gautier, T., Geary, J., Gould, A., Howell, S., Kjeldsen, H., Lissauer, J., Marcy, G., Meibom, S., Morrison, D., & Tarter, J. 2009, Science, 325, 709

Boss, A. P., Basri, G., Kumar, S. S., Liebert, J., Martín, E. L., Reipurth, B., & Zinnecker, H. 2003, in IAU Symposium, Vol. 211, Brown Dwarfs, 529

Boss, A. P., Butler, R. P., Hubbard, W. B., Ianna, P. A., Kürster, M., Lissauer, J. J., Mayor, M., Meech, K. J., Mignard, F., Penny, A. J., Quirrenbach, A., Tarter, J. C., & Vidal-Madjar, A. 2007, Transactions of the International Astronomical Union, Series A, 26, 183

Chabrier, G. & Baraffe, I. 2000, ARA&A, 38, 337

Charbonneau, D., Irwin, J., Nutzman, P., & Falco, E. E. 2008, in Bulletin of the American Astronomical Society, Vol. 40, American Astronomical Society Meeting Abstracts #212, 242

Fortney, J. J., Marley, M. S., & Barnes, J. W. 2007, ApJ, 659, 1661

Gillon, M., Anderson, D. R., Collier-Cameron, A., Doyle, A. P., Fumel, A., Hellier, C., Jehin, E., Lendl, M., Maxted, P. F. L., Montalbán, J., Pepe, F., Pollacco, D., Queloz, D., Ségransan, D., Smith, A. M. S., Smalley, B., Southworth, J., Triaud, A. H. M. J., Udry, S., & West, R. G. 2013, A&A, 552, A82

Gliese, W. & Jahreiss, H. 1995, VizieR Online Data Catalog, 5070, 0

Haswell, C. A. 2010, Transiting Exoplanets

Hellier, C., Anderson, D. R., Collier Cameron, A., Gillon, M., Jehin, E., Lendl, M., Maxted, P. F. L., Pepe, F., Pollacco, D., Queloz, D., Ségransan, D., Smalley, B., Smith, A. M. S., Southworth, J., Triaud, A. H. M. J., Udry, S., & West, R. G. 2011, A&A, 535, L7

Johnson, J. A., Aller, K. M., Howard, A. W., & Crepp, J. R. 2010, PASP, 122, 905

Johnson, J. A., Butler, R. P., Marcy, G. W., Fischer, D. A., Vogt, S. S., Wright, J. T., & Peek, K. M. G. 2007, ApJ, 670, 833

Kovács, G., Bakos, G. Á., Hartman, J. D., Torres, G., Noyes, R. W., Latham, D. W., Howard, A. W., Fischer, D. A., Johnson, J. A., Marcy, G. W., Isaacson, H., Sasselov, D. D., Stefanik, R. P., Esquerdo, G. A., Fernandez, J. M., Lázár, B. B. J., Papp, I., & Sári, P. 2010, ApJ, 724, 866

Lammer, H., Odert, P., Leitzinger, M., Khodachenko, M. L., Panchenko, M., Kulikov, Y. N., Zhang, T. L., Lichtenegger, H. I. M., Erkaev, N. V., Wuchterl, G., Micela, G., Penz, T., Biernat, H. K., Weingrill, J., Steller, M., Ottacher, H., Hasiba, J., & Hanslmeier, A. 2009, A&A, 506, 399

Lang, K. R. 1992, Astrophysical Data I. Planets and Stars.

Lépine, S. & Shara, M. M. 2005, AJ, 129, 1483

Li, S.-L., Miller, N., Lin, D. N. C., & Fortney, J. J. 2010, Nature, 463, 1054

Mandel, K. & Agol, E. 2002, ApJ, 580, L171

Matsuo, T., Shibai, H., Ootsubo, T., & Tamura, M. 2007, ApJ, 662, 1282

Muirhead, P. S., Johnson, J. A., Apps, K., Carter, J. A., Morton, T. D., Fabrycky, D. C., Pineda, J. S., Bottom, M., Rojas-Ayala, B., Schlawin, E., Hamren, K., Covey, K. R., Crepp, J. R., Stassun, K. G., Pepper, J., Hebb, L., Kirby, E. N., Howard, A. W., Isaacson, H. T., Marcy, G. W., Levitan, D., Diaz-Santos, T., Armus, L., & Lloyd, J. P. 2012, ApJ, 747, 144

Perryman, M. A. C. & ESA, eds. 1997, ESA Special Publication, Vol. 1200, The HIPPARCOS and TYCHO catalogues. Astrometric and photometric star catalogues derived from the ESA HIPPARCOS Space Astrometry Mission

Perryman, M. A. C., Lindegren, L., Kovalevsky, J., Hoeg, E., Bastian, U., Bernacca, P. L., Crézé, M., Donati, F., Grenon, M., Grewing, M., van Leeuwen, F., van der Marel, H., Mignard, F., Murray, C. A., Le Poole, R. S., Schrijver, H., Turon, C., Arenou, F., Froeschlé, M., & Petersen, C. S. 1997, A&A, 323, L49

Reed, B. C. 1998, JRASC, 92, 36

Snellen, I., Stuik, R., Otten, G., Bettonvil, F., Navarro, R., Kenworthy, M., de Mooij, E., ter Horst, R., Le Poole, R., Lesage, A.-L., & Spronck, J. 2013, in European Physical Journal Web of Conferences, Vol. 47, European Physical Journal Web of Conferences, 3008

Sozzetti, A., Bernagozzi, A., Bertolini, E., Calcidese, P., Carbognani, A., Cenadelli, D., Christille, J.-M., Damasso, M., Giacobbe, P., Lanteri, L., Lattanzi, M. G., & Smart, R. 2013, in European Physical Journal Web of Conferences, Vol. 47, European Physical Journal Web of Conferences, 3006

Spiegel, D. S., Burrows, A., & Milsom, J. A. 2011, ApJ, 727, 57

Tessenyi, M., Ollivier, M., Tinetti, G., Beaulieu, J. P., Coudé du Foresto, V., Encrenaz, T., Micela, G., Swinyard, B., Ribas, I., Aylward, A., Tennyson, J., Swain, M. R., Sozzetti, A., Vasisht, G., & Deroo, P. 2012, ApJ, 746, 45

Torres, G., Stefanik, R. P., Andersen, J., Nordstrom, B., Latham, D. W., & Clausen, J. V. 1997, AJ, 114, 2764

Wheatley, P. J., Pollacco, D. L., Queloz, D., Rauer, H., Watson, C. A., West, R. G., Chazelas, B., Louden, T. M., Walker, S., Bannister, N., Bento, J., Burleigh, M., Cabrera, J., Eigmüller, P., Erikson, A., Genolet, L., Goad, M., Grange, A., Jordán, A., Lawrie, K., McCormac, J., & Neveu, M. 2013, in European Physical Journal Web of Conferences, Vol. 47, European Physical Journal Web of Conferences, 13002

Williams, I. P. 2003, Celestial Mechanics and Dynamical Astronomy, 87, 13

Winn, J. N. 2010, ArXiv e-prints

Wright, J. T., Fakhouri, O., Marcy, G. W., Han, E., Feng, Y., Johnson, J. A., Howard, A. W., Fischer, D. A., Valenti, J. A., Anderson, J., & Piskunov, N. 2011, PASP, 123, 412

Wright, J. T., Kakhouri, O., Marcy, G. W., Han, E., Feng, Y., Johnson, J. A., Howard, A. W., Fischer, D. A., Valenti, J. A., Anderson, J., & Piskunov, N. 2013, VizieR Online Data Catalog, 612, 30412

Chapter 4: A catalogue of bright ($K < 9$) M dwarfs

The following chapter contains the unedited journal paper published by Frith et al. (2013), which was submitted and accepted for publication in the Monthly Notices of the Royal Astronomical Society (MNRAS) in volume 435, issue 3, pages 2161–2170. The associated catalogue produced by this article can be found on the MNRAS website at http://mnras.oxfordjournals.org/content/suppl/2013/08/30/stt1436.DC1/Frith_lep_comb_klessthan9.txt.

4.1 Abstract

Using the Position and Proper Motion Extended-L (PPMXL) catalogue, we have used optical and near-infrared colour cuts together with a reduced proper motion cut to find bright M dwarfs for future exoplanet transit studies. PPMXL's low proper motion uncertainties allow us to probe down to smaller proper motions than previous similar studies. We have combined unique objects found with this method to that of previous work to produce 8479 $K < 9$ M dwarfs. Low resolution spectroscopy was obtained of a sample of the objects found using this selection method to gain statistics on their spectral type and physical properties. Results show a spectral type range of K7-M4V. This catalogue is the most complete collection of $K < 9$ M dwarfs currently available and is made available here.

4.2 Introduction

Identification of M dwarfs in large surveys has been difficult even though they are the most numerous type of stars in the Galaxy. This is due to their colours and low luminosities often causing them to be confused with reddened stars or distant red giants. M dwarfs have become of particular interest in recent years for their applications to

exoplanet research. Their low masses and small radii lead to greater sensitivity to discovery of orbiting low mass planets via the radial velocity and transit techniques. Furthermore, due to an M dwarf's low luminosity, planets lying in the habitable zone around M dwarfs have short orbital periods as well as relatively favourable contrast ratios between the planet and the host star. New space facilities like the James Web Space Telescope (Clampin, 2010) (JWST) and the proposed Exoplanet charactersation Observatory (Tinetti et al., 2012) offer the potential to study exoplanet atmospheres for super Earths transiting M dwarfs but currently M dwarf transit detections are very rare.

5 M dwarfs are currently known to host transiting planets: GJ1214b, GJ3470, GJ436, KOI-961, and KOI-254. With the exception of the two Kepler systems (Johnson et al., 2012; Muirhead et al., 2012), the host stars are all bright in the near-infrared (K=6.1-8.8) and the systems are thus good targets for characterisation. Two of these were discovered using the radial velocity (RV) method (GJ436b and GJ3470b; Gillon et al. (2007); Bonfils et al. (2012)) and have masses similar to Neptune (15-20$M_{\oplus}$), while GJ1214b was discovered by the Mearth survey using the transit method (Charbonneau et al., 2009) and has a mass of 5.9$M_{\oplus}$. GJ1214b is currently the only known system with a Super-Earth transiting a bright M dwarf. The first step towards expanding this number is to identify all potential bright M dwarf host stars in the sky for future transit search campaigns.

Other recent studies in this area (overlapping with this work) include the catalogue of Lépine & Gaidos (2011;LG11). This sample was created from the LSPM catalogue (Lépine & Shara, 2005) and supplemented with Tycho-2 (Høg et al., 2000) objects but is limited at low proper motions due to the SUPERBLINK proper motion limit of 40 milli arcseconds (mas) per year. Our efforts attempt to optimize the search at the low proper motion extreme and thus expand on the existing sample. We have chosen to use the Position and Proper Motion Extended-L (PPMXL) (Roeser et al., 2010) as the starting point for a selection process that utilizes a multi-band colour selection and a reduced proper motion cut to isolate bright M dwarfs down to the lowest practical proper motion limits.

4.3 Sample Selection

4.3.1 The PPMXL Catalogue

The PPMXL catalogue represents a combination of the USNO-B1.0 (Monet et al., 2003) and 2MASS (Skrutskie et al., 2006) catalogues mapped onto the International Celestial Reference Frame (ICRF) (Ma et al., 1998). The ICRF is based on distant extragalactic radio sources observed by the Very Large Baseline Array as its reference points which allows proper motions to be described in a quasi-absolute manner as opposed to relative. Until the PPMXL catalogue was developed, only relative proper motions were available for the USNO-B1.0 objects and 2MASS did not have any proper motion information. PPMXL now provides low uncertainties for both the proper motion and position for many of the objects within the 2 catalogues. Typical uncertainties for proper motions are 4-10 mas/yr. The near-infrared (NIR) JHK magnitudes from 2MASS and the optical BVRI magnitudes from USNO-B1.0 also provides very useful colour information about the objects and is used during the sample selection process. At low proper motions, it is important to minimize measurement uncertainties so absolute proper motions will lead to less contamination as the astrometry becomes more noisy.

4.3.2 Magnitude Limit

A principal aim of this work is to target a stellar sample around which potential exoplanet atmospheres could be studied in the future. It was therefore appropriate to limit the selection to sufficiently bright targets that provide enough signal to probe the molecules of interest in exoplanet atmospheres. Even with bright host stars and favourable contrast ratios between the exoplanet and star, several observations of the transiting planet through both primary and secondary transits have to be co-added together to produce observations of any accuracy. Because of this, integration time can be equated to the number of transits necessary to achieve the needed signal to noise. Simulations were conducted by Tessenyi et al. (2012) to estimate the number of transits needed for a range of exoplanet sizes and host star brightnesses. They have

shown that for a space-based multi-channel spectrograph with a modest sized primary (1.2m) to achieve the signal to noise necessary to identify molecules in a transiting super earth in the habitable zone, the number of transits needed around M dwarfs with a magnitude of $K > 9$ becomes unrealistic when planning a space mission observing schedule. Therefore, a magnitude limit of $K < 9$ was implemented. Objects with uncertainties in JHK photometry greater than 0.05 magnitudes were also removed to limit saturated targets within the sample.

4.3.3 Guiding Samples

To help in our various colour and reduced proper motion selections, we identified several guiding samples using existing catalogues. Several M dwarf samples exist in the literature that have been observed spectroscopically and photometrically across many bands. In total, three M dwarf samples were used. One sample was produced by Bochanski et al. (2005) in a spectroscopic survey for cool stars within 100 parsecs of the Sun. These M dwarfs were selected using one optical (R-I) colour cut with no proper motion selection and later confirmed with spectroscopy. Another sample used was the Palomar/MSU (PMSU) spectroscopic survey (Reid et al., 1997) which is based on M dwarfs that were selected by using parallax measurements. Spectra were obtained of objects found in the Third Catalogue of Nearby Stars (CNS3) (Gliese & Jahreiß, 1991) which consists of stars within 25 parsecs of the Sun. The third M dwarf selection was done by Riaz et al. (2006) and was compiled to find active M dwarfs using X-ray observations from ROSAT. This had limited NIR colour selection and no kinematic bias. By using the combination of all 3 catalogues as guides, it is hoped that we can minimize any kinematic or photometric bias that may be incurred during our selection process. All 3 catalogues were cross-matched with PPMXL with a cone radius of 10 arcseconds and the best matched objects used as comparisons to our sample.

Distant M giants were a major source of potential contamination so a guiding sample of giants was also used from Famaey et al. (2005). This sample consists of giants with known distances and absolute magnitudes from the Hipparcos catalogue

(Perryman et al., 1997). Though the majority of the sample consists of K giants, there are a significant number of M giants identified that were used below when attempting to remove potential giant contamination. These objects were also cross matched with PPMXL so that all guiding samples had proper motion estimates mapped onto the ICRS.

To supplement the M giant guiding samples, we constructed a photometric selection using colour cuts. Our colour defined giant sample was created using a near infrared (NIR) colour selection from Sharma et al. (2011) which is reproduced here:

$$\begin{aligned} K &< 14 \\ J - K &\geq 0.85 \\ J - H &< 0.561(J - K) + 0.36 \\ J - H &> 0.561(J - K) + 0.19 \end{aligned}$$

This selection was applied to areas of sky avoiding the galactic plane to reduce the number of reddened stars selected. As seen in Figure 4.1, these cuts slightly overlap the region of M dwarfs in NIR colour space but the majority of the sample is well separated from the M dwarf region (described in the next section). This overlap illustrates how colour cuts alone don't completely isolate an M dwarf or M giant population.

4.3.4 Colour Selections

The initial colour selection for our sample was done using the 2MASS near-infrared JHK bands. These cuts were made to separate the M dwarfs from M giants as well as to limit K dwarf contamination. The guiding samples were used to define the colour regions where most M dwarfs lie as can be seen in Figure 4.1. Our resulting NIR selection criteria for M dwarfs are

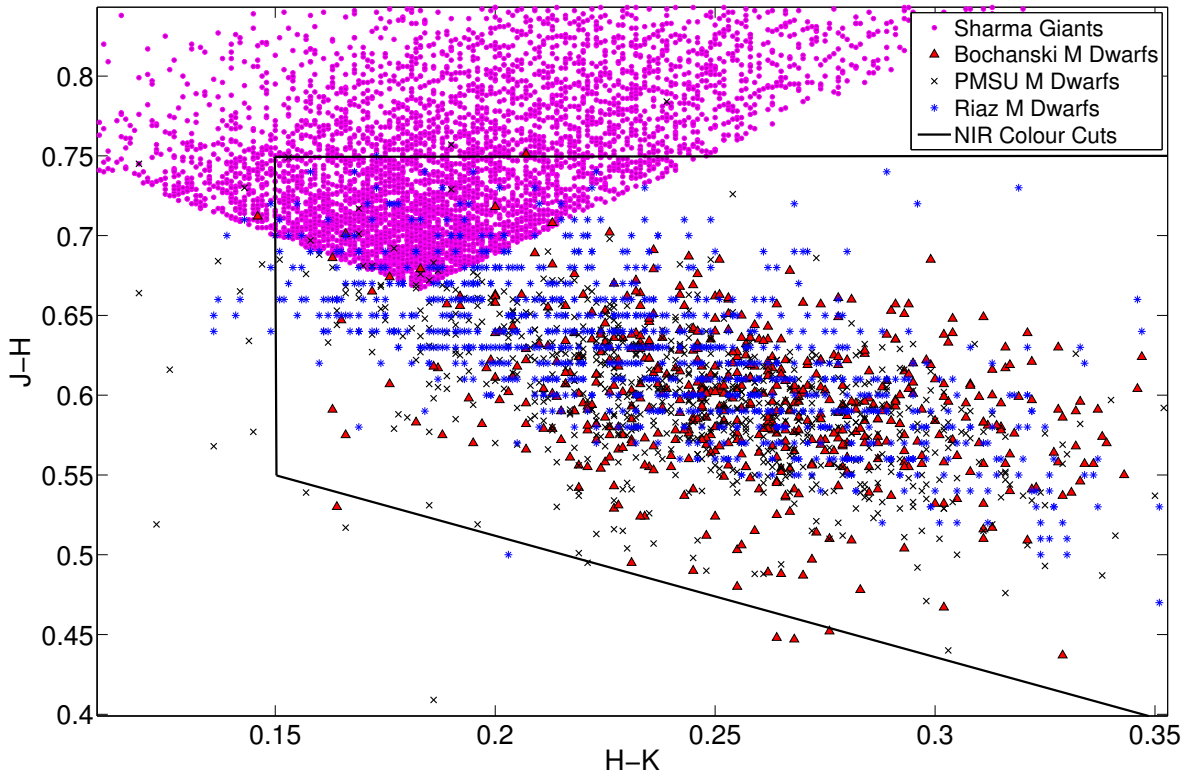

Fig. 4.1: Colour-colour plot showing the NIR selection and the M giant and M dwarf guiding samples. The different coloured triangles are known M dwarfs from previous surveys and are used to illustrate where M dwarfs can be expected to be found. Our colour defined M giant population created from PPMXL objects is shown as open squares. The overlap between the two populations demonstrates that M giants can overlap the same colour space as dwarfs and shows that futher cuts are needed.

$$J - K > 0.7$$

$$H - K > 0.15$$

$$J - H < 0.75$$

These regions isolate the general area of the M dwarf population. However, PPMXL also provides the photometry from USNO-B1 optical bands for many of its targets. Spectroscopically confirmed M dwarfs in PPMXL combined with K dwarfs from PMSU were used to determine where K dwarfs separate from M dwarfs in the colour space. All of the available colours were plotted against their spectral type and an example is seen in Figure 4.2. For the colours where the K dwarfs weren't available, the cut

was made on the blue end of the main body of the guiding samples. The following selections are used to isolate M dwarfs.

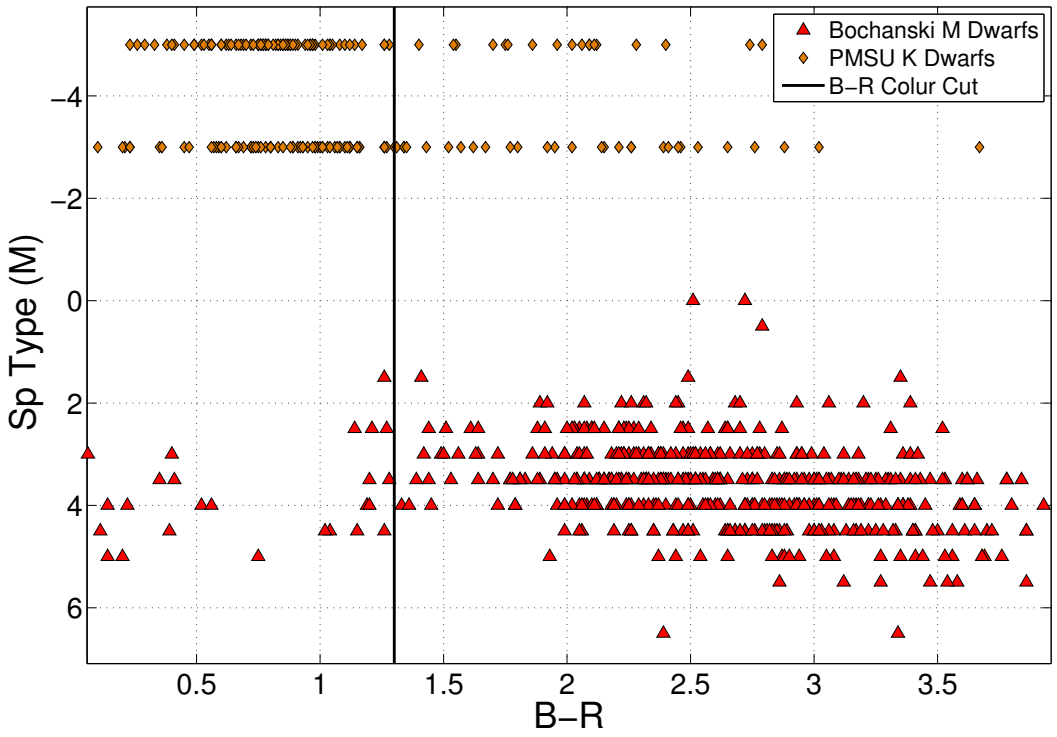

Fig. 4.2: Known M dwarfs plotted with PPMXL colours (red triangles) along with known K dwarfs (orange diamonds). The optical cut (vertical black line) was chosen to optimize the inclusion of M dwarfs and to minimize K dwarf contamination by removing all objects bluer than a B-R of 1.3. This process was repeated in all of the available optical pass bands in order to determine the optical colour cuts.

$$B - R > 1.3$$

$$B - I > 2.5$$

$$V - J > 2.7$$

$$R - I > 0.9$$

$$I - J > 0.6$$

Applying all of the NIR and optical colour cuts to the existing sample from PMSU removes approximately 88% of the K dwarfs and keeps 95% of the M dwarfs which gives

an indication of the amount of K dwarf contamination expected in the final selection of M dwarfs.

4.3.5 Proper Motion Uncertainty

Objects with high proper motion uncertainties were removed using the relationship

$$\mu < 5\sigma$$

where μ is the total measured proper motion of the object and σ is the listed uncertainty. Doing this removed any objects which had uncertainties that were a significant fraction of their total proper motions. This obviously tended to remove objects that had very low proper motions ($\mu < 15mas$) or non-moving objects and helped to minimize giant contamination.

4.3.6 Galactic Plane Removal

Due to overcrowding and dust, stars within the plane of the Milky Way can often have unreliable colours and proper motions. These objects were avoided by removing regions within the galactic plane that had a high density of stars and dust. These regions can be seen in Figure 4.3. After the initial K<9 cut, regions were removed where there was visible crowding or where there was an over density of red stars.

4.3.7 Reduced Proper Motion Selection

When distance to an object is not known, the reduced proper motion, H, can be used as a proxy for absolute magnitude. H is defined as

$$H = m + 5log\mu + 5,$$

where m is the observed magnitude and μ is the proper motion in arcseconds/year. This can also be used to separate different kinematic populations between the disk and

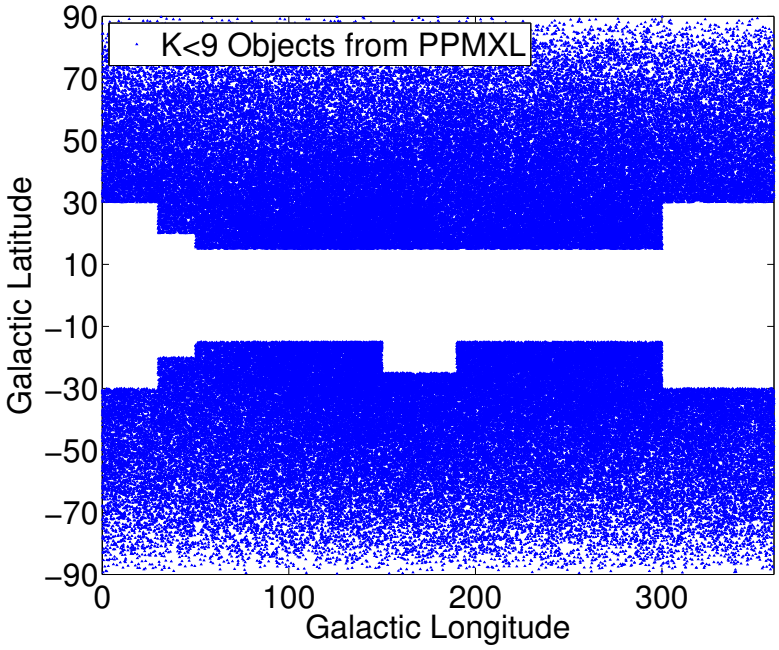

Fig. 4.3: This shows PPMXL K<9 objects across the sky. Regions where we detected an over density of red stars were removed. This roughly corresponded to areas of sky with a density above 45 stars per square degree. The majority of the regions cut can be defined by simply removing anything within 15 degrees of the galactic plane. Slightly higher galactic latitude regions near the galactic center where the density of stars was high (notably around a galactic longitude of 150-200) were also removed where there was an overdensity of very red objects.

halo but the primary use within this work is to separate the dwarfs from the giants within our sample. Because our brightness limit is defined using K magnitudes, we chose to use this band to determine our reduced proper motion cuts.

Since the reduced proper motion is analogous to absolute magnitude, plotting H along with a colour index provides us with a pseudo-equivalent of an Hertzsprung-Russell diagram where the brighter giant branch is separated vertically from the fainter red dwarfs. We use this, along with the giant and M dwarf guide samples (discussed in section 4.3.3), as a way of identifying the different populations within our sample. We were able to take advantage of PPMXL's wide range of colour space to precisely explore the completeness of the chosen H cut and this is illustrated Figure 4.4. These plots show the PPMXL objects that remain after the NIR and optical colour cuts as blue diamonds. The high proper motion (μ >150 mas/year) stars are plotted separately as filled in diamonds while those with μ <150 mas/year as empty diamonds. Giants from our guiding samples are plotted as red squares and magenta crosses. We can see

Table 4.1: This table shows how many objects are removed from the 4 other guiding catalogues (cross matched with PPMXL) if an $H_k \geq 6.0$ cut is applied.

Catalogue	Percent Rejected by $H_k \geq 6.0$
Bochanski M Dwarfs	3.7%
PMSU M Dwarfs	4.0%
Riaz M Dwarfs	18.7%
Famaey Giants	98.7%

a clear vertical separation between the giant populations and the majority of the our objects. The high proper motion objects extend in a clear manner down to an $H_{\rm K} = 6.0$. M dwarf candidates below $H_{\rm K} = 6.0$ begin to become mixed with the two giant populations and over densities in the PPMXL objects can be seen in the bluer regions of the B-R and V-J plots around an $H_{\rm K}$ of 5.8. After these considerations, objects with $H_{\rm K} \geq 6.0$ were chosen to best optimize giant removal and dwarf selection. This cut removed 293 objects.

To examine the completeness resulting from our reduced proper motion cut, we applied the same cut to our guiding samples as well. The results of this can be seen in Table 4.1. The Bochanski and PMSU M dwarfs only lose about 4% of their objects after this cut. Both catalogues are proper motion independent and target stars using an optical colour cut so a similar completeness level between the two is to be expected. However, almost 20% are lost from the Riaz M dwarfs. This is not surprising since the Riaz M dwarfs were selected primarily due to X-Ray activity and therefore have no lower proper motion cut off in their selection. Because of this, many of its targets have proper motions that lie well below the threshold of our reduced proper motion cut. From this, an incompleteness between 4 - 20% is a reasonable estimate for our selection methods. Encouragingly, 98% of our example giant star population is rejected using this reduced proper motion cut.

An $H_k \geq 6.0$ cut corresponds to a lower proper motion limit for the faintest objects of 25 mas/yr. This allows us to probe down below the LG11 limit of 40 mas/yr for for targets fainter than K = 8.0.

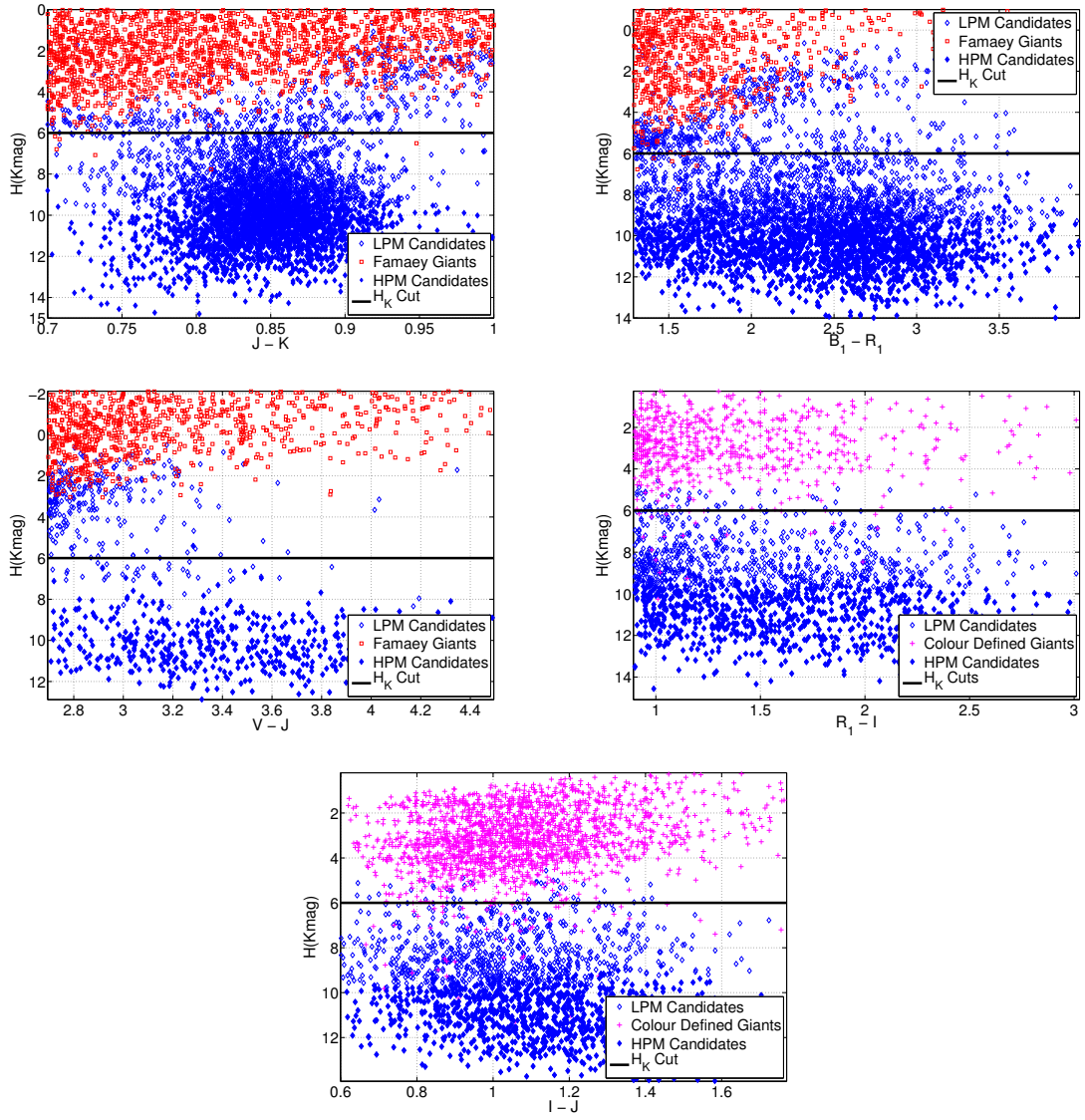

Fig. 4.4: Reduced proper motion vs the multiple colour indices available for the M dwarf candidates. The lines show the reduced proper motion cut used to remove the M giants from the sample. High proper motion candidates (HPM) with μ >150 mas/year from PPMXL have been plotted separately to better show the region where M dwarfs can be expected to lie since these objects are less likely to be mistaken for giants. Known giants have been taken from the samples described in Section 2.3 to illustrate where giants can be found. The Famaey giants did not have I magnitudes available so for the colours where I magnitude was needed, giants were defined using colour cuts from Sharma et al. A reduced proper motion cut of $H_k \geq 6$ was found to be high enough to safely remove objects that were likely to be giants and still low enough to include many low proper motion M dwarfs that were previously unclassified.

4.3.8 Tycho-2

For completeness, we have used the Tycho-2 catalogue (Høg et al., 2000) to augment our existing PPMXL sample. The above NIR colour cuts were applied to 2MASS objects that shared a Tycho-2 detection and the reduced proper motion cut applied using proper motions from Tycho-2. The resulting objects were crossmatched with PPMXL using a 5 arcsec radius and the other cuts were applied. Many of the resulting objects were already included in the sample from PPMXL, however 93 of the objects were found to be unique and were added to the total catalogue.

4.4 Final Sample

After application of all the above cuts, 4054 bright M dwarf candidates remain. In Table 4.3, we list the number of M dwarf candidates that remain across different K band magnitude ranges. Many of these candidates fall into the same parameter space as LG11 so we have also listed objects from their catalogue. A cross match was done between the two at a separation of 5 arcseconds and 2861 of the candidates were found to be shared. The common object's are also included in Tabel 4.3 for comparison.

The two catalogues targeted slightly different magnitude ranges (K<9 and J<10 for this work and LG11 respectively) so to facilitate a comparison between this work and the LG11 sample we have applied two simple cuts to the catalogue of LG11. We only select objects with K<9 and reject objects from the region of the galactic plane not included in our selection. In this way, we can focus on the main differences between the two catalogues: colour selection, reduced proper motion selection, and using PPMXL or SUPERBLINK for the proper motion measurements. As seen in Figures 4.6 and 4.7, this work's sample is able to identify M dwarf candidates down to a lower proper motion whereas LG11 does better at higher proper motions. This is expected, however, because PPMXL objects are cross matched between USNO-B1 and 2MASS with a cone radius of 2 arcseconds whereas the SUPERBLINK comparisons can be as large as 1.5 arcminuts. This difference gives SUPERBLINK greater sensitivity to objects with higher proper motions.

Figure 4.5 show's this work and LG11 in NIR colour space. This shows that many of the objects in LG11 lie in a region that is bluer than the scope of this work and thus includes stars of earlier spectral types.

A machine readable file has been created containing all of the M dwarfs in this work as well as those that were found to be unique to LG11 in the $K < 9$ magnitude range. This file is thus the most complete sample in the $K < 9$ brightness range currently available. An example of entries in the catalogue can be seen in Table 4.2.

Table 4.2: Example of final bright M dwarf catalogue.

Index	α (°)	δ (°)	μ_α (mas yr^-1)	μ_δ (mas yr^-1)	$\sigma\mu_\alpha$ (mas yr^-1)	$\sigma\mu_\delta$ (mas yr^-1)	K[a] (mag)	$J-K$ (mag)	$H-K$ (mag)	B[b] (mag)	R (mag)	Fl[c]
FR0001	0.028530	69.717120	136.0	-2.0	–	–	8.84	0.86	0.28	–	12.60	2
FR0002	0.087700	-8.037150	29.0	-96.0	–	–	8.27	0.85	0.20	–	11.80	2
FR0003	0.144917	-5.552002	187.8	67.5	5.3	5.3	8.17	0.83	0.22	13.50	11.16	1
FR0004	0.163530	18.488850	335.0	195.0	–	–	7.64	0.80	0.15	12.91	10.30	2
FR0005	0.195287	-35.168330	355.6	-114.9	4.1	4.1	8.28	0.84	0.20	13.20	10.86	1
FR0006	0.195902	16.402781	12.4	-135.1	4.8	4.8	8.46	0.86	0.23	14.40	11.38	1
FR0007	0.303580	13.972050	25.0	144.0	–	–	7.53	0.83	0.18	13.67	–	2
FR0008	0.357630	-16.948410	299.0	-255.0	–	–	7.22	0.80	0.19	12.14	9.80	2
FR0009	0.371550	47.414660	170.0	-4.0	–	–	8.83	0.84	0.19	–	11.40	2
FR0010	0.399370	-8.244880	97.0	-77.0	–	–	8.91	0.88	0.21	–	11.70	2

[a]JHK magnitudes taken from 2MASS (mean uncertainty ∼0.02).
[b]B and R magnitudes taken from USNO-B1 (mean uncertainty ∼0.3 magnitudes).
[c]Flag identifying origin of proper motion information(1:PPMXL, 2:SUPERBLINK, 3:Tycho-2).

Table 4.3: Number of bright M dwarfs that have been found by this work and LG11.

K	This Work	LG11	Common Objects	Total
<4	0	3	0	3
4-5	14	28	13	29
5-6	62	140	57	145
6-7	195	490	169	516
7-8	675	1626	523	1778
8-9	3108	4999	2099	6008

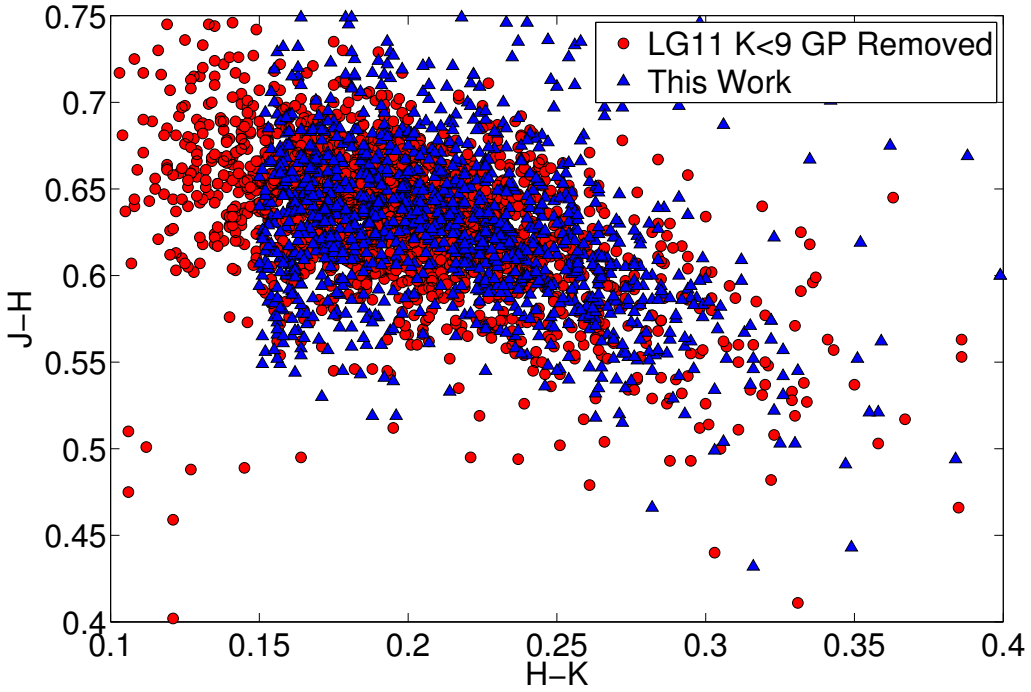

Fig. 4.5: Colour-colour diagram with the PPMXL selected M dwarfs as well as M dwarfs from LG11 (with magnitude and galactic plane cuts applied) to compare the two M dwarf selection methods. The LG11 sample's cut in H-K space allowed slightly more blue objects into that selection than this work.

4.5 Low Resolution Spectroscopy

4.5.1 Observations

Spectra were taken for a group of objects to give an indication of how effective the selection process weeded out giant contamination and to gain statistics on spectral type, temperature and metalicity of the M dwarf candidates. Candidates were chosen solely based on whether they had observationally favourable locations on the sky at the time and place of the observations.

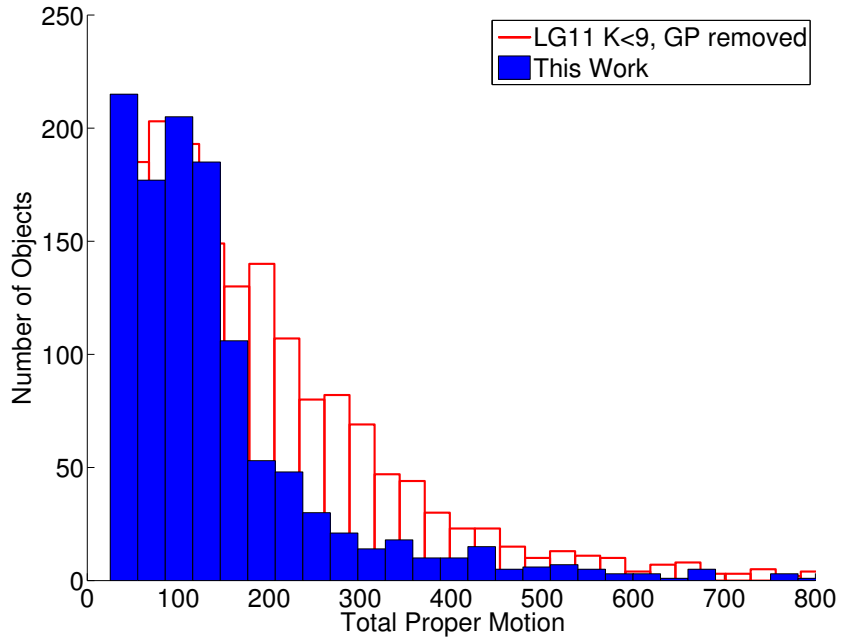

Fig. 4.6: Histogram showing the proper motion distribution of the objects that were unique to each sample. The LG11 has had the same galactic plane cut as this work and a magnitude cut of K< 9 to better compare the selection methods. LG11 is better on the high proper motion end whereas this work does slightly better at the low proper motion objects.

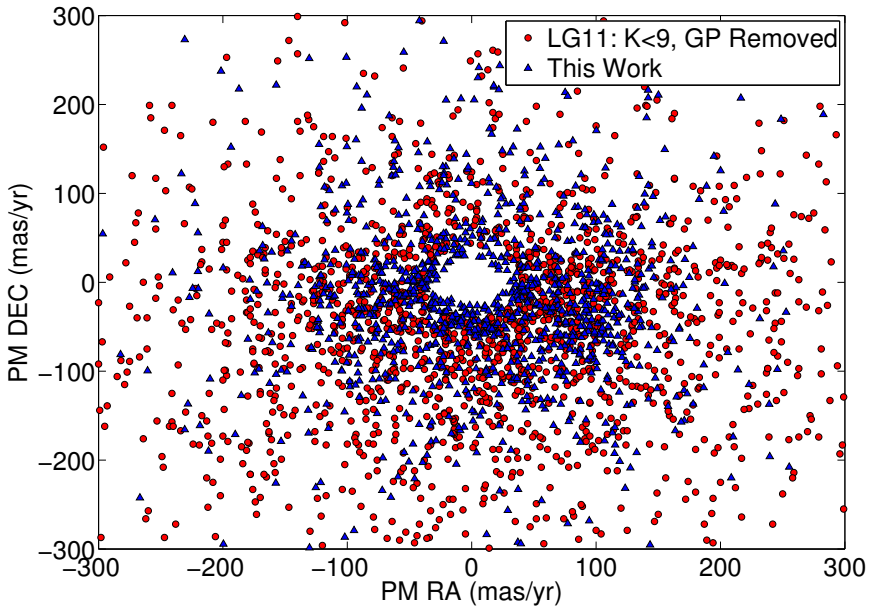

Fig. 4.7: Proper motion plot showing the unique objects from each catalogue and the low proper motion objects this work identifies that lie below 40 mas.

One set of low resolution spectra were obtained using the Telescopio Nazionale Galileo (TNG) telescope on La Palma, Spain in May 2011. These spectra were taken using the Device Optimized for the LOw RESolution (DOLORES) instrument using

the LR-R grism. The resolution of these spectra was approximately R∼700. Flux and wavelength calibration was performed using spectrophotometric standard stars and the Ne+Hg standard lamps. The reduction process was carried out using IRAF routines. Flats were median combined, bias subtracted, trimmed to remove any edge effects, and applied to the object images. The spectra were extracted using IRAF.APALL which identified the apertures as well as calculated and subtracted the background. The spectra of the spectrophotometric standard stars were used with the package IRAF.TELLURIC to determine the wavelength shift and scaling needed to account for the telluric lines in the atmosphere.

Spectra were also collected in September 2011 from Ritchey-Chretien Focus Spectrograph at the 4-m telescope in Kitt Peak, Arizona (KPNO) using the BL-181 grism. The standard IRAF routines were also used for sky subtraction, wavelength and flux calibration employing the use of ThAr lamps and spectrophotometric standards. After calibration and trimming, both sets of spectra cover a wavelength range of 6000-8000 Å. The KPNO spectra had a resolution of R∼1000.

4.5.2 Analysis

An initial spectral type was determined by comparing each of the observed spectra to that of known M dwarf standards from Kirkpatrick et al. (1991) as well as M giant spectra from Garcia (1989). The standard spectra included K7-M9 dwarfs and K4-M4.5 giants. The observed spectra were normalized using the mean value between 7450 and 7550 $\AA$. The comparison standard stars were linearly interpolated so their resolution matched that of the observed spectra and normalized using the same region. A least squares minimization was then performed to find the standard spectra that was the best fit to the observed spectra. As well as providing a preliminary spectral type, this also provided an initial temperature estimate for later model fitting.

Further refinement of spectral type and determination of whether the objects were giants was made by using the calcium hydride (CaH3) and titanium oxide (TiO) molecular bands. The CaH3 (6960-6990Å) region has been shown to display weaker absorp-

tion in giants than in dwarfs (Allen & Strom, 1995) and the full depth of the TiO5 (7126-7135Å) feature has been shown to also be a good indication of spectral types for early M dwarfs (Kirkpatrick et al., 1993; Reid et al., 1997).

Since the CaH3 region is sensitive to gravity, when plotted together with the TiO5 bandstrenghth, any giants should stand out as clear outliers. Figure 4.8 shows the observed spectra in such a plot along with CaH3/TiO5 measurements taken of the M standards interpolated to the same resolution. The M dwarf and M giant standards show a vertical separation as expected with our observed spectra falling in the region consistent with M and K dwarfs. Though this analysis only covers a small selection of objects within our sample, it is still encouraging that no giants were detected.

We used the relationship between the TiO band strength and spectral type, derived by Ried et al, as an independent check of our own best fit spectral types. Ried et al found this linear relationship to be

$$S_p = -10.775 \times TiO5 + 8.2$$

Our spectral type fits agreed to within 0.5 spectral types of our least squares fit which is the stated uncertainty found by Ried et al with the above relationship. The resulting spectral types can be found in Table 4.4 and all of the observed spectra along with the M dwarf standard spectra used can be seen in Figures 4.9 and 4.10.

Using the initial temperature estimations found in the spectral template least square fits above, a grid of synthetic spectra were generated using local thermal equilibrium models from the NextGen code of Hauschildt et al. (1999) by the program WITA6 (Pavlenko, 1997). Opacity line lists for TiO were taken from Plez (1998) and other opacity sources are cited in Pavlenko et al. (2006). A range of effective temperatures, metallicities, and gravities were generated at increments of 100 K, 0.5 dex, and 0.5 log g. The synthetic spectra were created for 2600 K$<$ T $<$ 4600 K, 4.0 $<$ log g $<$ 5.5, $-0.5 <$ [Fe/H] < 0.5. We used the fitting procedure described in Pavlenko & Jones (2002) and Jones et al. (2002) across 6000 - 8000Å. Only effective temperature's were iterated for the initial fit. Metallicities and gravities were fixed such that [Fe/H] = 0.0

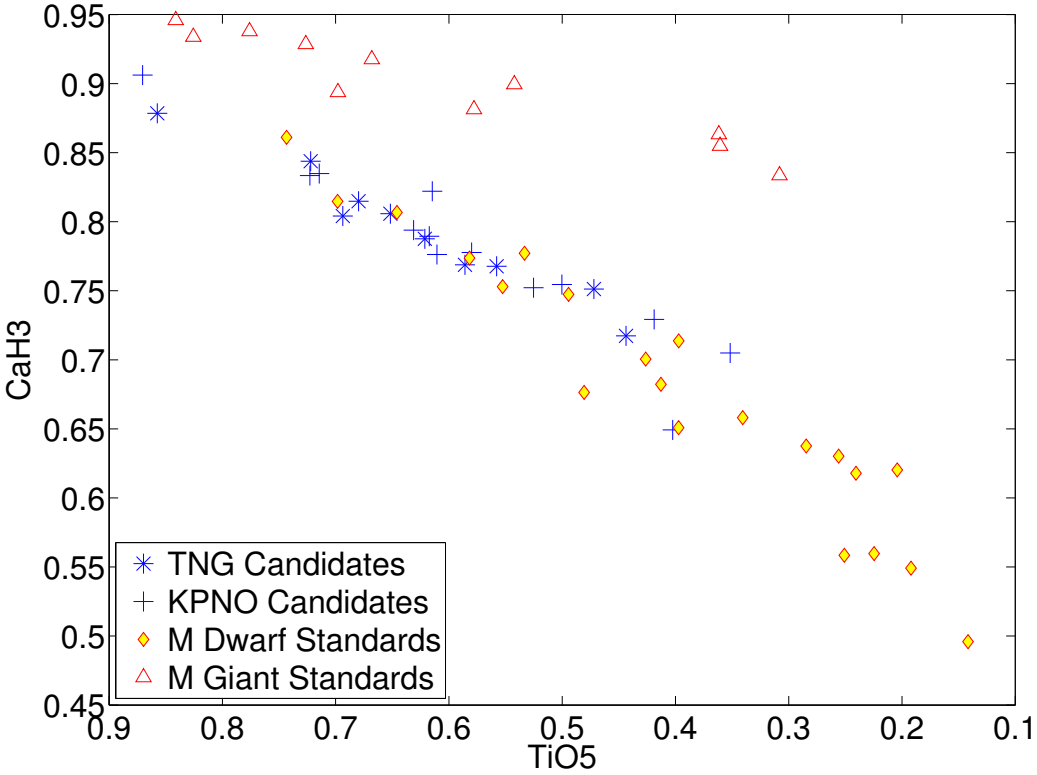

Fig. 4.8: CaH3 and TiO5 values for the observed targets. M dwarf and M giant standards are plotted here as yellow diamonds and red triangles, respectfully, and show a vertical separation. None of the candidate spectra fall within the region of the M giant standards indicating they are all likely to be M dwarfs.

and a $\log g = 5.0$. After the best fit for temperature was determined, [Fe/H] and $\log g$ were iterated until the fitting parameter was minimized. The results from the fits can be seen in Table 4.4.

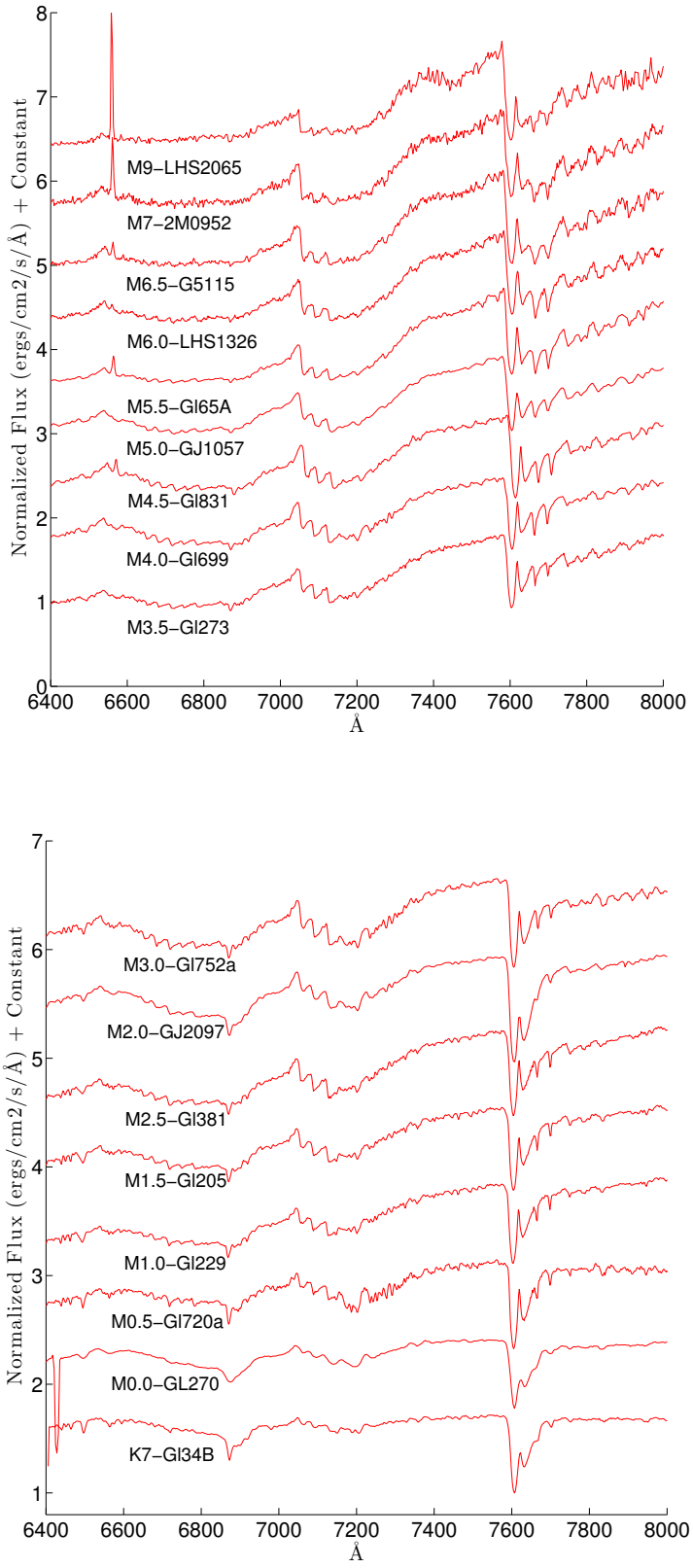

Fig. 4.9: M dwarfs used to determine spectral types of our targets.

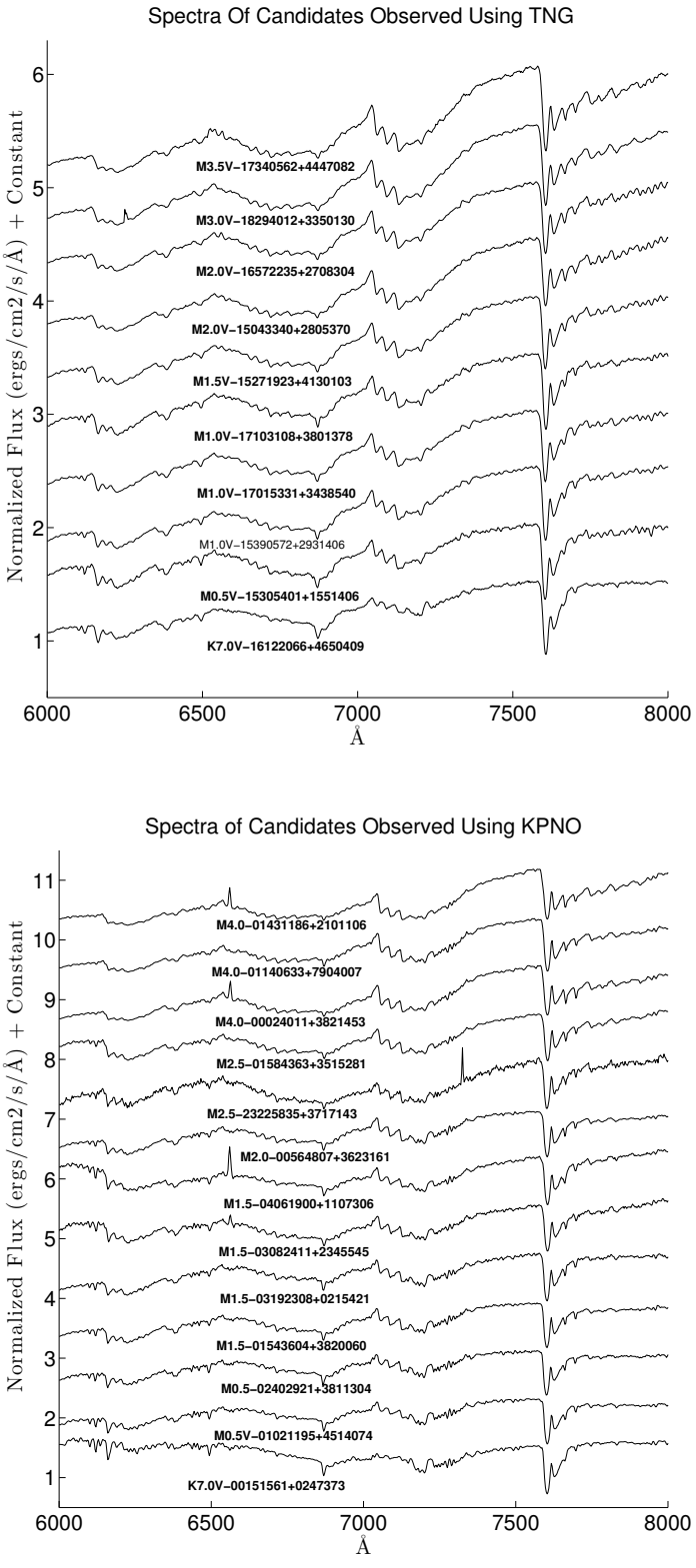

Fig. 4.10: All observed spectra of M dwarf candidates. The spectra are labelled with our determined spectral type and 2MASS designation.

Table 4.4: Results of physical parameter fits for a selection of M dwarfs from this work.

$2MASSDesignation$	α (°)	δ (°)	K (mag)	$J-K$ (mag)	$SpTyp$	$Teff$[a] (k)	log g (cgs)	$[Fe/H]$ (dex)
15305401+1551406	232.725081	15.861243	8.97	0.843	M 0.5 V	3800	5.0	0.0
15043340+2805370	226.139194	28.093640	8.98	0.836	M 2.0 V	3300	4.5	+0.5
15390572+2931406	234.773838	29.527944	8.94	0.817	M 1.0 V	3600	5.0	0.0
15271923+4130103	231.830081	41.502949	7.52	0.843	M 1.5 V	3600	5.0	0.0
16572235+2708304	254.343100	27.141781	8.51	0.845	M 2.0 V	3500	5.0	0.0
17015331+3438540	255.472140	34.64834 5	8.80	0.966	M 1.0 V	3500	4.5	+0.5
16122066+4650409	243.086139	46.844694	8.20	0.761	K 7.0 V	3900	5.0	0.0
17103108+3801378	257.629549	38.027209	8.62	0.864	M 1.0 V	3700	5.0	0.0
17340562+4447082	263.523338	44.785632	7.91	0.837	M 3.5 V	3300	5.0	0.0
18294012+3350130	277.417172	33.836978	8.95	0.892	M 3.0 V	3400	5.0	0.0
23225835+3717143	350.743198	37.287263	7.96	0.839	M 2.5 V	3600	5.0	0.0
00024011+3821453	0.667193	38.362543	8.91	0.796	M 4.0 V	3400	5.0	0.0
00564807+3623161	14.200329	36.387792	8.92	0.837	M 2.0 V	3700	5.0	0.0
01021195+4514074	15.549841	45.235351	8.85	0.892	M 0.5 V	4000	5.0	0.0
01140633+7904007	18.526638	79.066892	8.81	0.856	M 3.0 V	3500	5.0	0.0
01543604+3820060	28.650189	38.334976	8.97	0.784	M 1.5 V	3800	5.0	0.0
02402921+3811304	40.121777	38.191774	8.78	0.815	M 0.5 V	3900	5.0	0.0
03192308+0215421	49.846142	2.261704	8.99	0.839	M 1.5 V	3800	5.0	0.0
00151561+0247373	3.815086	2.793711	8.66	0.867	K 7.0 V	4200	5.0	0.0
01431186+2101106	25.799383	21.019610	8.36	0.890	M 4.0 V	3200	5.0	0.0
01584363+3515281	29.681783	35.257797	8.90	0.753	M 2.5 V	3500	5.0	0.0
03082411+2345545	47.100472	23.765137	8.85	0.860	M 1.5 V	3300	5.0	0.0
04061900+1107306	61.579243	11.125108	8.91	0.836	M 1.5 V	3800	5.0	0.0

[a]Uncertainties for fitted stellar parameters: Teff ±100k, log g ±0.5,$[Fe/H]$±0.5

4.6 Summary and Future Work

This work has classified 4054 M dwarfs with magnitudes of K< 9 from the PPMXL catalogue. By probing down to lower proper motions, this work has produced 1193 new bright M dwarf candidates that were not included in previous catalogues. By combining these objects with M dwarfs from LG11, we present a catalogue with 8479 K<9 late K and M dwarfs for future transit studies.

Good progress in transit discovery can be made by targeting this expansive M dwarf catalogue for low and high resolution spectroscopy. Low resolution spectra will confirm the cool dwarf nature and high resolutions spectra will provide constraints on inclination angles of potential transiting planetary systems using the method outlined in Herrero et al. (2012). Such observations would allow prioritization of bright M dwarfs for light curve follow-up and transit searches.

Target lists can then be expanded or refined for facilities such as Mearth (Charbonneau et al., 2008), Apache (Sozzetti et al., 2013), and LCOGTN (Brown et al., 2013) as the search for transiting Super Earth's moves forward.

4.7 Acknowledgements

DJP, HRAJ, YP, JRB, and ELM have received support from and JF, MKK, MC, and RT were supported by RoPACS, a Marie Curie Initial Training Network funded by the European Commissions Seventh Framework Programme. This research has benefitted from the M, L and T dwarf compendium housed at DwarfArchives.org and maintained by Chris Gelino, Davy Kirkpatrick and Adam Burgasser. This research is based on observations made with the Italian Telescopio Nazionale Galileo (TNG) operated on the island of La Palma by the Fundacin Galileo Galilei of the INAF (Istituto Nazionale di Astrofisica) at the Spanish Observatorio del Roque de los Muchachos of the Instituto de Astrofisica de Canarias and the Kitt Peak National Observatory which is operated by the Association of Universities for Research in Astronomy (AURA) under cooperative agreement with the National Science Foundation.

References

Allen, L. E. & Strom, K. M. 1995, AJ, 109, 1379

Bochanski, J. J., Hawley, S. L., Reid, I. N., Covey, K. R., West, A. A., Tinney, C. G., & Gizis, J. E. 2005, AJ, 130, 1871

Bonfils, X., Gillon, M., Udry, S., Armstrong, D., Bouchy, F., Delfosse, X., Forveille, T., Fumel, A., Jehin, E., Lendl, M., Lovis, C., Mayor, M., McCormac, J., Neves, V., Pepe, F., Perrier, C., Pollaco, D., Queloz, D., & Santos, N. C. 2012, A&A, 546, A27

Brown, T. M., Baliber, N., Bianco, F., Bowman, M., Burleson, B., Conway, P., Crellin, M., Depagne, É., De Vera, J., Dilday, B., Dragomir, D., Dubberley, M., Eastman, J. D., Elphick, M., Falarski, M., Foale, S., Ford, M., Fulton, B. J., Garza, J., Gomez, E. L., Graham, M., Greene, R., Haldeman, B., Hawkins, E., Haworth, B., Haynes, R., Hidas, M., Hjelstrom, A. E., Howell, D. A., Hygelund, J., Lister, T. A., Lobdill, R., Martinez, J., Mullins, D. S., Norbury, M., Parrent, J., Paulson, R., Petry, D. L., Pickles, A., Posner, V., Rosing, W. E., Ross, R., Sand, D. J., Saunders, E. S., Shobbrook, J., Shporer, A., Street, R. A., Thomas, D., Tsapras, Y., Tufts, J. R., Valenti, S., Vander Horst, K., Walker, Z., White, G., & Willis, M. 2013, ArXiv e-prints

Charbonneau, D., Berta, Z. K., Irwin, J., Burke, C. J., Nutzman, P., Buchhave, L. A., Lovis, C., Bonfils, X., Latham, D. W., Udry, S., Murray-Clay, R. A., Holman, M. J., Falco, E. E., Winn, J. N., Queloz, D., Pepe, F., Mayor, M., Delfosse, X., & Forveille, T. 2009, Nature, 462, 891

Charbonneau, D., Irwin, J., Nutzman, P., & Falco, E. E. 2008, in Bulletin of the American Astronomical Society, Vol. 40, American Astronomical Society Meeting Abstracts #212, 242

Clampin, M. 2010, in Astronomical Society of the Pacific Conference Series, Vol. 430, Pathways Towards Habitable Planets, 167

Famaey, B., Jorissen, A., Luri, X., Mayor, M., Udry, S., Dejonghe, H., & Turon, C. 2005, A&A, 430, 165

Frith, J., Pinfield, D. J., Jones, H. R. A., Barnes, J. R., Pavlenko, Y., Martin, E. L., Brown, C., Kuznetsov, M. K., Marocco, F., Tata, R., & Cappetta, M. 2013, MNRAS

Garcia, B. 1989, Bulletin d'Information du Centre de Donnees Stellaires, 36, 27

Gillon, M., Pont, F., Demory, B.-O., Mallmann, F., Mayor, M., Mazeh, T., Queloz, D., Shporer, A., Udry, S., & Vuissoz, C. 2007, A&A, 472, L13

Gliese, W. & Jahreiß, H. 1991, Preliminary Version of the Third Catalogue of Nearby Stars, Tech. rep.

Hauschildt, P. H., Allard, F., Ferguson, J., Baron, E., & Alexander, D. R. 1999, ApJ, 525, 871

Herrero, E., Ribas, I., Jordi, C., Guinan, E. F., & Engle, S. G. 2012, A&A, 537, A147

Høg, E., Fabricius, C., Makarov, V. V., Urban, S., Corbin, T., Wycoff, G., Bastian, U., Schwekendiek, P., & Wicenec, A. 2000, A&A, 355, L27

Johnson, J. A., Gazak, J. Z., Apps, K., Muirhead, P. S., Crepp, J. R., Crossfield, I. J. M., Boyajian, T., von Braun, K., Rojas-Ayala, B., Howard, A. W., Covey, K. R., Schlawin, E., Hamren, K., Morton, T. D., Marcy, G. W., & Lloyd, J. P. 2012, AJ, 143, 111

Jones, H. R. A., Pavlenko, Y., Viti, S., & Tennyson, J. 2002, MNRAS, 330, 675

Kirkpatrick, J. D., Henry, T. J., & McCarthy, Jr., D. W. 1991, ApJS, 77, 417

Kirkpatrick, J. D., Kelly, D. M., Rieke, G. H., Liebert, J., Allard, F., & Wehrse, R. 1993, ApJ, 402, 643

Lépine, S. & Gaidos, E. 2011, AJ, 142, 138

Lépine, S. & Shara, M. M. 2005, AJ, 129, 1483

Ma, C., Arias, E. F., Eubanks, T. M., Fey, A. L., Gontier, A.-M., Jacobs, C. S., Sovers, O. J., Archinal, B. A., & Charlot, P. 1998, AJ, 116, 516

Monet, D. G., Levine, S. E., Canzian, B., Ables, H. D., Bird, A. R., Dahn, C. C., Guetter, H. H., Harris, H. C., Henden, A. A., Leggett, S. K., Levison, H. F., Luginbuhl, C. B., Martini, J., Monet, A. K. B., Munn, J. A., Pier, J. R., Rhodes, A. R., Riepe, B., Sell, S., Stone, R. C., Vrba, F. J., Walker, R. L., Westerhout, G., Brucato, R. J., Reid, I. N., Schoening, W., Hartley, M., Read, M. A., & Tritton, S. B. 2003, AJ, 125, 984

Muirhead, P. S., Johnson, J. A., Apps, K., Carter, J. A., Morton, T. D., Fabrycky, D. C., Pineda, J. S., Bottom, M., Rojas-Ayala, B., Schlawin, E., Hamren, K., Covey, K. R., Crepp, J. R., Stassun, K. G., Pepper, J., Hebb, L., Kirby, E. N., Howard, A. W., Isaacson, H. T., Marcy, G. W., Levitan, D., Diaz-Santos, T., Armus, L., & Lloyd, J. P. 2012, ApJ, 747, 144

Pavlenko, Y. V. 1997, AZh, 74, 608

Pavlenko, Y. V. & Jones, H. R. A. 2002, A&A, 396, 967

Pavlenko, Y. V., Jones, H. R. A., Lyubchik, Y., Tennyson, J., & Pinfield, D. J. 2006, A&A, 447, 709

Perryman, M. A. C., Lindegren, L., Kovalevsky, J., Hoeg, E., Bastian, U., Bernacca, P. L., Crézé, M., Donati, F., Grenon, M., Grewing, M., van Leeuwen, F., van der Marel, H., Mignard, F., Murray, C. A., Le Poole, R. S., Schrijver, H., Turon, C., Arenou, F., Froeschlé, M., & Petersen, C. S. 1997, A&A, 323, L49

Plez, B. 1998, A&A, 337, 495

Reid, I. N., Hawley, S. L., & Gizis, J. E. 1997, VizieR Online Data Catalog, 3198, 0

Riaz, B., Gizis, J. E., & Harvin, J. 2006, AJ, 132, 866

Roeser, S., Demleitner, M., & Schilbach, E. 2010, AJ, 139, 2440

Sharma, S., Johnston, K. V., Majewski, S. R., Bullock, J., & Muñoz, R. R. 2011, ApJ, 728, 106

Skrutskie, M. F., Cutri, R. M., Stiening, R., Weinberg, M. D., Schneider, S., Carpenter, J. M., Beichman, C., Capps, R., Chester, T., Elias, J., Huchra, J., Liebert, J., Lonsdale, C., Monet, D. G., Price, S., Seitzer, P., Jarrett, T., Kirkpatrick, J. D., Gizis, J. E., Howard, E., Evans, T., Fowler, J., Fullmer, L., Hurt, R., Light, R., Kopan, E. L., Marsh, K. A., McCallon, H. L., Tam, R., Van Dyk, S., & Wheelock, S. 2006, AJ, 131, 1163

Sozzetti, A., Bernagozzi, A., Bertolini, E., Calcidese, P., Carbognani, A., Cenadelli, D., Christille, J. M., Damasso, M., Giacobbe, P., Lanteri, L., Lattanzi, M. G., & Smart, R. 2013, ArXiv e-prints

Tessenyi, M., Ollivier, M., Tinetti, G., Beaulieu, J. P., Coudé du Foresto, V., Encrenaz, T., Micela, G., Swinyard, B., Ribas, I., Aylward, A., Tennyson, J., Swain, M. R., Sozzetti, A., Vasisht, G., & Deroo, P. 2012, ApJ, 746, 45

Tinetti, G., Beaulieu, J. P., Henning, T., Meyer, M., Micela, G., Ribas, I., Stam, D., Swain, M., Krause, O., Ollivier, M., Pace, E., Swinyard, B., Aylward, A., van Boekel, R., Coradini, A., Encrenaz, T., Snellen, I., Zapatero-Osorio, M. R., Bouwman, J., Cho, J. Y.-K., Coudé de Foresto, V., Guillot, T., Lopez-Morales, M., Mueller-Wodarg, I., Palle, E., Selsis, F., Sozzetti, A., Ade, P. A. R., Achilleos, N., Adriani, A., Agnor, C. B., Afonso, C., Allende Prieto, C., Bakos, G., Barber, R. J., Barlow, M., Batista, V., Bernath, P., Bézard, B., Bordé, P., Brown, L. R., Cassan, A., Cavarroc, C., Ciaravella, A., Cockell, C., Coustenis, A., Danielski, C., Decin, L., De Kok, R., Demangeon, O., Deroo, P., Doel, P., Drossart, P., Fletcher, L. N., Focardi, M., Forget, F., Fossey, S., Fouqué, P., Frith, J., Galand, M., Gaulme, P., Hernández, J. I. G., Grasset, O., Grassi, D., Grenfell, J. L., Griffin, M. J., Griffith, C. A., Grözinger, U., Guedel, M., Guio, P., Hainaut, O., Hargreaves, R., Hauschildt, P. H., Heng, K., Heyrovsky, D., Hueso, R., Irwin, P., Kaltenegger, L., Kervella, P., Kipping, D., Koskinen, T. T., Kovács, G., La Barbera, A., Lammer, H., Lellouch, E., Leto, G., Lopez Morales, M., Lopez Valverde, M. A., Lopez-Puertas, M., Lovis, C., Maggio, A., Maillard, J. P., Maldonado Prado, J., Marquette, J. B., Martin-Torres, F. J., Maxted, P., Miller, S., Molinari, S., Montes, D., Moro-Martin, A., Moses, J. I., Mousis, O., Nguyen Tuong, N., Nelson, R., Orton, G. S., Pantin, E., Pascale, E., Pezzuto, S., Pinfield, D., Poretti, E., Prinja, R., Prisinzano, L., Rees, J. M., Reiners, A., Samuel, B., Sánchez-Lavega, A., Forcada, J. S., Sasselov, D., Savini, G., Sicardy, B., Smith, A., Stixrude, L., Strazzulla, G., Tennyson, J., Tessenyi, M., Vasisht, G., Vinatier, S., Viti, S., Waldmann, I., White, G. J., Widemann, T., Wordsworth, R., Yelle, R., Yung, Y., & Yurchenko, S. N. 2012, Experimental Astronomy, 34, 311

Chapter 5: High Resolution Spectroscopy of HD179949b

5.1 Introduction

Some of the efforts to place limits on and fully characterize exoplanet atmospheres were mentioned in Section 1.3.2. The first to establish albedo constraints using reflected light studies was done by Charbonneau et al. (1999) on the Close Orbiting Giant Planet (CEGP) orbiting τ Boo. Collier Cameron et al. (1999) also reported directly detecting the reflected light of the same system; however, later observations ruled out the planet candidate signature with a higher level of confidence and put constraints on the planets geometric albedo (Leigh et al., 2003). More reflected light studies were done by Collier Cameron et al. (2002) using high resolution spectroscopy and a similar Doppler tomographic signal-analysis technique establishing constraints on υ And's innermost planet. Snellen et al. (2010) were able to discern a highly blue shifted carbon monoxide signal within HD 209458 b which suggested strong winds flowing from the day to the night side. Carbon monoxide was also reported to be detected on the non-transiting planet τ Boo by Brogi et al. (2012). Little work has been done to detect the light emitted directly from the planet. This is partly due to the fact that to the planet's light is most strong in the infrared (IR) and near-infrared (NIR) and instrumentation has only recently come to fruition for these wavelengths for ground based observatories.

Barnes et al. (2008) obtained high resolution spectroscopy of HD 179949 in the NIR and established contrast ratio constraints between the planet and host star at those wavelengths. Cubillos et al. (2011) performed similar NIR infrared analysis on HD 217107b to Barnes et al. (2008) and did not detect the planet but set limits on the flux ratio. More recently, Rodler et al. (2013) compared various analysis methods and detected carbon monoxide absorption in HD 189733b using NIR spectroscopy.

In this chapter, high resolution spectroscopy is used to set constraints on the pres-

ence of titanium oxide (TiO) in the non-transiting planet HD 179949b.

5.1.1 HD 179949

HD 179949 and its exoplanet have been heavily studied since its discovery by (Tinney et al., 2001) and has helped define the term 'Hot Jupiter'. Table 5.1 lists the most up to date known physical properties and their associated uncertainties.

Table 5.1: Stellar Parameters for HD 179949 and its planet

Parameters	Value	Reference
Star:		
Spectral type	F8V	Valenti (2005)
$T_{\rm eff}$	6124 ±44	Valenti (2005)
$M_{\odot}$	1.181 +.039/−0.26	Takeda (2007)
$R_{\odot}$	1.226 ±0.041	Torres (2010)
$[Fe/H]$	0.137 ±0.03	Valenti (2005)
log g	4.341 ±0.06	Valenti (2005)
$v \sin i (\mathrm{km\,s^{-1}})$	7.02 ±0.5	Valenti (2005)
Distance(pc)	27.55 +0.54/-0.52	van Leeuwen (2007)
K(mag)	4.936	Skrutskie (2006)
Planet:		
$m \sin i (M_{\rm Jup})$	0.902 ±0.033	Butler (2006)
a(au)	0.04392±0.000073	Butler (2006)
e	0.022±0.015	Butler (2006)
$K_*(ms^{-1})$	112.6±1.8	Butler (2006)
$K_p(\mathrm{km\,s^{-1}})$	123.4 ±29.1	This work
i	52.5571	This work
$\sin i$	0.7939699	This work

HD 179949 b does not appear to be a multi-planet system as Eggenberger et al. (2007) found no evidence of a companion in their search for stellar duplicity and Wittenmyer et al. (2007) could not detect another planet orbiting at a longer period. Santos et al. (2004) found the metallicity of HD 179949 to be similar to that of other systems known to host exoplanets ($[Fe/H] = 0.22 \pm 0.05$ dex) which is in slight disagreement with the more recent measurements found in Valenti & Fischer (2005) that reported a slightly lower metallicity (value in Table 5.1). Initially, there were observations by Shkolnik et al. (2003) of the Ca II H&K lines of the host star that found evidence of periodic coronal activity that coincided with the orbit of the planet which

implied a possible interaction between the two. Later, similar observations were done by Gurdemir et al. (2012) that were consistent with this result. Additionally, spectropolarimetric observations done by Fares et al. (2012) found the possibility of low amplitude fluctuations with a period close to that of the planet. However, Scandariato et al. (2013) performed a simultaneous optical and X-ray spectroscopic campaign over 5 orbital periods and 2 stellar rotations and found there to be no clear signature coincident with the planet's orbit.

While the planet-induced stellar activity remains ambiguous, progress has been made in the characterisation of the atmospheres of a few select hot Jupiters as well as HD 179949b. Using the Spitzer telescope, (Knutson et al., 2009) was able to determine the atmosphere of HD 189733b is highly efficient at transporting heat from the day to the night side of the planet and this was also reproduced with simulations conducted by Showman et al. (2008). Spitzer was also used by Cowan et al. (2007) to obtain light curves of HD 179949, HD 209458 and 51 Peg. They found phase dependent variation in the light curve of HD 179949b but no detectable variation in the other two systems. They set a lower limit of 21 per cent of the stellar flux being recirculated from the day to the night side. The lack of similar findings in the other two systems implied the possibility that HD 179949b's atmosphere may differ compared to the others. υ And b has many similar physical characteristics to HD 179949b and also shows an offset between its superior conjunction and the peak of its light curve (Harrington et al., 2006). One explanation of why both υ And b and HD 179949b are apparently inefficient at redistributing energy from the day to the night side of the planet has been suggested by Harrington et al. (2007) and to be caused by heavy elements within the planets' atmospheres creating an inversion layer which allows incident flux to be re-radiated quickly before it can be carried to other parts of the planet. If this were true, then the absence of such a stratosphere could be an explanation for the observations of HD 209458 and 51 Peg and would suggest a possible bifurcation in the make-up of hot Jupiter atmospheres.

5.1.2 Two Possible Atmospheres for HD179949b

Hubeny et al. (2003) and later Burrows et al. (2008) and Fortney et al. (2008) have described such a division between hot Jupiter atmospheres separating them using similar criteria to the distinction between dM and dL spectral types. Because of this, they designate the two types of atmospheres as pM and pL.

The fundamental difference between the two atmospheres is caused by a combination of the mass of the planet and the amount of flux it receives from its host star. The pM type has a hotter $(2000 + K)$ atmosphere due in part to TiO and vanadium oxide (VO) absorbing incident flux at higher altitudes leading to the formation of a hot stratosphere. If the atmosphere receives less radiation from its parent star and is cooler, TiO and VO solidifies in the upper atmosphere and "rains out" falling to lower altitudes over time and eventually depletes the upper atmosphere of those molecules. These atmospheres would then have no temperature inversion and are described as pL atmospheres by Fortney et al. Cooler atmospheres have a lower temperature differential between the night and day side of the planet due to the lack of flux absorbing molecules. Figure 5.1 shows model temperature-pressure profiles for a 1 M_J planet at various orbital distances. For this case, planets further away than 0.035 AU would be cool enough for Ti and V silicates to condense.

As described in 5.1.1, there have been observations of hot Jupiters that have hinted at this separation of atmospheric types. For the pM type atmospheres, the expected observables would be the presence of TiO and VO, a hot stratosphere, the location of the hottest point in the atmosphere at the superior conjunction, and a large day/night temperature contrast (Fortney et al., 2008). υ And b, Wasp-1b, TrES-4b, TrES-3b, HD 149026b, and a few others show certain qualities that could put them in the pM category.

Conversely, the pL class is more difficult to predict observables since it has less extreme conditions than the pM type. However, the pL atmosphere is expected to have strong absorption caused by H_2O, Na, CO, and K and should have small day/night contrasts. HD 189733b, 51 Peg b, and HD 209458b are possible examples for the pL

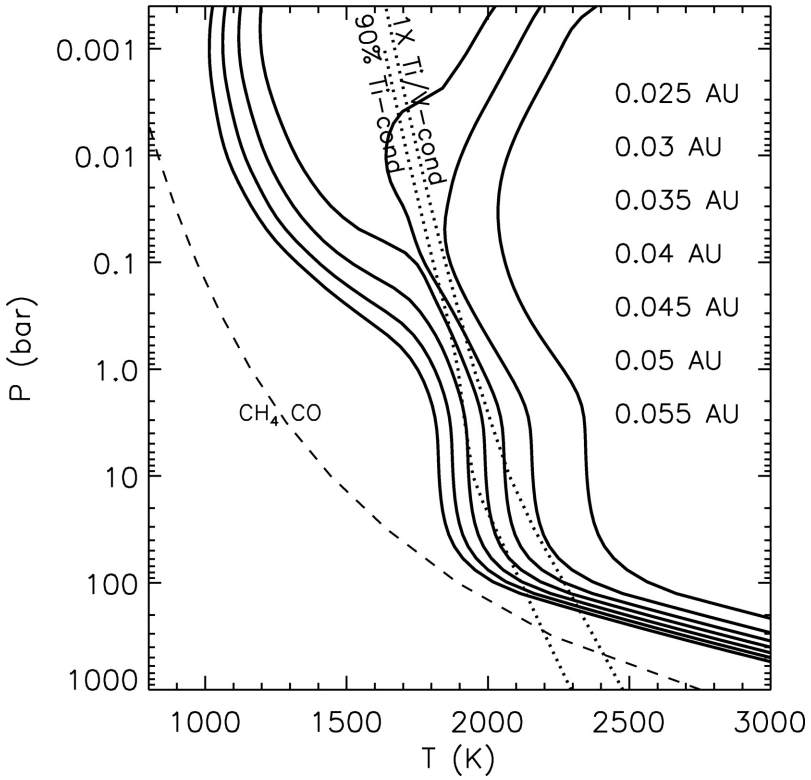

Fig. 5.1: Temperature-pressure profile predictions taken from Fortney et al. (2008) using their models. The lines show profiles for planets with g = 15 ms^{-2} and an internal temperature of 200 K at different orbtial distances from a Sun-like star. Of note are the dashed lines showing the location of Ti and V condensation. For planets with enough incident flux to increase the atmospheric temperature above the condensation point (for pressures found in the upper atmosphere, this occurs at around 1800 K) a temperature inversion can be seen. For this type of planet, an inversion can be seen for orbits less than 0.035 astronomical units.

class and observations by Tinetti et al. (2007) and Swain et al. (2009) have found evidence of these molecules. However, since the rain out of Ti and V is one that could happen over a long period of time, it is entirely possible (especially for young systems) that some hot Jupiters could be found to be in transition between pM and pL.

Figure 5.2 shows Fortney et al's predictions of which atmosphere is expected for a selection of exoplanets and find it likely that HD 179949b has a pM atmosphere.

Fortney et al. also developed synthetic spectra using model planetary atmospheres for both the pM and pL type atmosphere. The spectra were generated using a code originally designed to study the atmosphere of Titan by McKay et al. (1989). This was further modified over several iterations to be applied to Solar System giant planets, brown dwarfs, and hot Jupiters (Marley et al., 1996; Burrows et al., 1997; Marley & McKay, 1999; Fortney, 2005; Saumon et al., 2006; Fortney et al., 2006; Fortney, 2007).

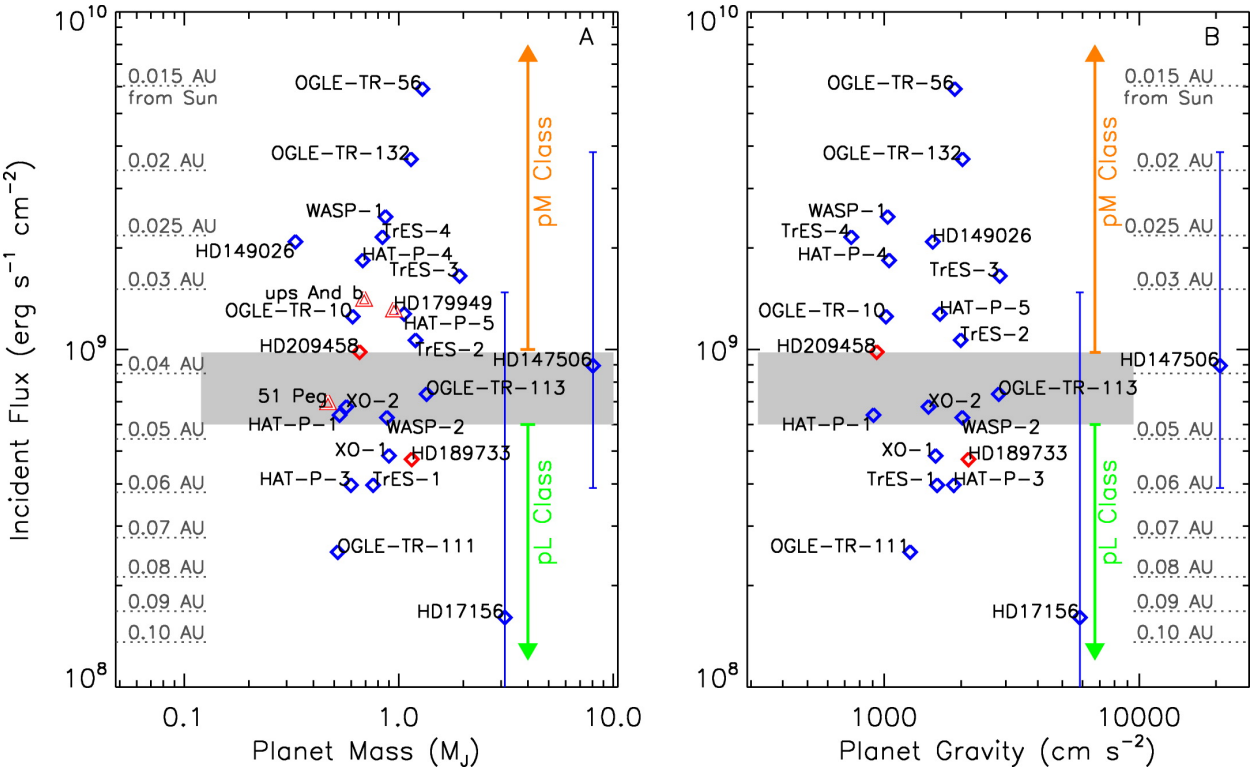

Fig. 5.2: Figure taken from Fortney et al. (2008), this shows the incident flux received by various hot Jupiters and their associated masses and gravities. Based on these models, HD179949 is expected to have a pM atmosphere and TiO present in its atmosphere.

The code takes into account both the flux received from the planet's host star as well as the thermal energy produced from the planet itself.

Similar spectra of irradiated atmospheres were used by Barnes et al. (2008) to investigate the possibility of a stratosphere on HD 179949b. High resolution spectra of the system were taken in the NIR, where the contrast ratios between the planet and star are favourable, and then searching for signal directly emitted from the planet. This was done by modelling the combined planet/star light as a phase dependent combination of the two signals (using the model spectra provided by Fortney et al) and deconvolving the two signals. Their attempt to detect emitted light directly through high resolution molecular features from HD 179949b was not successful using either the pM or pL atmosphere but they were able to rule out a pL (absorption dominated) atmosphere at a maximum contrast ratio of $F_p/F*$=1/3350 with 99 per cent confidence. Their conclusion for the detection of the pM atmosphere was limited by their sensitivities being too low in comparison to the expected contrast ratios produced by the model.

Specifically, the model pM expected a $F_p/F*$ of about 1/2900 and their 95.4 per cent upper confidence level at the most probable orbital velocity amplitude was 1/2000.

5.1.3 Motivation

This work focuses on setting further limits on the contrast ratios between the emitted light of HD 179949b and its star towards the eventual characterisation of its atmosphere as being either pM or pL. High resolution spectra are utilised in the optical regime where TiO transitions appear and where many more spectral lines are available. This is hoped to lead to greater sensitivities, but is complicated by the fact that the modelled contrast ratio is expected to be less favourable at these wavelengths.

5.1.4 Expected Contrast Ratios

To predict the kind of sensitivities needed, it is necessary to understand the contrast ratios expected from a planetary system like HD 179949. To this end, an F8V spectrum was simulated using the Vienna Atomic Line Database (VALD) (Piskunov et al., 1995) with a $T_{eff} = 6250$ and a log $g = 4.5$. The simulated stellar spectrum's wavelength positions are given to 0.0001 angstroms which translates to an uncertainty of 3 m/s in velocity space. Subsequently, using the atmospheres described in Section 5.1.2, model pM and pL planetary spectra were generated (provided by Didier Saumon and Jonathan Fortney via private communication) and are plotted in Figure 5.3 and Figure 5.4 along with the simulated F8V stellar spectrum. These flux levels are generated when the planet is at a phase such that it is emitting at its maximum possible level, i.e. superior conjunction (equivalent to a secondary eclipse in an eclipsing system), and thus represent the maximum flux/lowest contrast. The resulting F_p/F_* can be seen in Figure 5.3 and 5.4. As discussed in Section 5.2, observations for this work were timed such that the obtained spectra were as close as possible to this optimal phase angle (ϕ=0.5) to maximize the signal received from the planet.

In the bluest end of the spectrum, we can see contrast ratios as great as 10^{-7} - 10^{-8} for both atmospheres indicating that the pL atmosphere is more difficult to detect.

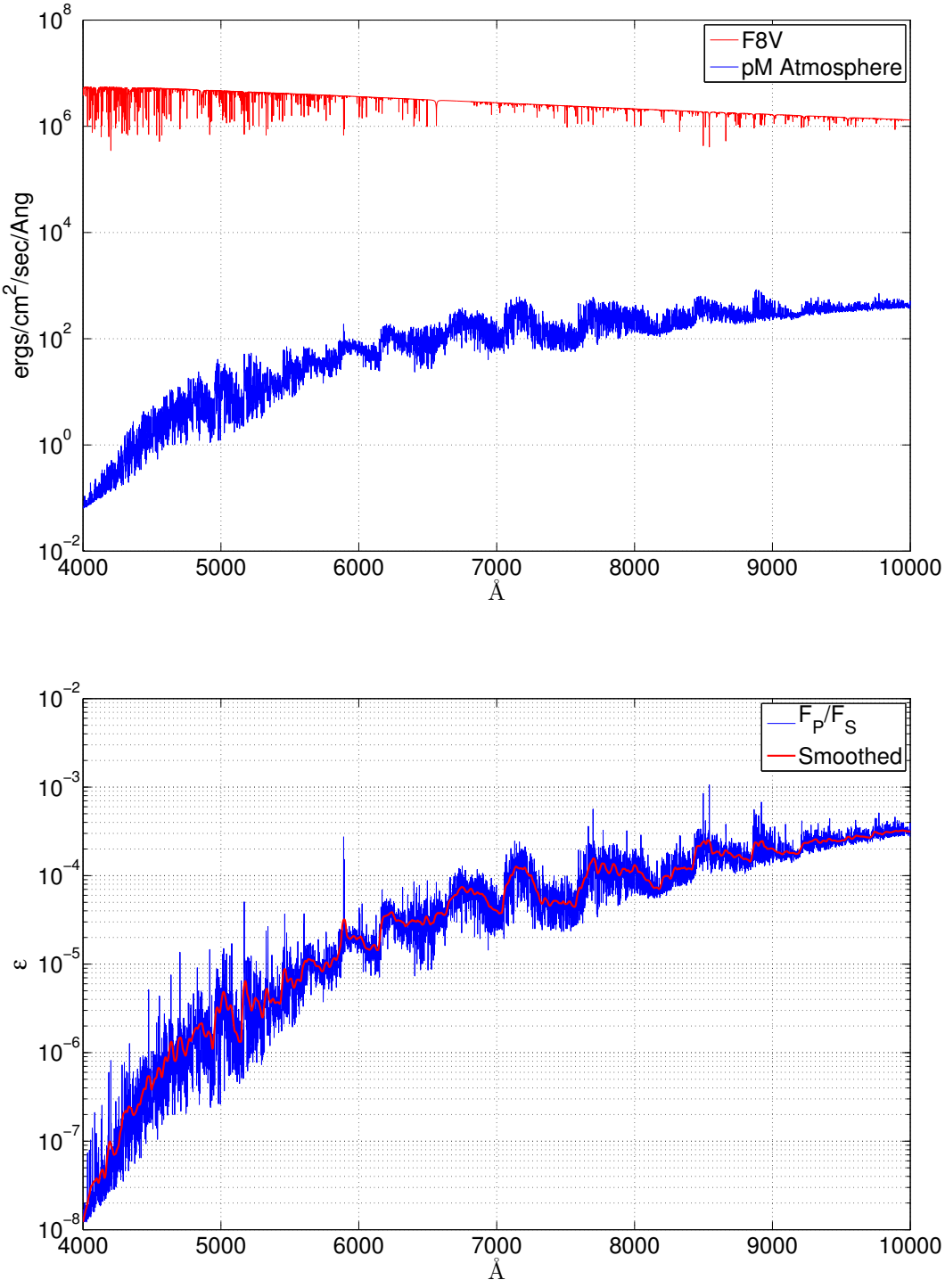

Fig. 5.3: Top: Plotted in red is the modelled F8 V spectrum produced using VALD. The much lower flux model pM atmosphere is seen in blue dominated by emission lines and molecular bands produced by TiO. Bottom: Contrast ratio, ϵ, of the light from the planet to that of the host star. At the central wavelength of the observations, this model atmosphere predicts an ϵ between 10^{-5} to 10^{-4}.

However, at around 6000$\mathring{A}$, the contrast ratio is 3 orders of magnitude greater. A search in the red optical is therefore a possibility given a high enough signal to noise

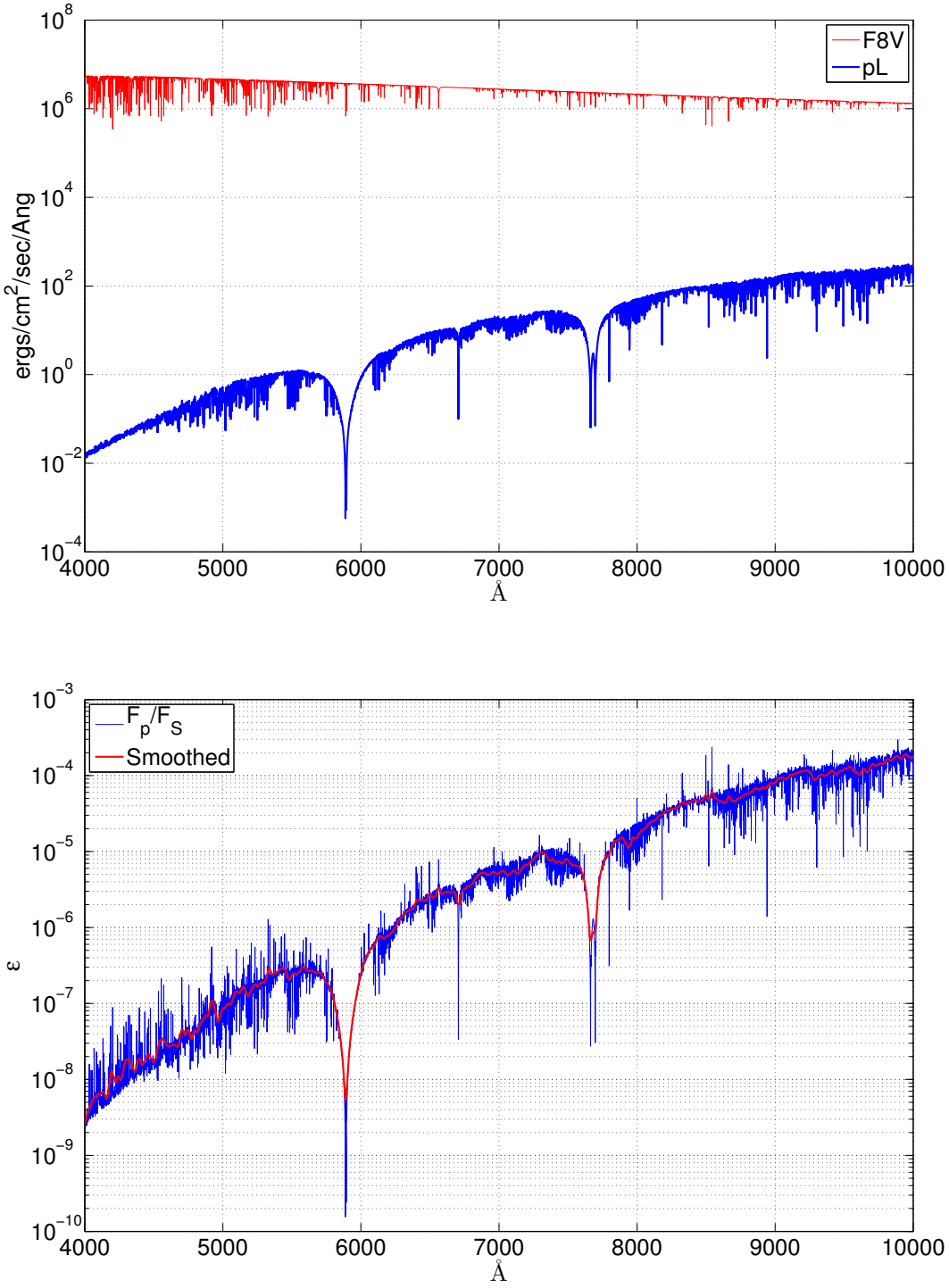

Fig. 5.4: Same as Figure 5.3 but showing the spectra for the pL atmosphere. The spectra is dominated by large absorption lines caused by H_2O, Na, and K. Contrast ratios between a planet of this atmospheric type and its host star are expected to fall between 10^{-6} and 10^{-5} for the central wavelength of observations in the red optical.

which can be achieved with many spectra and using the information content from many molecular transitions of TiO and VO.

5.2 Observations

HD 179949 was observed continuously on the night of May 25th and 28th 2009 using the Ultraviolet and Visual Echelle Spectrograph (UVES) located at the Nassmyth B focus of on the Very Large Telescope (VLT) at the Paranal observatory in Chile. These nights and times were specifically chosen so the planet would be as close to superior conjunction as possible (i.e. ϕ close to 0.5). The spectra were spread across two CCDs. The"blue" chip was an EEV CCD-44 2Kx4K with 15 μm pixels that observed a wavelength range of 300-500 nm. The "red" chip was a combination of the same EEV chip and the MIT/LL CCID-20 chip which has better quantum efficiency in red optical and near-infrared. The red chip covered a wavelength range of 420-1100 nm. Details of the spectrograph's design can be found in Dekker et al. (2000) and up to date or observing epoch specific updates can be found on the ESO UVES web page. Thorium-Argon (ThAr) lamps were observed for wavelength calibration.

5.3 Data Reduction

The reduction and extraction of the spectra was done using the Starlink package `ECHOMOP` which uses algorithms based Horne (1986) to implement an optimal extraction of the echelle spectra. A series of C shell scripts developed by Collier Cameron et al. (2002) for reflected light studies and modified by Barnes et al. (2007, 2010) were also used to further automate the `ECHOMOP` routines for the reduction and analysis of the data.

5.3.1 Preparing The Data

A single master bias frame was constructed by median combining all biases for each chip per night. A single median combined flat-field image was similarly created for each night and science frames were bias subtracted and trimmed to remove overscan regions.

5.3.2 Echomop Reduction Steps

Firstly, the individual orders were traced using a polynomial fit. Any orders that didn't span the entirety of the chip were not included in the analysis. A total of 37 orders were traced in all. Flat fields were used to determine the dekker and the object extent. The flat field was modelled to account for pixel to pixel variations along the traced orders and the sky intensity modelled along each order using a quadratic polynomial fit. The object profile was modelled and the object and arc spectra extracted simultaneously. The wavelength calibration was done using the ThAr arc lamp reference spectra obtained during the observations. Each of the 37 extracted orders had a minimum of 10 arc lines identified and a best fit was obtained. The line positions were further iterated by fitting Gaussians (allowing for Gaussian fits to nearby lines) and then performing a 2D wavelength solution to all extracted orders for each chip (Barnes et al., 2012).

Spectra were binned in order to increase signal to noise and decrease the processing time necessary. A weighted mid-point exposure time was calculated for the combined spectra to retain precision in the calculation of the planet's phase angle. The minimum exposure time was 65.99 seconds with a mean exposure time of 115.50 seconds. The maximum combined exposure time of the binned images was 299.99 seconds which corresponds to a $\Delta\phi$ =0.0011. With an observed K_p of 123.4 km s^{-1}, the change in RV signal for a $\Delta\phi$ of 0.0011 is 0.135 km s^{-1} ($\Delta RV = K_p \Delta\phi$). The planet profile width, which is a combination of the instrumental resolution and planet FWHM, was found to be $\sim$ 6 km s^{-1}. Therefore, the smearing of the planetary signal is not significant since the velocity shift in this time frame is much less than the profile width.

5.4 Constructing a Deconvolved Time Series

After the individual spectra have been extracted and reduced, there are many steps necessary to produce a deconvolved time-series composite of the residual spectra. The details of many of the numerical analysis procedures are outlined thoroughly in the appendices of Collier Cameron et al. (2002). The procedures have been updated for use with emission spectra rather than reflection spectra by Barnes et al. (2007, 2010)

and also further in this work. The following is an overview of the processing steps.

5.4.1 Registering Spectra and night template

All the spectra are first registered and aligned to within one pixel of a given spectral frame using a cross-correlation of selected stellar spectral lines. For each night, all aligned spectra are summed together to produce a spectral template containing the stellar spectra, the tellurics, and a smeared planetary signal. The night template is then scaled, shifted, and broadened to the individual spectra by performing a spline fit to the night template and obtaining scale factors at 96 different points. The scaled template is described as a linear combination of derivatives in the spectra (essentially a Taylor expansion) and enables changes in shift and line width to be modelled. Once the night template is scaled correctly, it is subtracted from the individual spectra producing residual spectra containing noise and signal from the planet.

5.4.2 Principle Component Analysis

To help mitigate any systematic effects that may be contained within the residual spectra, principal component analysis (PCA) is performed on a pixel by pixel basis on the stacked residual spectra data cube in a way similar to that used by Collier Cameron et al. (2002). This reduces the spatially fixed but time-varying effects possibly caused by defects in the CCD, a drift in the flat field sensitivity, thermal flexure, or telluric lines that vary in strength with airmass throughout the night. In this case, the eigen values of the principle components were compared and the 3 strongest removed. Similarly to the night template subtraction, this process did not greatly affect the signal from the planet since the planet's signal was smeared in velocity space.

5.4.3 Weighted Least Squares Deconvolution using atmospheric models

After the PCA is performed, the resultant residual spectra should contain a Doppler shifted version of the signal from HD179949b. However, this signal is lost deep within

the noise. Using a method originally outlined by Donati et al. (1997) and Barnes et al. (1998), we use a line list and appropriate line depths taken from the model atmosphere described in 5.1.2 to perform a weighted least-squares deconvolution at the location of the planetary lines, thus amplifying any signal from the planet that may be buried in the residual spectra. The method is similar to doing a cross-correlation which co-adds all the aligned spectra while removing any side lobes that may have occurred due to line broadening, effectively being a weighted mean of all the line profiles. The centroidal wavelength of the deconvolution is defined by

$$\langle\lambda\rangle = \frac{\sum_i s_i d_i \lambda_i}{\sum_i s_i d_i} \tag{5.1}$$

where d_i is the central depth of the unbroadened line, s_i is the S/N ratio of the line taken from the variances in the input spectrum or a scaled standard continuum, and λ_i is the wavelength of the pixel in the spectrum (taken from Barnes et al. (2000)). For the pM model, $\langle\lambda\rangle = 6891$ $\mathring{A}$ and for the pL model, $\langle\lambda\rangle = 7249$ $\mathring{A}$.

5.4.4 Phase Alignment

The final result, therefore, consists of a series of deconvolved residual spectra. Because the observations were taken between two nights at various phase angles, the spectral time series is displayed in terms of orbital-phase to more easily combine the two nights of data. This allows the observations to be folded together and for the Doppler shifted planetary signal to be analyzed.

5.5 Planetary Signal Analysis

5.5.1 Matched Filter

Using a method similar to Collier Cameron et al. (2002) and Barnes et al. (2007), the aim of this work is to detect the planetary spectrum within the residual spectra which should appear as Doppler shifted and phase dependent with respected to the stellar signal. The phase dependence is caused by the geometry of the planet's orbit where

its maximum irradiated surface area is visible at the point of superior conjunction or a phase (ϕ) equal to 0.5 (Barman et al., 2005). These Doppler shifts and brightness variations are modelled as a function of time using a Gaussian-matched filter as described in Barnes et al. (2007). Specifically, the planet-star flux ratio, ϵ, can be expressed as a function of wavelength and the orbital phase.

$$\epsilon(\alpha, \lambda) \equiv \frac{f_p(\alpha, \lambda)}{f_*(\lambda)} = \epsilon_0(\lambda) g(\alpha, \lambda) \tag{5.2}$$

Here, ϕ and inclination, i, are expressed in terms of α which is defined as

$$cos(\alpha) = -sin(i)cos(\phi) \tag{5.3}$$

The phase function $g(\alpha, \lambda)$ can be either empirically derived or based on a model. In this case, it is modelled using the phase function of Venus which was shown by Barnes et al. (2007) to be consistent with an empirically observed phase function of HD 208457b produced by Barman et al. (2005). Discrepancies in the phase function are mitigated with observations taken close to ϕ=0.5 where $g(\alpha, \lambda)$ is at its maximum. Using this model and the above relationships, it is possible to derive the maximum flux ratio between the planet and the star (ϵ_0) as well as the velocity amplitude of the planet (K_p).

5.5.2 Estimating System Orbital Parameters

No transit of HD 179949b has been detected so its inclination cannot be easily constrained. Having estimations of both the inclination and K_p is necessary to estimate the intensity and the location of the planetary signal in velocity space. Using the empirically determined stellar parameters and their associated uncertainties from Table 5.1, a Monte Carlo simulation similar to that done by Collier Cameron et al. (2002) was performed to generate a distribution of most probable sin i and K_p values. Previously calculated values of stellar rotation period, P_{rot}, v sin i, stellar radius, R_*, semi-major axis of the planet's orbit, a, and the amplitude of the star's reflex orbital velocity, K_*, were run through a one million iteration Monte Carlo simulation to determine the most

probable values for sin i and K_p.

$$\sin i = \frac{P_{rot} v \sin i}{2\pi R_*} \tag{5.4}$$

$$K_p = \frac{2\pi}{P_{orb}} \frac{\sin i}{1+q} \tag{5.5}$$

where $q = M_p/M_*$ and is determined using

$$\frac{q}{1+q} = \frac{K_*}{\sin i} \frac{P_{orb}}{2\pi a} \tag{5.6}$$

The results, as stated in Table 5.1, are a $\hat{K_p}$=123.4 km s^{-1} and an $\hat{i}$=52.557.

5.5.3 Simulated Planet Injection

It is necessary to calibrate the recovered planet signal by injecting a simulated planet signal into the residual spectra with a known contrast ratio and K_p. This calibration allows for the recovered value for $log_{10}(\epsilon)$ to be representative of the true contrast between the planet and star signal and not just an arbitrary value. This enables the equivalent width of the Gaussian matched filter to be properly scaled to the simulated, and subsequently, the observed data. Since deconvolution yields a single line profile from potentially thousands of lines that are weighted according to line depth and continuum counts, the Gaussian scaling value cannot be determined easily in advance and must be determined empirically.

A planet signal is injected into the extracted spectra before any analysis is done so that its signal is processed in the same way as would be done for a non-simulated signal. This is achieved by first normalizing the observed spectrum along the continuum and then multiplying the result by the spectral energy distribution of the star. This produces an observed stellar spectrum with the correct slope for a star at the temperature of HD 179949 (∼6100 K) normalized to 1 at the mean wavelength. The planet spectrum is then normalized to 1 at the mean wavelength and attenuated according to the desired contrast ratio and added to the stellar spectrum. The resultant sum of

the two spectra is then normalized again to ensure that the continuum is set to 1 and is multiplied by the observed continuum of a mean observation. The final output is a stellar spectrum with a planetary spectrum injected at the desired contrast ratio.

This was done for both the pM and pL atmospheres and the results of this process can be seen in Figure 5.5. In these plots, the deconvolved time series for both nights of observations folded together in terms of the orbital phase of the planet are shown along with a surface plot of χ^2 results from the matched filter analysis. For the pM atmosphere, the planet signal was injected at ϵ_0=-4.14 and -3.4 for the pL atmosphere. The signal is calibrated to recover the planet at the correct (injected) ϵ_0. This calibration essentially scales the strength of the Gaussian matched filter. This is necessary to take the deconvolved profile strength into account which is dependent on the input line list, wavelength range and least squares weightings.

Plotted on top of the χ^2 surface plot are contours showing confidence levels and, thus, the significance of the results. These were determined using bootstrap statistics where the phase of the residual spectra were randomized, which shuffled any signal from the planet. This allows for any detection caused by systematic or spurious signals to be retained and provides statistics on what can be considered a random detection. The scrambling is performed 3000 times and the contour lines plotted from bottom to top show a 68.4, 95.4, 99.0 and a 99.9 per cent confidence level of the detection of planet's signal. The dotted line shows the most likely value for K_p. This procedure is outlined in Appendix D and E of Collier Cameron et al. (2002).

5.6 Results

The process above was carried out for both the pM and pL atmospheres and the initial runs for both can be seen in Figures 5.6 and 5.7. χ^2 for the pM atmosphere was found to have the greatest enhancement at an ϵ_0 = -4.14 and a K_p = 109.6 km s^{-1} with a confidence level of approximately 99.9 percent. The best solution for the pL atmosphere was found at ϵ_0 = -3.79 and a K_p = 141.8 km s^{-1} with a confidence level of approximately 95.4 per cent.

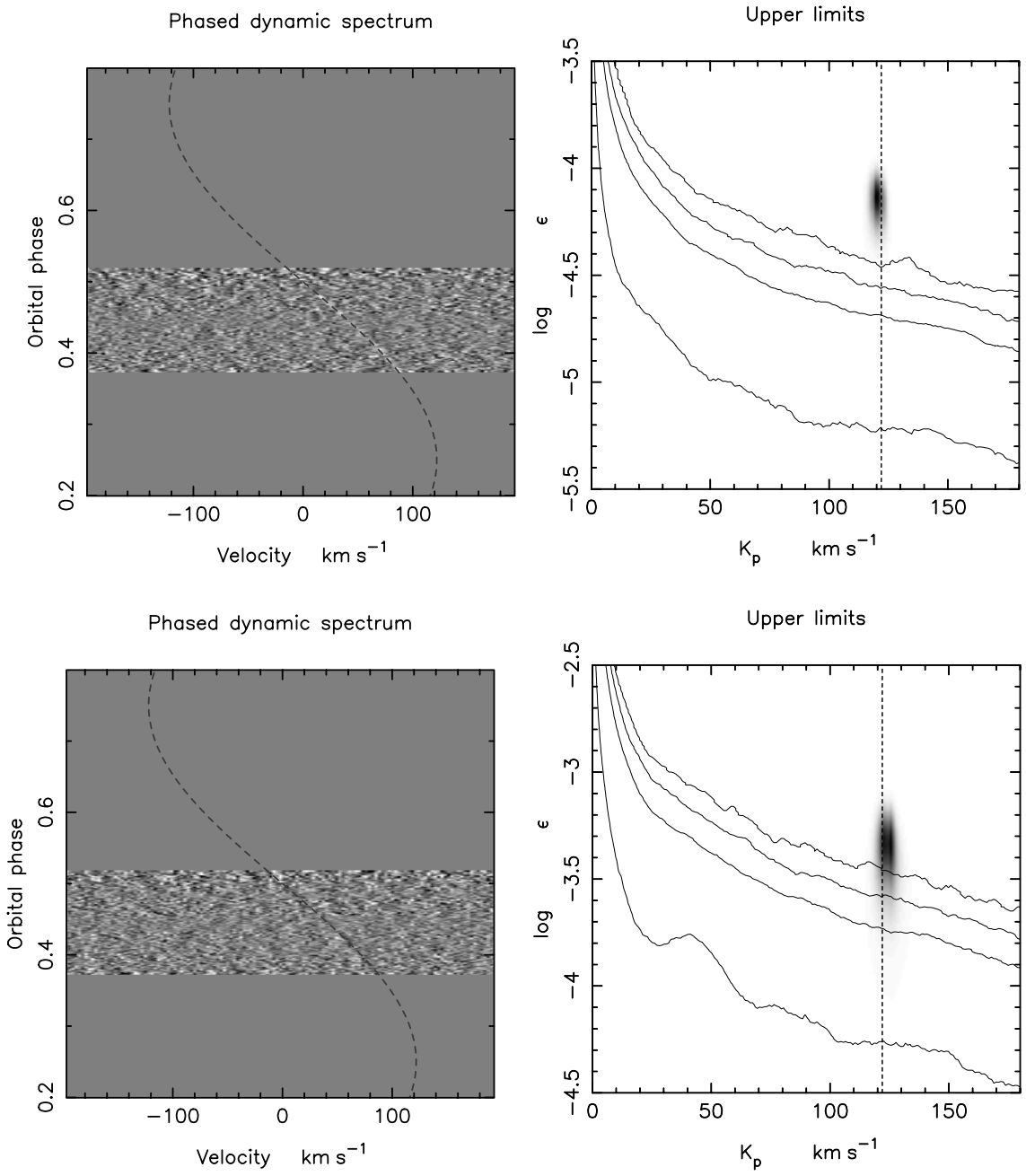

Fig. 5.5: Left Panels: Time series of the deconvolved residual spectra plotted in terms of orbital phase containing the injected planetary signal used for calibration. The dashed line represents where a planetary signal would be found using the velocity amplitude $\hat{K_p}$ calculated in Section 5.5.2. The top panel contains a signal generated using a pM atmosphere and the lower panel contains a pL atmosphere. Right Panels: Relative χ^2 surface plot showing the best solution for a signal detection as a function of log_{10} ϵ_0 versus K_p. The contour lines are the result of a bootstrap Monte Carlo analysis showing the significance of a detection when compared to a random alignment of noisy residuals. From bottom to top, the contour lines represent 68.4, 95.4, 99.0, and a 99.9 per cent confidence.

The best enhancement in χ^2 for the pL class atmosphere is found at an ϵ_0 and K_p that are not consistent with expectations. Given the analysis in 5.1.2, we expect an ϵ_0 no greater than -4.0. The more confident signal found in the pM model is, however,

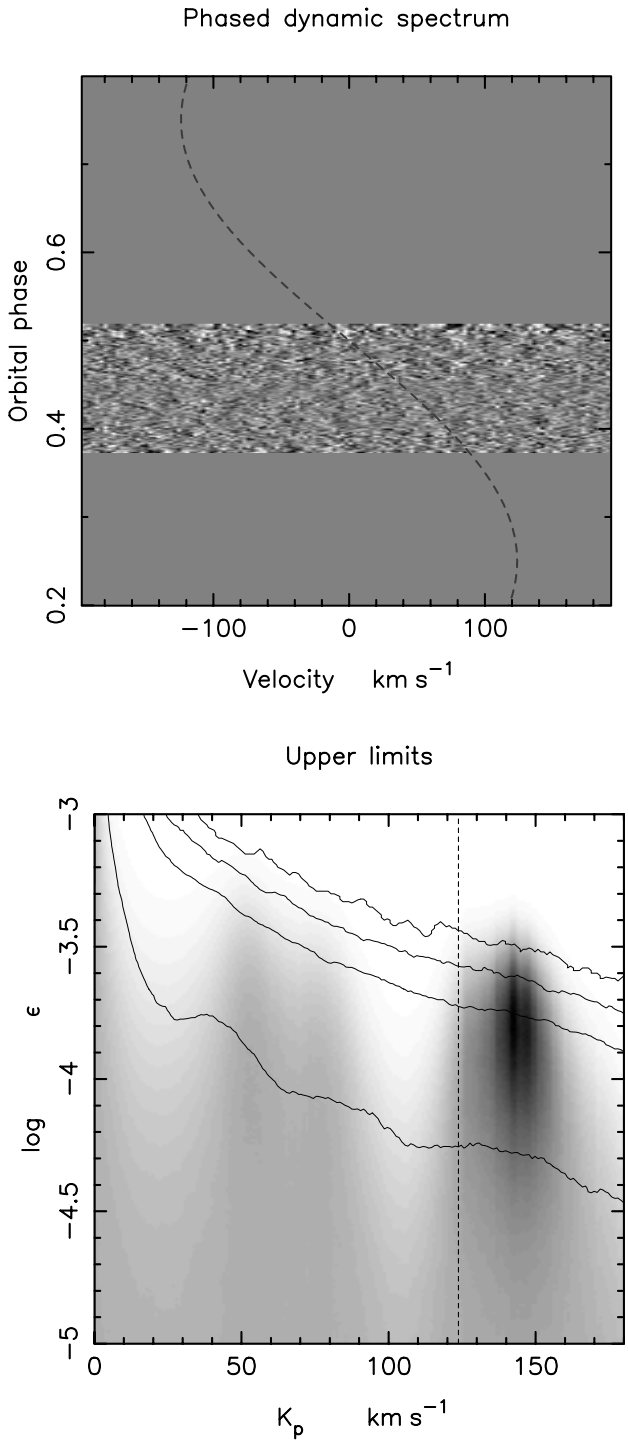

Fig. 5.6: Phased residual time series as in Figure 5.5 using the pL model spectra for the deconvolution. A signal is detected with low confidence (less than 95.4 percent) at a contrast ratio 3 orders of magnitude stronger than expected.

located at an ϵ_0 that is consistent with predictions. However, further confirmation of this result was necessary before coming to the conclusion that a real and significant detection of TiO was made.

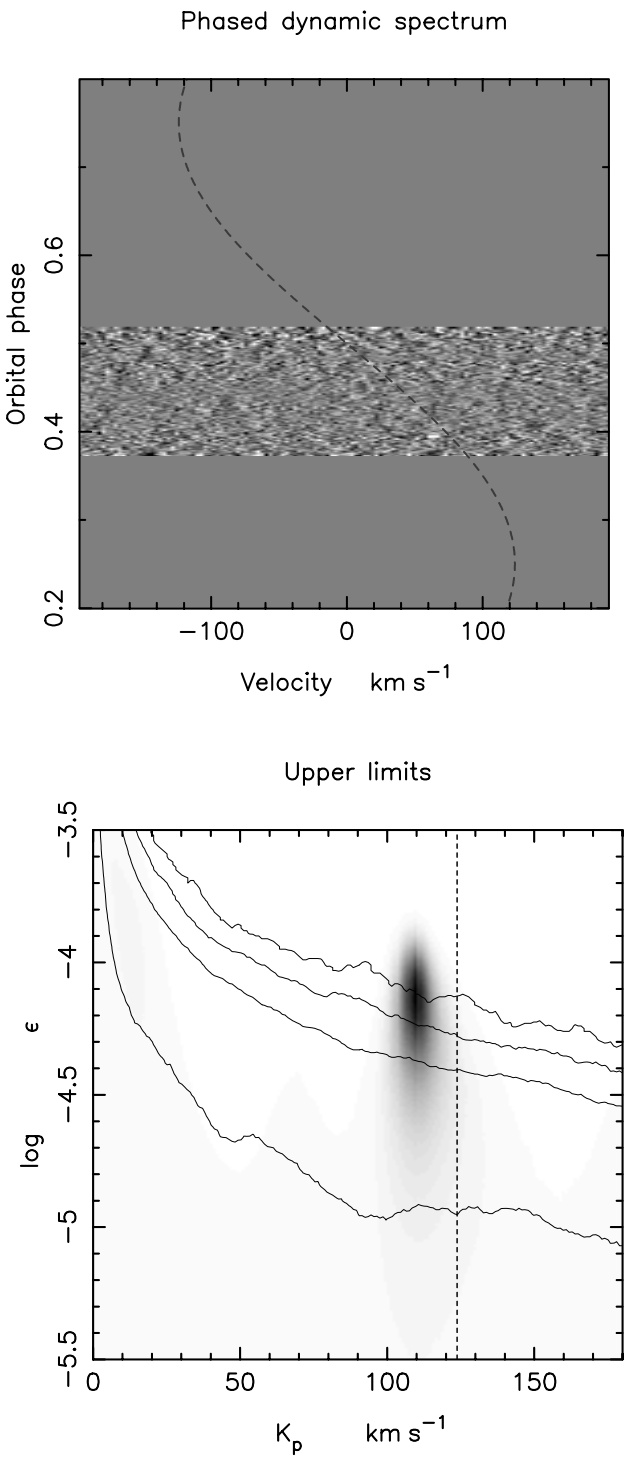

Fig. 5.7: Phased residual time series as in Figure 5.5 using the pM model spectra for the deconvolution. A signal is detected with relatively high confidence (approximately 99.9 per cent) at a contrast ratio within the range of predictions made in Section 5.1.4 ($log_{10}\epsilon$=-4.14).

5.7 Further Analysis

Before accepting the results of our initial analysis, further checks were performed to confirm its validity.

5.7.1 Individual Night Analysis

Each night was processed separately to check if a few spurious spectra from one night were causing the matched filter to produce a false signal. The results can be seen in Figure 5.8.

While we see a slightly more spread out maximum in the χ^2 surface plot and the signal has dropped in confidence, the planetary signal is still recovered at the same values as both nights combined.

5.7.2 Analysis from Planet's Reference Frame

Taking results from both nights of analysis, instead of looking at the residual spectra from the star's rest frame, the deconvolved spectra were shifted into the rest frame of the planet. This required the phaseshift for each observed spectra to be recalculated using the K_p found to be the most likely (109.6 km s^{-1}). Looking at the time series in this way constrained the location of the detected signal to the center vertical column of plot as seen in Figure 5.9.

While the results of the matched filter analysis detected a planetary signal with a 3 sigma confidence, no obvious planetary signal could be seen within the data upon visual inspection of Figure 5.9(a). For comparison, a fake planetary signal was injected into the time series spectra at $F_p/F_* = 10^{-4.14}$ and rotated the resulting deconvolved time series into the reference frame of the planet as was done in Figure 5.9(a). At this contrast ratio, the fake signal can be still be seen visually above the noise in Figure 5.9(b)

Because no obvious signal was seen in Figure 5.9(a), the observed deconvolved time series was re-examined by eye and any pixels along the column that coincided with a $Kp = 109.6$ km s^{-1} with a signal that was significantly above the background was

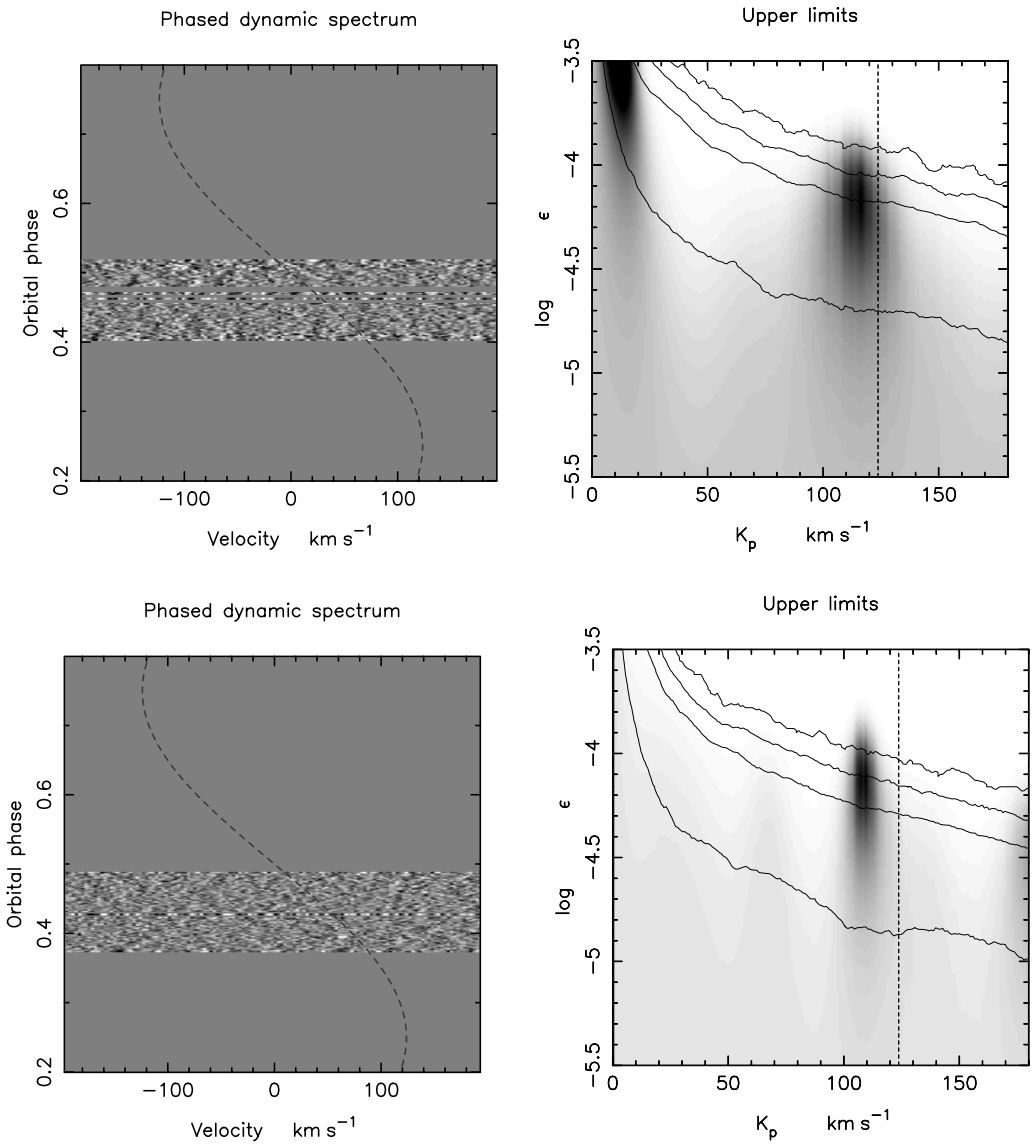

Fig. 5.8: Top: Phased time series and χ^2 map as before showing the pM atmosphere deconvolution for spectra only obtained on the first night (July 25th 2009). The detected signal from Figure 5.7 has lowered in confidence levels from 99.9 to 95.4 per cent and is a less constrained but is still detected. Bottom: As above for spectra only obtained on the second night (July 28th 2009). The detected signal from Figure 5.7 has lowered in confidence levels from 99.9 to 99.0 per cent.

noted. The matched filter analysis was then re-run while masking out the rows that contained these bright pixels and the result can be seen in Figure 5.10.

The original detection was found at $log_{10}\epsilon_0$ = -4.14, with a confidence level of approximately 99.9 per cent. After masking out 13 spectra that had high values in the residuals at a K_p = 109.6 km s^{-1}, the best enhancement in χ^2 is found at a confidence level of 96.1 percent (down from 99.9 percent). If the signal of the planet were genuine, there would not be this large of a drop in significance from losing only 13 spectra out

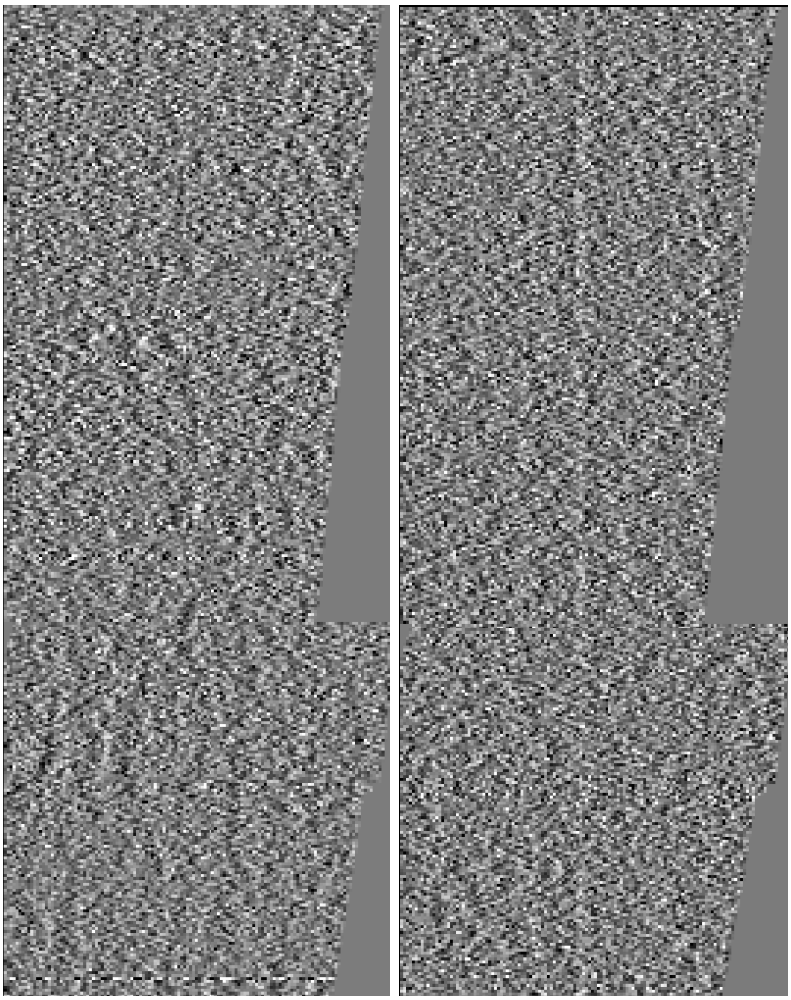

(a) (b)

Fig. 5.9: Left: Deconvolved time series of both nights shifted to the reference frame of the planet so that any planetary signal should appear as a line down the center of the image (0 kms^{-1} in velocity space). Right: Same as the left but with a fake planet signal injected at the $log_{10}\epsilon_0$ = -4.14. It is faint, but there is a clear, visible signal found directly in the center of the image. The lack of a similarly visible signal in the original data suggest that a few individually bright spectra were causing a false detection in earlier analysis.

of the total 338.

5.8 Sensitivity

5.8.1 Estimating theoretical sensitivity levels

In order to investigate the theoretical sensitivity of our observations, a series of spectra, based on the VALD atmospheres with a T_{eff}= 6250 K, were generated. The original synthetic stellar spectra was convolved with a moving Gaussian using the a Fortran

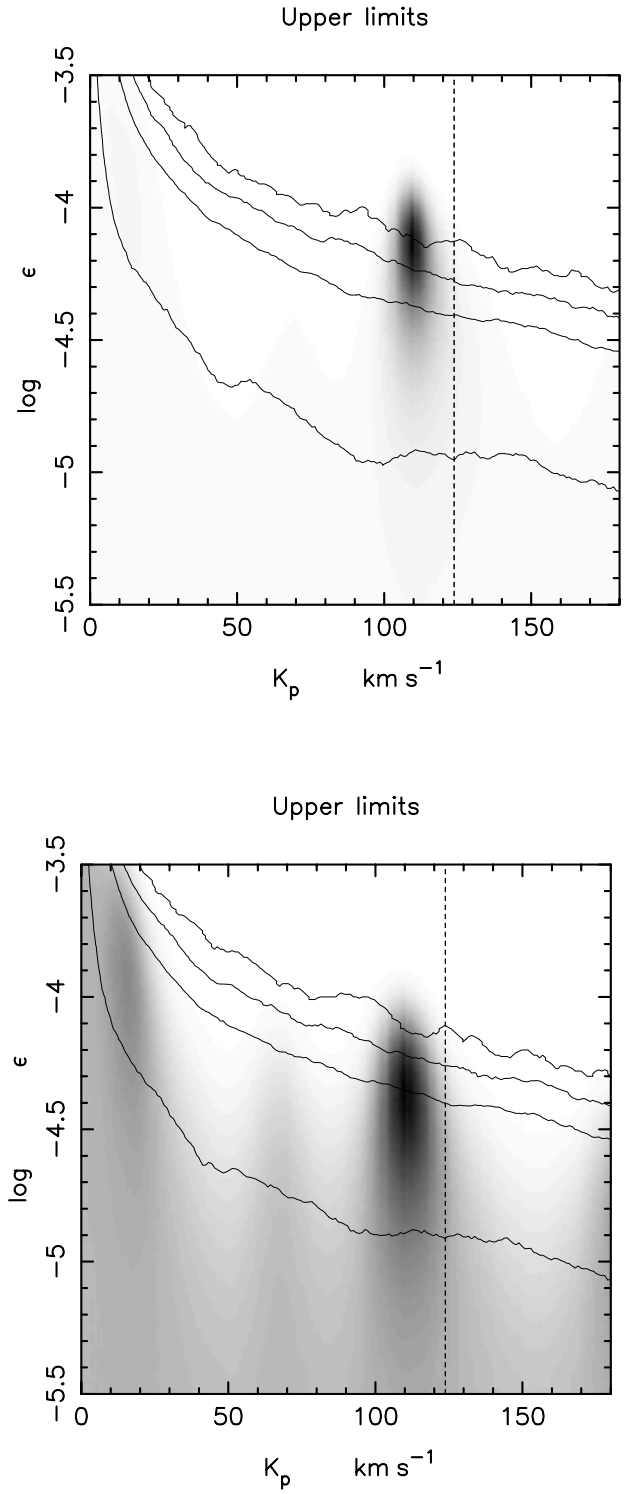

Fig. 5.10: Left: The original detection showing the most likely signal, at $log_{10}\epsilon_0$ = -4.14, found at a confidence level of approximately 99.9 per cent. Right: Same as left after masking out 13 spectra that had high values in the residuals at a $K_p = 109.6$ km s^{-1}. The best enhancement in χ^2 is found at a confidence level of 96.1 percent (down from 99.9 percent) after removing the 13 spectra. If the signal of the planet were genuine, it would be found in all of the 338 spectra and a loss of 13 should not affect the detection significantly as seen here.

routine so that the synthetic spectrum matched the instrumental resolution of our observations (FWHM = 5.995 km s^{-1}, σ= 3.523 km s^{-1}). A mean representative continuum was used so the frames should have exactly the same mean signal to noise and blaze function as the observed spectra. 338 copies of the spectrum were made with Poisson noise added to each one separately. Using the simulated spectra, a fake planet signal was then injected into each spectra using the same phase information as our observations. The spectra were then processed in the same way as our observations and a deconvolved time series created.

The bootstrap Monte Carlo simulation resulted in Figure 5.11 and provided us with our expected Poisson noise limited sensitivity levels. When compared to Figure 5.7, the 99.9 per cent confidence contour (top line) for the simulated spectra intersects the predicted K_p at a $log\ \epsilon$ of roughly -4.6 where our original data produced a sensitivity level of at the same K_p of $log\ \epsilon \simeq$-4.1.

From this discrepancy, one can infer that a loss of sensitivity is occurring either due to varying observing conditions or due to an issue in the extraction, or subsequent analysis, of the observed spectra. This test also shows that if the models are correct and HD179949b does have a pM atmosphere, these observations should be sensitive enough to detect it.

5.8.2 Telluric Masking

Telluric lines can shift in location and strength throughout the night due to variations in temperature and pressure in the atmosphere and the airmass of the observations. One possible contributor to the loss of sensitivity is that these variable telluric lines could have affected the continuum fit during the template spectra subtraction process.

In the process of subtracting the night template from the individual spectra, the night template needs to be adjusted to fit the individual spectra before subtraction. This is done by by using 24 points along each quarter of the spectra (96 points in total) to determine any scaling, shifting or blurring/sharpening needed. It is possible that, during this process, in addition to the template derivatives that are calculated and used

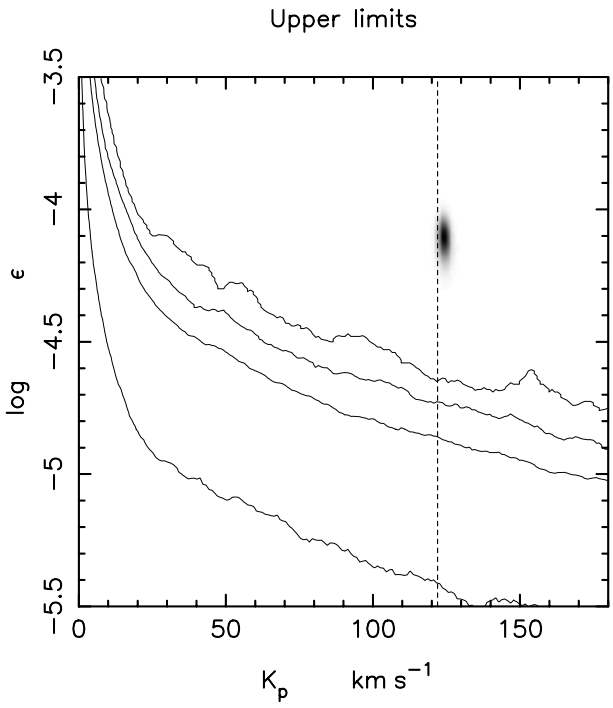

Fig. 5.11: Results of the deconvolution after using a VALD generated F8V spectra convolved with a moving Gaussian to match the instrumental resolution of the observations, adding Poisson noise, and processing as before with a planetary signal injected. This shows the expected sensitivities of this instrumental set up assuming no systematic or time varying effects. The 99.9 per cent confidence level at the most likely K_p is found at a log_{10} ϵ_0=-4.63 which. The equivalent confidence level in the non-simulated data is found at log_{10} ϵ_0=-4.12 which shows a discrepancy of about 3.2 times worse than expected

to determine any shifting, telluric lines could affect the fits which could result in a non-optimal template subtraction. Even outside the telluric regions (which were omitted from the deconvolution), small differences in the continuum normalisation could be seen.

To investigate this as a possible source of our loss of sensitivity, a telluric mask was introduced into the fitting process which prevented any of the individual scaling points from falling onto a, possibly variable, telluric line.

After introducing this telluric mask, the data were processed in the same way and the result can be seen in Figure 5.12. The confidence levels have a very slight improvement and the noise level decreases by 1% but this does not account for the discrepancy between our expected sensitivity and our observed.

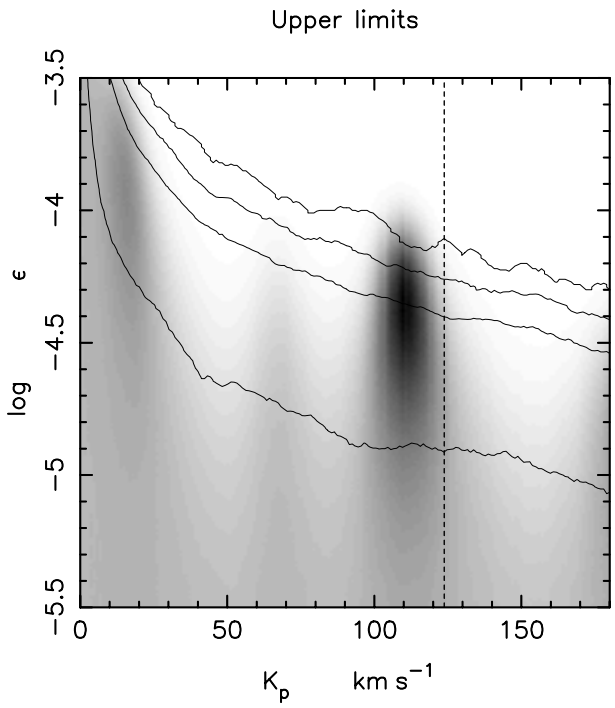

Fig. 5.12: The data reprocessed masking out the known telluric lines from the continuum fitting process. A very slight improvement in confidence levels can be seen when compared to Figure 5.10(b) but this increase does not account for the discrepency between our observed and expected sensitivities.

5.9 Conclusions and Future Work

Initial results suggested a high confidence detection of TiO in the atmosphere of HD 179949b but after further analysis it seems likely that a small number of spurious residual spectra are responsible for the signal. After removing these spectra, no strong signal is detected using either the pM or the pL model atmospheres during the deconvolution process. While the sensitivities of the data are too low to rule out the possibility of a pL atmosphere, the data is sufficiently sensitive to put clear limits on whether HD 179949b has an atmosphere dominated by emission lines caused by TiO. We can rule out the presence of TiO down to a $log_{10}\ \epsilon_0$ = -4.09 or (1 part in 12,300) with 99.9 per cent confidence. We can further rule out the presence of a signal at the most probable $\hat{K_p}$ as no candidate signal appears there. At $\hat{K_p}$ = 123.4 km s^{-1}, we do not detect TiO down to an ϵ_0 = -4.11 with 99.9 per cent confidence.

However, the simulations carried out using a non-varying residual spectra representative of this instrumental set up (Section 5.8.1) imply that we should be sensitive down to a contrast ratio of 1 part in 42,500. This suggests that there are some unaccounted

for systematics causing the sensitivities to be much lower. Possible causes for these effects could be changes in observing conditions such as airmass or varying telluric lines or possibly spectrograph/CCD response changes throughout the night. These effects need to be better understood, modelled, and corrected for during processing in order to bring down these sensitivities.

A path towards reducing these systematics will include investigating the possibility of fringing on either of the 2 CCDs on UVES as well as a more in depth analysis of the order by order noise levels to ascertain if any of the orders differ significantly from the expected Poission noise. A preliminary look at this can be seen in Figure 5.13 where the noise of each order was plotted before and after the PCA was performed. Further work needs to be done to analyse the significance of the deviations from Poisson noise and the causes for such deviations.

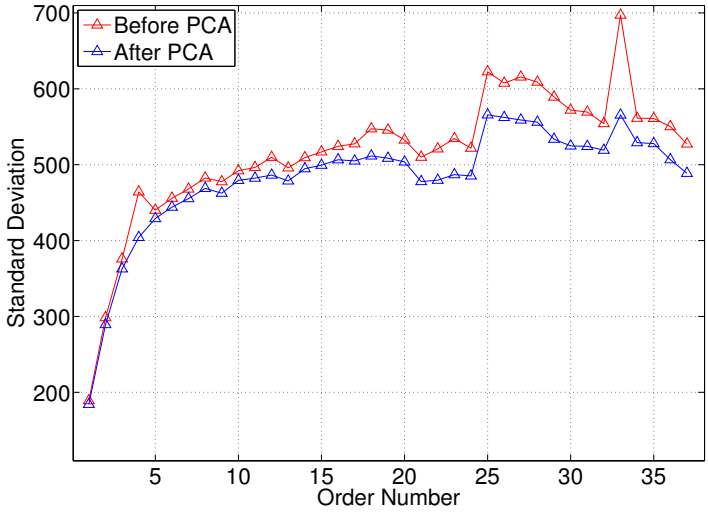

Fig. 5.13: Order to order noise levels of a selected residual spectra. The global increase in noise at order 25 is where the "Blue" chip on UVES ends and the "Red" chip takes over. The jump in noise at order 33 is still being investigated.

A more iterative approach to the PCA can also be implemented where, rather than removing the strongest 3 eigenvalue exclusively, the removal could be tailored to each order so that only the significant components are removed. Additionally, an investigation into the effect of using a non-Gaussian matched filter should be conducted to test whether a Lorentz or Voigt profile would more accurately fit the observed data. These and potentially other tests will be conducted before the work in this chapter is

submitted for publication.

References

Barman, T. S., Hauschildt, P. H., & Allard, F. 2005, ApJ, 632, 1132

Barnes, J. R., Barman, T. S., Jones, H. R. A., Barber, R. J., Hansen, B. M. S., Prato, L., Rice, E. L., Leigh, C. J., Collier Cameron, A., & Pinfield, D. J. 2010, MNRAS, 401, 445

Barnes, J. R., Barman, T. S., Jones, H. R. A., Leigh, C. J., Collier Cameron, A., Barber, R. J., & Pinfield, D. J. 2008, MNRAS, 390, 1258

Barnes, J. R., Collier Cameron, A., James, D. J., & Donati, J.-F. 2000, MNRAS, 314, 162

Barnes, J. R., Collier Cameron, A., Unruh, Y. C., Donati, J. F., & Hussain, G. A. J. 1998, MNRAS, 299, 904

Barnes, J. R., Jenkins, J. S., Jones, H. R. A., Rojo, P., Arriagada, P., Jordán, A., Minniti, D., Tuomi, M., Jeffers, S. V., & Pinfield, D. 2012, MNRAS, 424, 591

Barnes, J. R., Leigh, C. J., Jones, H. R. A., Barman, T. S., Pinfield, D. J., Collier Cameron, A., & Jenkins, J. S. 2007, MNRAS, 379, 1097

Brogi, M., Snellen, I. A. G., de Kok, R. J., Albrecht, S., Birkby, J., & de Mooij, E. J. W. 2012, Nature, 486, 502

Burrows, A., Budaj, J., & Hubeny, I. 2008, ApJ, 678, 1436

Burrows, A., Marley, M., Hubbard, W. B., Lunine, J. I., Guillot, T., Saumon, D., Freedman, R., Sudarsky, D., & Sharp, C. 1997, ApJ, 491, 856

Butler, R. P., Wright, J. T., Marcy, G. W., Fischer, D. A., Vogt, S. S., Tinney, C. G., Jones, H. R. A., Carter, B. D., Johnson, J. A., McCarthy, C., & Penny, A. J. 2006, ApJ, 646, 505

Charbonneau, D., Noyes, R. W., Korzennik, S. G., Nisenson, P., Jha, S., Vogt, S. S., & Kibrick, R. I. 1999, ApJ, 522, L145

Collier Cameron, A., Horne, K., Penny, A., & James, D. 1999, Nature, 402, 751

Collier Cameron, A., Horne, K., Penny, A., & Leigh, C. 2002, MNRAS, 330, 187

Cowan, N. B., Agol, E., & Charbonneau, D. 2007, MNRAS, 379, 641

Cubillos, P. E., Rojo, P., & Fortney, J. J. 2011, A&A, 529, A88

Dekker, H., D'Odorico, S., Kaufer, A., Delabre, B., & Kotzlowski, H. 2000, in Society of Photo-Optical Instrumentation Engineers (SPIE) Conference Series, Vol. 4008, Society of Photo-Optical Instrumentation Engineers (SPIE) Conference Series, 534–545

Donati, J.-F., Semel, M., Carter, B. D., Rees, D. E., & Collier Cameron, A. 1997, MNRAS, 291, 658

Eggenberger, A., Udry, S., Chauvin, G., Beuzit, J.-L., Lagrange, A.-M., Ségransan, D., & Mayor, M. 2007, A&A, 474, 273

Fares, R., Donati, J.-F., Moutou, C., Jardine, M., Cameron, A. C., Lanza, A. F., Bohlender, D., Dieters, S., Martínez Fiorenzano, A. F., Maggio, A., Pagano, I., & Shkolnik, E. L. 2012, MNRAS, 423, 1006

Fortney, J. J. 2005, MNRAS, 364, 649

Fortney, J. J. 2007, in In the Spirit of Bernard Lyot: The Direct Detection of Planets and Circumstellar Disks in the 21st Century

Fortney, J. J., Cooper, C. S., Showman, A. P., Marley, M. S., & Freedman, R. S. 2006, ApJ, 652, 746

Fortney, J. J., Lodders, K., Marley, M. S., & Freedman, R. S. 2008, ApJ, 678, 1419

Gurdemir, L., Redfield, S., & Cuntz, M. 2012, PASA, 29, 141

Harrington, J., Hansen, B. M., Luszcz, S. H., Seager, S., Deming, D., Menou, K., Cho, J. Y.-K., & Richardson, L. J. 2006, Science, 314, 623

Harrington, J., Luszcz, S., Seager, S., Deming, D., & Richardson, L. J. 2007, Nature, 447, 691

Horne, K. 1986, PASP, 98, 609

Hubeny, I., Burrows, A., & Sudarsky, D. 2003, ApJ, 594, 1011

Knutson, H. A., Charbonneau, D., Cowan, N. B., Fortney, J. J., Showman, A. P., Agol, E., Henry, G. W., Everett, M. E., & Allen, L. E. 2009, ApJ, 690, 822

Leigh, C., Collier Cameron, A., Horne, K., Penny, A., & James, D. 2003, MNRAS, 344, 1271

Marley, M. S., Guillot, T., Saumon, D., & Freedman, R. S. 1996, in Bulletin of the American Astronomical Society, Vol. 28, Bulletin of the American Astronomical Society, 1114

Marley, M. S. & McKay, C. P. 1999, Icarus, 138, 268

McKay, C. P., Pollack, J. B., & Courtin, R. 1989, Icarus, 80, 23

Piskunov, N. E., Kupka, F., Ryabchikova, T. A., Weiss, W. W., & Jeffery, C. S. 1995, A&AS, 112, 525

Rodler, F., Kürster, M., & Barnes, J. R. 2013, MNRAS, 432, 1980

Santos, N. C., Israelian, G., & Mayor, M. 2004, A&A, 415, 1153

Saumon, D., Marley, M. S., Cushing, M. C., Leggett, S. K., Roellig, T. L., Lodders, K., & Freedman, R. S. 2006, ApJ, 647, 552

Scandariato, G., Maggio, A., Lanza, A. F., Pagano, I., Fares, R., Shkolnik, E. L., Bohlender, D., Cameron, A. C., Dieters, S., Donati, J.-F., Martínez Fiorenzano, A. F., Jardine, M., & Moutou, C. 2013, A&A, 552, A7

Shkolnik, E., Walker, G. A. H., & Bohlender, D. A. 2003, ApJ, 597, 1092

Showman, A. P., Cooper, C. S., Fortney, J. J., & Marley, M. S. 2008, ApJ, 682, 559

Skrutskie, M. F., Cutri, R. M., Stiening, R., Weinberg, M. D., Schneider, S., Carpenter, J. M., Beichman, C., Capps, R., Chester, T., Elias, J., Huchra, J., Liebert, J., Lonsdale, C., Monet, D. G., Price, S., Seitzer, P., Jarrett, T., Kirkpatrick, J. D., Gizis, J. E., Howard, E., Evans, T., Fowler, J., Fullmer, L., Hurt, R., Light, R., Kopan, E. L., Marsh, K. A., McCallon, H. L., Tam, R., Van Dyk, S., & Wheelock, S. 2006, AJ, 131, 1163

Snellen, I. A. G., de Kok, R. J., de Mooij, E. J. W., & Albrecht, S. 2010, Nature, 465, 1049

Swain, M. R., Tinetti, G., Vasisht, G., Deroo, P., Griffith, C., Bouwman, J., Chen, P., Yung, Y., Burrows, A., Brown, L. R., Matthews, J., Rowe, J. F., Kuschnig, R., & Angerhausen, D. 2009, ApJ, 704, 1616

Tinetti, G., Vidal-Madjar, A., Liang, M.-C., Beaulieu, J.-P., Yung, Y., Carey, S., Barber, R. J., Tennyson, J., Ribas, I., Allard, N., Ballester, G. E., Sing, D. K., & Selsis, F. 2007, Nature, 448, 169

Tinney, C. G., Butler, R. P., Marcy, G. W., Jones, H. R. A., Penny, A. J., Vogt, S. S., Apps, K., & Henry, G. W. 2001, ApJ, 551, 507

Torres, G., Andersen, J., & Giménez, A. 2010, A&A Rev., 18, 67

Valenti, J. A. & Fischer, D. A. 2005, ApJS, 159, 141

van Leeuwen, F., ed. 2007, Astrophysics and Space Science Library, Vol. 350, Hipparcos, the New Reduction of the Raw Data

Wittenmyer, R. A., Endl, M., & Cochran, W. D. 2007, ApJ, 654, 625

Chapter 6: Summary and Conclusion

This thesis has approached the problem of exoplanet atmospheric characterisation from several different directions. The future of this field will depend on novel space and ground based instruments as well as new observing techniques and this work has provided new information to help pave the way for such endeavours as well as provided its own insights into the structure of exoplanet atmospheres. It has done so in the following way.

6.1 Preliminary Design Studies for EChO

Work was done in collaboration with Astrium Engineers on the preliminary design of the EChO spacecraft: a proposal for ESA's M3 slot as part of their Cosmic Visions program. Studies were done focusing on the spacecraft's AOCS and sun shield taking into consideration the many design concerns necessary for a spacecraft of this nature. The trade studies concluded that a cold gas thruster system with the possibility of a hybrid design that would include reaction wheels would best suit EChO's requirements for its AOCS. For the sun shield, a V-groove cone option is recommended based on both its thermal abilities, mechanical stability, and it symmetric design allows easier slewing between targets. These recommendations were folded in the the Phase-A design studies conducted by Astrium. The final design recommended to ESA was consistent with the results of this trade study.

6.2 Planet Simulations

Chapter 3 produced statistics for the number of transiting planets that can be expected to be found around known stars less than 50 parsecs away in the next 10 years. The current exoplanet population was used as a guide to produce a mass and semi-major

axis distribution consistent with observations. After estimating the stars physical characteristics such as mass and radius from empirical relationships, a planet population was produced using input from models to produce radii for terrestrial and gas giant planets. The stars and simulated planets were sorted by mass and the most massive star was assigned the most massive planet consecutively down to the least massive of the star and planet but maintained an orbital radius based on a power law fit to empirical data. After iterating the simulations 6000 times, an average of 27 planets were found to have a detectable transit amongst this stellar population.

6.3 M Dwarf Catalogue

In Chapter 4, the PPMXL catalogue was used to find previously overlooked M dwarfs for future transit and RV surveys. This was done by using tailored colour cuts across multi bands and using PPMXL's highly accurate proper motions and a reduced proper motion cut to surpass the lower proper motion limit of previous catalogues. This method produced 1193 new M dwarf candidates and combined previous work with this work to produce the complete complication of K<9 M dwarfs currently available.

The applications of this catalogue are many but this catalogue has already been distributed to several groups who are applying it to their various scientific endeavours. These include the Apache program and CARMENES programs (mentioned in Section 1.5.1), a University of Hertfordshire-based campaign to search for benchmark brown dwarfs, as well as providing targets for a high resolution spectroscopy survey to obtain constraints on inclination angles of potential transiting planetary systems.

6.4 High Resolution Spectroscopy of HD 179949

Chapter 5 used high resolution spectroscopy and spectra of planetary atmospheres based on models to perform spectral deconvolution in an attempt to detect the Doppler shifted signal of the non-transiting planet HD 179949 b. The signal was not detected but new upper limits were set ruling out the presence of TiO down to a $\log_{10} \epsilon_0 = -4.09$

with 99.9 per cent confidence. Though the data did produce new results, simulations conducted by this work imply a loss of sensitivity occurring possibly due to varying telluric interference or instrumental systematics.

6.5 Future Work

An obvious next step is to combine the planet simulations and the new M dwarfs discovered to produce new statistics for a more complete stellar sample. Some care is necessary in this, however, due to the lack of distance measurements of the M dwarfs as well as the current exoplanet populations statistics being heavily skewed towards higher mass stars. This can be accomplished in a basic way with distance estimations based on colour and a planet population that is scaled down to not include the most massive planets. Some significant alterations to the code will need to be done to accomplish this but it is a step that would be worthwhile pursing.

Additional M dwarfs may also be able to be found by pushing the reduced proper motion limit lower and exploring the regions of the galactic plane that were cut out of this sample. Both would need to be done with great care as both would introduce far more possibilities for giants and reddened objects to contaminate the selection process. However, it may be possible to use galactic plane reddening maps to pick out the brightest candidate objects and could yield a significant number of additional M dwarfs. A proper motion limit lower than 20 mas using the method in Chapter 4 would most likely become impractical due to M giant contamination but that these limits could be explored further to find additional objects.

For the analysis of observations of HD 179949 b, a more thorough investigation into what is causing the drop in sensitivity is needed. Some ideas for this would be the way in which the principle component analysis is conducted where fewer or more components are removed depending on the time of observation. This is still under investigation. These results plan to be submitted to a journal so the community will have access to the new constraints put on the atmospheric characteristics of HD 179949 b.